1985

Hydrodynamic model of an inlet sound system in southern New Jersey /

Frederick E. Scbueprer
Lehigh University

HYDRODYNAMIC MODEL OF AN INLET SOUND SYSTEM IN SOUTHERN NEW JERSEY

by

Frederick E. Schuepfer

A Thesis

Presented to the Graduate Committee

of Lehigh University

in Candidacy for the Degree of

Master of Science

in

Civil Engineering

Lehigh University
1985

Certificate of Approval

This thesis is accepted and approved in partial fulfillment of the requirements for the degree of Master of Science.

5/13/85
(date)

Gerard P. Lennon
Professor in Charge

T. A. Sorensen
Chairman of Department

ACKNOWLEDGMENTS

This report was made possible by funds from the Office of Sea Grant and is part of an ongoing project in the Department of Civil Engineering at Lehigh University. The Acting Head of the Department of Civil Engineering is Dr. Robert M. Sorensen. The Acting Research Director is Dr. John W. Fisher.

The computer program HYDTID was furnished by the Coastal Engineering Research Center, Vicksburg, Mississippi. Support services were provided by the Lehigh University Computing Center.

Drs. Gerard P. Lennon and Richard N. Weisman were the co-principal investigators for the project. Their expertise and patient guidance helped to bring this study to fruition.

I am also grateful to Captain Ralph J. Gabriel whose generous, timely advice during the early days of my stay was most appreciated. I am obliged to Mr. John M. Gera for his assistance in drafting the figures and to Mrs. Catherine Miller for her help in typing the manuscript. Finally, I wish to thank my family and friends for their indispensible kindness and support.

Table of Contents

List of Figures

List of Tables

ABSTRACT

The two-dimensional, hydrodynamic, numerical model HYDTID was used to predict flows and tidal heights for a range of tidal conditions in Great Sound, New Jersey. The vertically averaged momentum and continuity equations for a specific set of initial and boundary equations are solved using an explicit finite difference scheme. Potential inputs include forcing tides, wind, rainfall and evaporation data, topography, bathymetry, friction, and external inflows.

The model was calibrated against observed discharges and tidal elevations for selected spring and neap tide events. Subsequently, the model was verified by simulating a mean tide event using an independent set of data. To demonstrate the model's predictive capability, two hypothetical scenarios were run. In the first simulation, channel geometries were modeled without an Intracoastal Waterway. In the second simulation, a two-foot sea level rise was modeled.

Because spring tide in Great Sound involves inundation of most of the marsh, a method of modeling the flooding and draining of an expanse of marshland was developed. If the simulation began at a high or low tide, a preliminary startup interval was not required. The predicted flows and water levels were sensitive to marsh cell

elevations, feeder channel arrangement, and allocation of forcing cells, and were insensitive to friction values and bathymetry.

1. INTRODUCTION

1.1 Overview and Study Objectives

Increasing human activity near the southern New Jersey wetlands has introduced new issues involving the sensitive tidal marsh ecosystem. Currently, balancing the need for environmental protection against urban growth and increased recreational demand has become more difficult. Additionally, possible sedimentation in the back bays and channels requires attention due to the negative effects on commerce and navigation. For these reasons, the hydrodynamics of a tidal inlet-bay area were studied with respect to the many driving mechanisms affecting water elevations and flows, including tides, precipitation, river inflow, evaporation, and wind. Although many factors affect the hydraulics of the sound, the astronomical tides are most important during typical, fair-weather conditions.

The study area includes Great Sound, a back bay located behind the barrier island of Avalon and Stone Harbor, New Jersey (see Fig. 1-1). The sound is connected to the Atlantic Ocean by Great Channel and Ingram Thorofare which receive waters from Hereford Inlet and Townsend Inlet, respectively. This effort utilized a mathematical model to simulate the hydrodynamics of Great Sound, its feeder channels, and the surrounding wetlands.

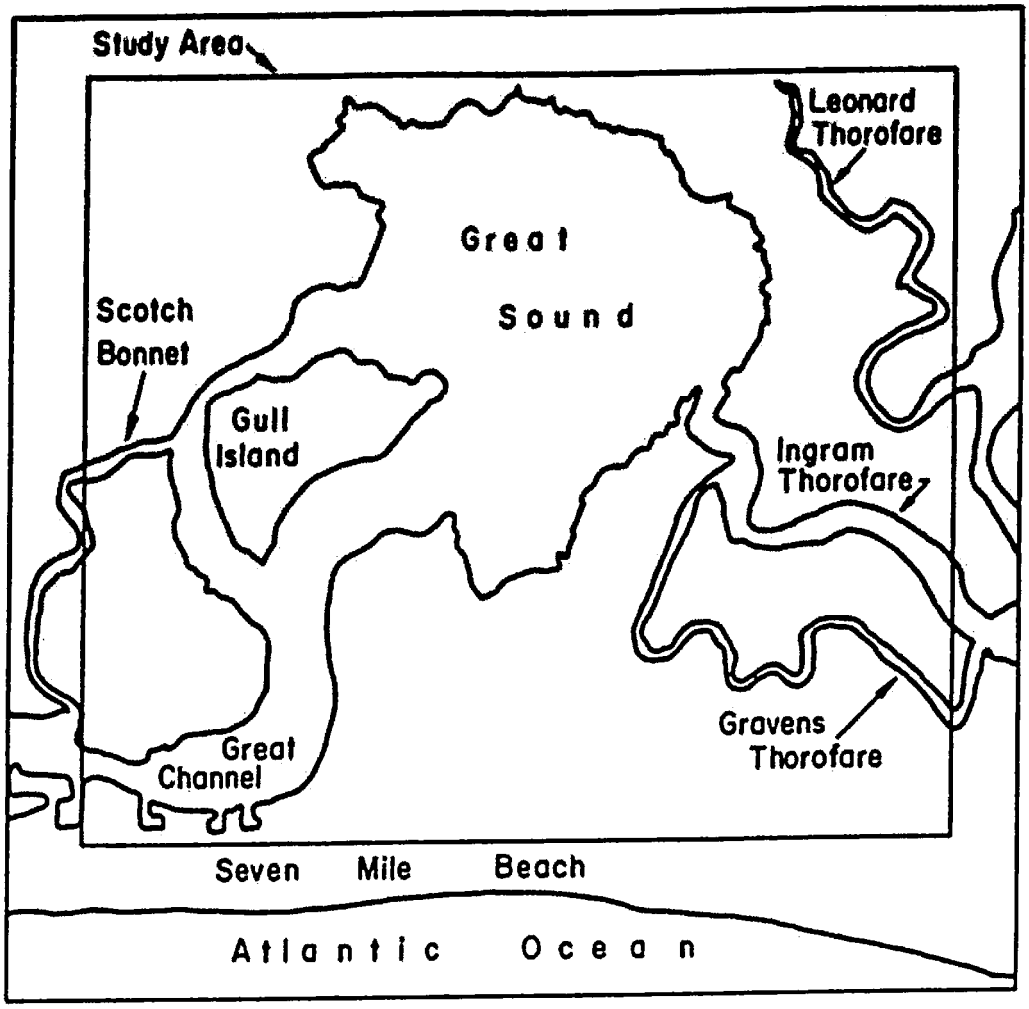

Figure 1-1: Map of Study Area

The objectives of this effort are:

1. to accurately simulate the flow field and tidal elevations throughout Great Sound for selected periods of record;
2. to predict the effect of manmade or natural changes to the hydraulic environment;
3. to assess the importance of modeling the relatively smaller channels which permeate the marsh adjacent to Great Sound;
4. to simulate the inundation of marshland using the hydrodynamic model; and
5. to obtain in the field observed values of Manning's roughness coefficient for the main channels feeding Great Sound.

A critical part of any modeling study is the calibration and verification of the model. Consequently, comprehensive elevation and discharge data for the range of tidal conditions were taken in the field and were supplemented by data obtained by the National Ocean Survey (NOS) [23].

The hydrodynamic model is based on a numerical technique using the equations of motion and the continuity equation. A synopsis of the important principles and applications of hydraulics of inlet-sound systems is now presented.

1.2 Tidal Hydraulics

In a classic examination of tidal hydraulics, Brown [2] modeled a simple inlet-bay system. He first presented a wide-ranging discussion on wave action, littoral drift, ocean currents, inlet formation, inlet currents, inlet migration, and scour-deposition. Brown studied the elementary case of an enclosed back bay attached to the sea by one inlet. His simplifying assumptions included vertical bay walls, an inlet of uniform cross-section, uniform water density, and negligible energy due to acceleration. He also assumed that the surface elevations of the bay and sea varied sinusoidally, and he neglected fresh-water flow into the bay.

Brown then used these simplifications to formulate two equations. The first expression, the conservation of mass, equated the quantity of water exiting the ocean to the amount of water entering the basin. The second expression, the energy equation, utilized energy considerations to relate the change in water elevation to the energy loss in the channel. These two expressions in turn yielded expressions for mean tidal range, maximum current velocity, and potential volume of tidal discharge (the tidal prism).

Brown's approach has inherent limitations. The assumption that the quantity of water exiting the ocean equals the amount of water entering the basin is valid only if there is minimal discharge from

rivers. The inlet channel in reality is seldom uniform, and energy is rarely dissipated in a linear fashion in the channel (as assumed). Also, as a result of Brown's simplifying assumptions several constants were incorporated into the formulation which tend to vary through the actual tidal cycle. While Brown's model is instructive, the extent of the simplifying assumptions make the method insufficient for describing tidal hydraulics.

Keulegan [18] developed a simple but useful technique for estimating inlet flows and tidal-bay water levels. In Keulegan's formulation, the basin responds only to a sinusoidal ocean tide where the inertia of the inlet flow is neglected and the basin walls are vertical. Also, inlet depth is assumed to be large compared to the tidal range. A differential equation involving dimensionless ocean and bay elevations and the bay elevation's derivative with respect to time was developed. Keulegan presented a "repletion coefficient" relating these quantities; the coefficient incorporates the influence of bay and inlet geometry, roughness, and tidal amplitude and period. Because Keulegan conveniently summarized inlet paramters in a single coefficient, an analytical solution to the differential equation was found by using a Fourier series presented in tabular format. Keulegan's approach was an improvement over Brown's because Keulegan allowed for a nonsinusoidal water level in the bay and retained the nonlinear nature of the energy

equation.

Oliveira [27] made Keulegan's method more practical by considering small values for the channel depth to tidal range ratio--a prime characteristic of shallow, non-navigable channels needing navigation improvements. An expression for Keulegan's repletion coefficient was developed and was then integrated numerically. Huval and Wintergerst's model [17] is also based on Keulegan's technique but was extended to include variable inlet and basin surface area, variable inlet depths, nonsinusoidal tides, inlet inertia effects, and bay inflows or outflows other than the ocean.

Recently, the application of the equations of continuity and motion has proceeded in conjunction with numerical solution techniques for use with a digital computer. Lamb [20] presented the general forms of the equations, and Dronkers [8] presented the more useful discretized forms. Dronkers [9] examined difficulties in practical applications of tidal computations, including a discussion of both implicit and explicit finite difference methods.

Snyder [33], noting the nearly harmonic nature of estuarine tidal flow, drew an analogy between the hydraulics of estuaries and alternating current flow. By applying this analogy, slack tidal

current tables can be generated. Also, the concept of reactance was applied to verify if a particular estuarine system is close to resonance. Chu and Yeh [6] applied a semi-implicit finite-difference approach in modeling, taking into account the effect of the salinity density gradient on hydrodynamics. Two hypothetical estuaries were modeled neglecting Coriolis force, wind stress and temperature variation.

Masch et al. [21] developed a two-dimensional finite difference model called HYDTID. Originally developed as a hurricane surge model, HYDTID was further enhanced to account for irregular bathymetry, bottom roughness, islands, and small, inundated areas. The model was used to simulate the hydrodynamics of Masonboro Inlet in North Carolina by first using a coarse grid model on the entire area. The coarse grid results were used as external inputs to a fine grid sub-model of a more localized area of greater interest.

Himwood and Wallis [15] surveyed the hydraulic and water quality modeling of tidal waters. They developed a classification system for models by grouping them by the number of spatial dimensions, Eulerian or non-Eulerian reference frame, and the theoretical type (hydrodynamic, kinematic, or transport model). Some general considerations in selecting a model are offered, along with an exhaustive review of approximately 100 water and waste

movement models for tidal bays and estuaries.

1.3 Accomplishments

In this study the two-dimensional, hydrodynamic, numerical model HYDTID was used to hydraulically describe Great Sound. HYDTID is an explicit, finite difference simulation model written in the FORTRAN source language. Based on its successful application to Masonboro Inlet by Masch et al. [21] and to Hereford Inlet by Gabriel et al. [10], the model was deemed the best choice for this effort.

The model was first calibrated for neap and spring tidal data collected during 1983. To accomplish this calibration, additional data concerning bathymetry, topography, and Manning's roughness coefficient were also collected during site visits in 1984. Refinement of the model completed the calibration process, yielding accurate water elevations, discharges, and tidal prisms which compared well with field data.

The model was then verified by comparing results for an independent set of tidal forcing data obtained from NOS. Finally, the model was applied by simulating hypothetical flow geometries. The relative effects of manmade or natural changes on the discharges and velocities in Great Sound could then be determined.

From this project the following conclusions are made:

1. The model accurately simulates the flow field and tidal elevations throughout Great Sound for selected spring, mean, and neap tide events. The model can be used to provide relative estimates of the effects of introducing certain changes to the back-bay area, such as dredging or sea-level rise.

2. Accurate modeling of feeder channels can be achieved by using one wide channel to represent several channels.

3. The model need not be run for a preliminary startup interval so long as the simulation period begins at a high or a low tide.

4. The empirical formulas relating Manning's n to elevation recommended by Masch et al. [21] are inappropriate for the Great Sound inlet-channel-sound system based on the 1984 data collection effort.

Some recommendations for future work emerged from this effort. More accurate discharge measurements should be obtained to improve calibration of the model and calculation of Manning's roughness coefficient. Manning's n should be calculated specifically for Great Sound, Great Channel, and the small feeder channels. Another set of water level data for neap tide should be collected to check the set used in the model calibration. Also, the linear equations for Manning's n used by Masch et al. [21] were not appropriate for elevations less than zero Mean Low Water (MLW). These equations should be checked for elevations greater than zero. A field study of Manning's n for flow over marshland should be undertaken to substantiate Manning's n values found in the literature.

2. HYDTID MODEL FORMULATION

2.1 Finite Difference Technique

To mathematically describe tidal hydrodynamics requires simultaneous solution of the nonlinear partial differential equations of motion and the general continuity equation for an incompressible fluid. Because the spatial and temporal complexities of actual tidal systems make purely analytical approaches impractical, numerical methods implemented on mainframe computers are used to obtain an approximate representation of a hydrodynamic system.

As described by Masch et al. [21] and Gabriel et al. [10], the HYDTID model is based on an explicit, finite difference technique. Since numerical modeling necessitates a discretization of the study area, a grid composed of square cells in two-dimensional Cartesian coordinates is used to represent the physical characteristics of the system. The relevant parameters defined at the center of a cell include: the water surface elevation, h, the bottom elevation, z, the water depth, d (equal to h-z), Manning's roughness coefficient, n, rainfall, r, and evaporation, e (see Fig. 2-1.) Also, the discharges per unit width q_x and q_y are defined in the x and y directions, respectively, across the right and upper sides of each cell.

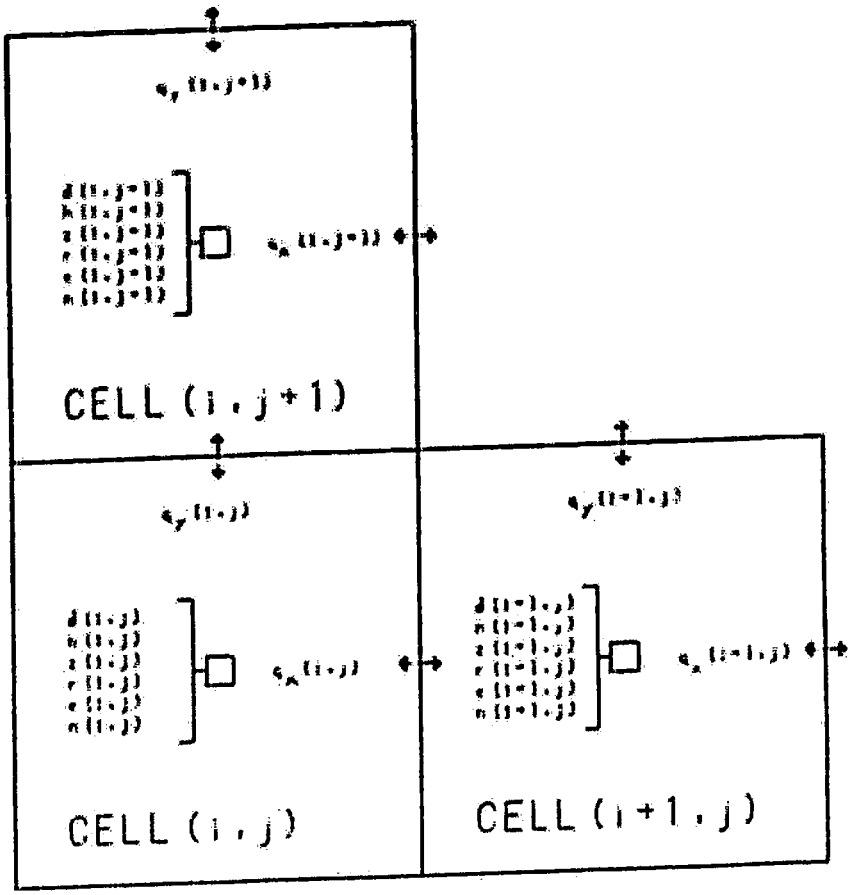

Figure 2-1: Variable Positions in HYDTID
(after Gabriel et al. [10])

To calculate q_x, q_y, and h, the initial and boundary conditions must first be specified. The finite difference approximation of the equations of motion and the continuity equation must be solved for these three unknowns at the first time step. After these calculations are performed in every cell, the boundary conditions are re-calculated for the next time step. This procedure is repeated for the new boundary conditions at the new time step for the required simulation period. The finite difference approximation of the hydrodynamic equations are derived in Appendix I.1.

The accuracy of the results obtained by this procedure is partly a function of the time interval and the cell size chosen. Decreasing the time interval or cell size will improve the accuracy of the results but increases cost. An additional constraint on cell size and time interval is imposed by the mathematical considerations of stability and convergence [21]:

$$\Delta t \leq \frac{\Delta s}{\sqrt{2\ g\ d_{max}}} \qquad (1)$$

where Δt is the time step, Δs is the cell width, d_{max} is the maximum water depth in the model, and g is the gravitational acceleration. Usually, stability of the finite difference technique is a more stringent requirement than convergence, as is the case

here [6].

2.2 Boundary Conditions

Numerical solution of the theoretical equations can yield accurate results in an open-water area. However, where land or barriers are adjacent to water special flow boundaries must be mathematically described. The HYDTID model includes seven special boundary types:

1. water-land boundaries
2. submerged barrier boundaries
3. overtopping barrier boundaries
4. external flow boundaries
5. artificial offshore tidal boundaries
6. artificial tidal storage boundaries
7. inundation boundaries.

Water-land boundaries have, by definition, no flow normal to the boundary. Applications of this boundary are non-inundated land, islands, spoil banks, dikes and impermeable jetties.

For submerged barrier boundaries, the barrier-crest elevation is always less than the two adjacent water levels. This condition is used to model submerged reefs, sand bars, spoil banks and pipelines.

An overtopping barrier boundary describes a situation where normally the water level on only one side at a time may exceed the barrier crest elevation. This boundary can be used to simulate periodic flow over dikes, jetties, or bridge embankments or can be used to model water storage by salt water pannes in marshland.

External flow boundaries describe the inflow or outflow due to rivers, diversions, or sewage outfalls. Also, fine-grid sub-models of localized areas may require external flow boundaries along the sub-model's perimeter.

Artificial offshore tidal boundaries describe the ocean water level as a function of time. During non-storm conditions, for most tidal inlet-bay systems, the tidal function is the most significant excitation force. Consequently, accurate output from the model requires accurate hourly tidal forcing functions.

Similarly, artificial tidal-storage boundaries lie along the model's perimeter and require hourly input tidal elevations. These boundaries lie between back bays or in channels connecting bays and assist in providing the proper exchange of water throughout an inlet-bay system.

Inundation boundaries describe the flooding and draining of

cells as a consequence of tide-induced water level oscillations. If the water level in a cell is higher than the elevation of an adjoining cell, flow occurs, and the boundary is regarded as open water. If not, the boundary remains a water-land boundary and no flow occurs.

The HYDTID model uses a system of flags to facilitate the use of these boundary conditions. Cells are classified by the boundary conditions on their top and right sides. Masch et al. [21] originally defined 45 combinations of different boundary conditions [21] as shown in Figs. 2-2 and 2-3.

This study utilized four of the seven boundary condition types: water-land boundaries, overtopping barrier boundaries, artificial offshore tidal boundaries, and inundation boundaries. However, because the model's creators originally designed HYDTID to model Masonboro Inlet, a site with much less inundatable marshland than Great Sound, it seems possible that the model was not designed for extensive marshland areas. Even with the special boundary conditions provided by HYDTID, an expanse of inundatable marshland cannot be adequately modeled in this simulation. Hence, marshland inundation will be examined further in the next section.

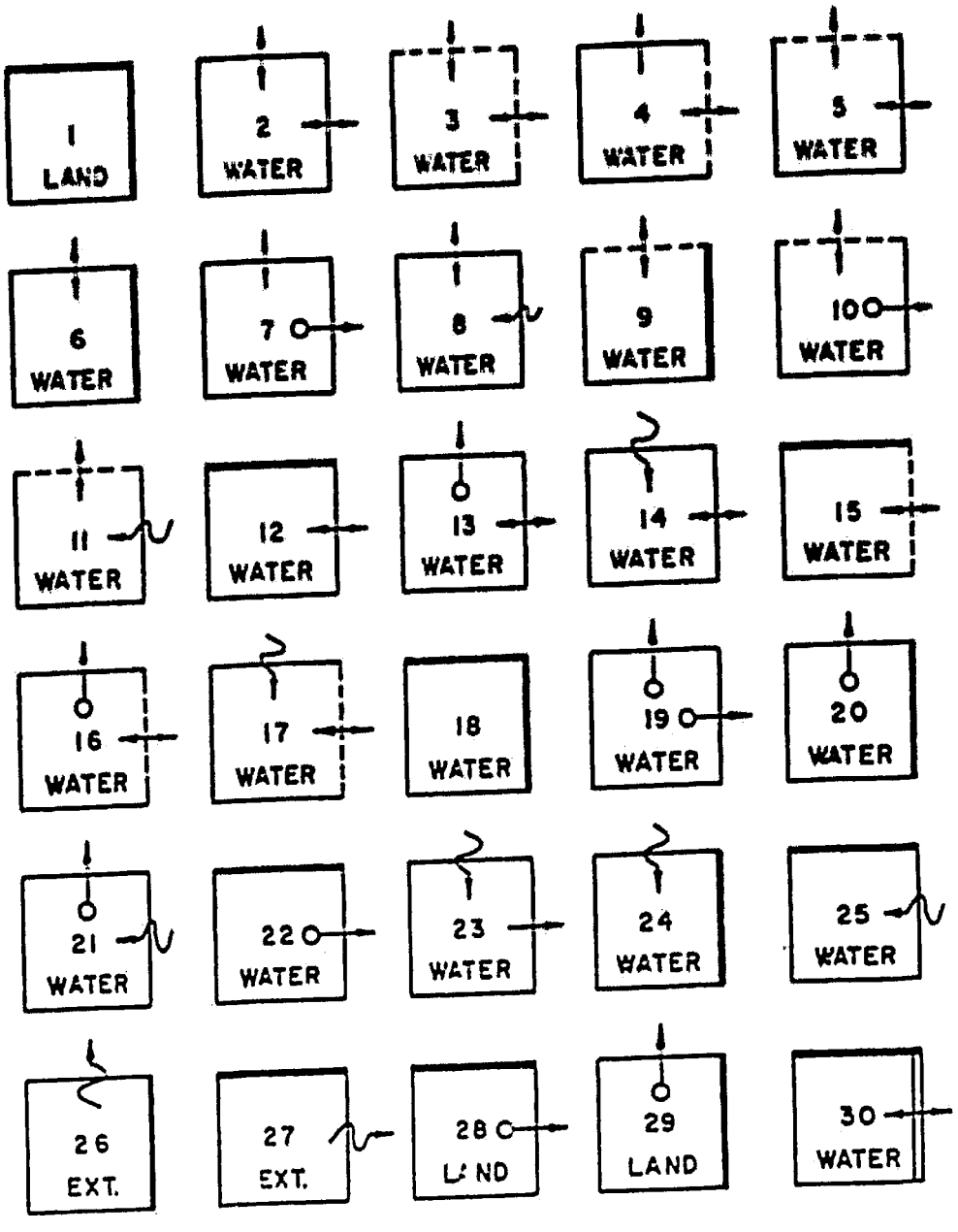

Figure 2-2: Cell Flags Defining Flow Boundary Conditions (after Masch et al. [21])

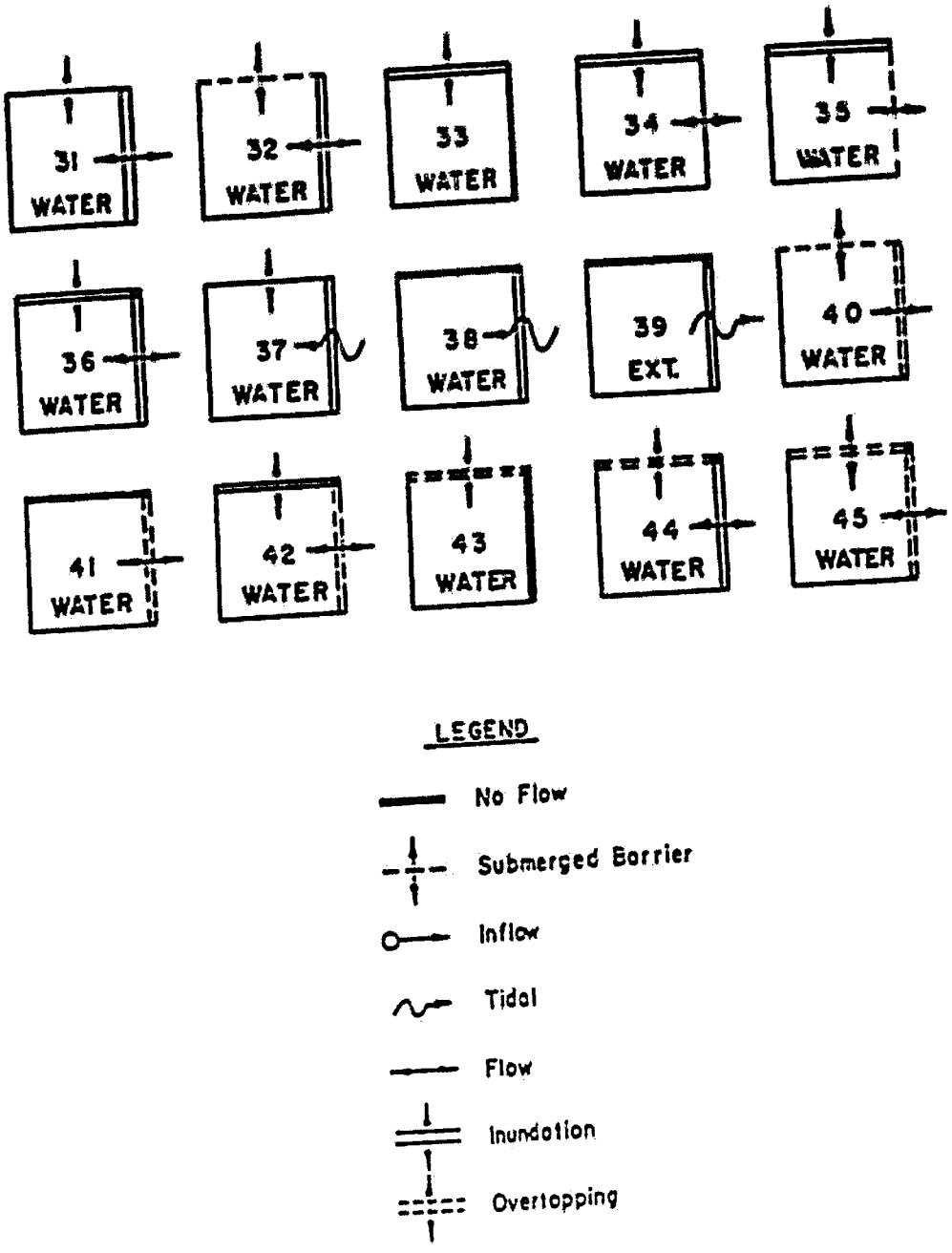

Figure 2-3: Cell Flags, Continued
(after Masch et al. [21])

2.3 Marshland Inundation

Of all the various boundary conditions, perhaps the marsh-water interface is the most important one for Great Sound. Specifically, the rise and fall of the tides cause an expanse of marshland to be cyclically inundated and drained. Few modeling efforts have attempted to simulate this extensive wetting-drying process. The U. S. Army Corps of Engineers Waterways Experiment Station (WES) developed a finite difference model with the capability of inundation simulation of low-lying terrain. This model, known as WIFM, has found application in delineating flood limits of tsunamis, as well as hindcasting surge and coastal flooding from hurricanes [4]. The WIFM model was also compared to HYDTID in simulating hydrodynamics at Masonboro Inlet, North Carolina [21], and was used to model Great Egg Harbor and Corson Inlets [5]. While these applications do not involve as large a flooded area as in Great Sound, these applications demonstrate that WIFM can model inundation. However, its ability to model the draining of large areas apparently remains untested [4].

Accurate values of roughness are necessary to adequately model marshland flow. Consequently, several studies have been done to determine the roughness due to flow through vegetation. Petryk and Basmajian [29] presented a flow model for unsubmerged vegetation conditions. The model was used to predict the variation of

Manning's n with depth given the vegetation density as a function of depth. Values for Manning's n were determined empirically for wheat and two kinds of sorghum by planting the crops in diversion terraces [31]. The roughness coefficient has also been estimated for Bermuda grass, waterplantain, pondweed, and floating mannagrass [19]. Free surface flow through marsh grass was studied by Burke and Stolzenbach from a fluid mechanics perspective [3]. The effort involved developing a numerical model to predict the vertical variation of a basically horizontal fluid flow through vertically oriented obstructions, such as vegetation. Their results are not readily applicable to hydrodynamic modeling efforts, because Burke and Stolzenbach's model used the drag coefficient C_D, whereas most hydrodynamic models use Manning's n.

Salt marshes are permeated by tidal creeks which meander and form a dendritic pattern [30]. This network of channels expedites the flooding and draining of the marsh. Because of the smallness of many of these channels, it is difficult to spatially represent each one without resorting to an excessively small cell size. Instead, one large channel that is one grid cell wide can represent several of the small, prototype channels in that vicinity. Consequently, the correct discharge is transferred in and out of the sound and is distributed in a realistic manner.

By defining the boundary conditions for each cell in the discretized study area, the model can be implemented as discussed in the next chapter.

3. MODEL IMPLEMENTATION

3.1 Implementation Procedure

To accurately portray a tidal inlet-bay system using HYDTID, a variety of physical characteristics must be provided as input. The following basic steps are required [21]:

1. Define the grid resolution, Δs, and choose a time step, Δt.
2. Determine the study area boundaries and overlay a mesh of cells on a hydrographic map of the area.
3. Obtain bathymetric and topographic data; calculate the average elevation for each grid cell.
4. Define the cell computation flag on the top and right boundary of the cell.
5. Identify convective acceleration flags (see App. I.1.)
6. Assign discharge coefficients and crest elevations to all submerged or overtopping barriers.
7. Determine Manning's n for each cell.
8. Collect necessary tidal elevations and discharge data for the selected calibration period.
9. Format the input data.
10. Operate the model for the selected simulation period.
11. Refine the model by varying friction values, barrier characteristics, cell elevations, feeder channel arrangement, and allocation of forcing cells until calibrated against observed water level and discharge data.
12. Perform production runs using the calibrated model. Simulate historical or hypothetical geometries.

3.2 Modeling Feeder Channels

The network of small feeder channels plays a prime role in the flooding and draining of Great Sound. Rather than flowing overland directly into the sound, most of the draining water empties by way of these channels. The role of feeder channels in draining was verified by test runs on an experimental grid using the HYDTID model. These tests revealed that if feeder channels are ignored when modeling an expanse of marshland, the marshland will require an unrealistically long time to drain, and computational difficulties occur [32].

Horton's ordering scheme is useful in describing stream systems [16]. In his method, fingertip or unbranched tributaries are classified as order 1. Streams which receive flow from first-order streams (but these only) are of order 2. A third order stream must receive one or more tributaries of the second and possibly first order, and so on. The main stream is of the highest order and defines the order of the drainage system.

Consequently, it can be seen that the Great Sound inlet-bay system is of order 5 with Hereford Inlet and Townsends Inlet of the highest order. Modeling channels that are narrower than one grid cell wide (streams of order 1, 2, and 3, that are less than 500 feet wide) was done using a single one-grid-cell wide channel to

represent several of the lower-order channels in that vicinity. The resulting network of channels is shown in Fig. 3-1.

Because the flows in these feeders channels were relatively small, it was decided to neglect the convective acceleration term for these channels. Hence, all convective acceleration flags for feeder channels were encoded as "22". A discussion of the convective acceleration term and its significance in the equations of motion is presented in Appendix I.1.

3.3 Bathymetry and Topography

The bathymetry for Great Sound was determined by Hall and Nadeau by repeatedly traversing the bay with a Si-Tex HE-356A Fathometer depth recorder [12]. The traverses, as well as beginning and ending traverse points, are shown in Fig. 3-2. From the depth recorder instrument, water depth at a point was found. The depth was converted to the bottom elevation at that location by subtracting the depth from the water surface elevation. Surface elevations were obtained from the National Oceanic and Atmospheric Administration (NOAA) Tide Tables [26] for the date and times the depth recorder data was taken. Although the NOAA surface elevations referred to one location in Great Sound, it was assumed that the elevations were valid for the entire region of the sound that was traversed.

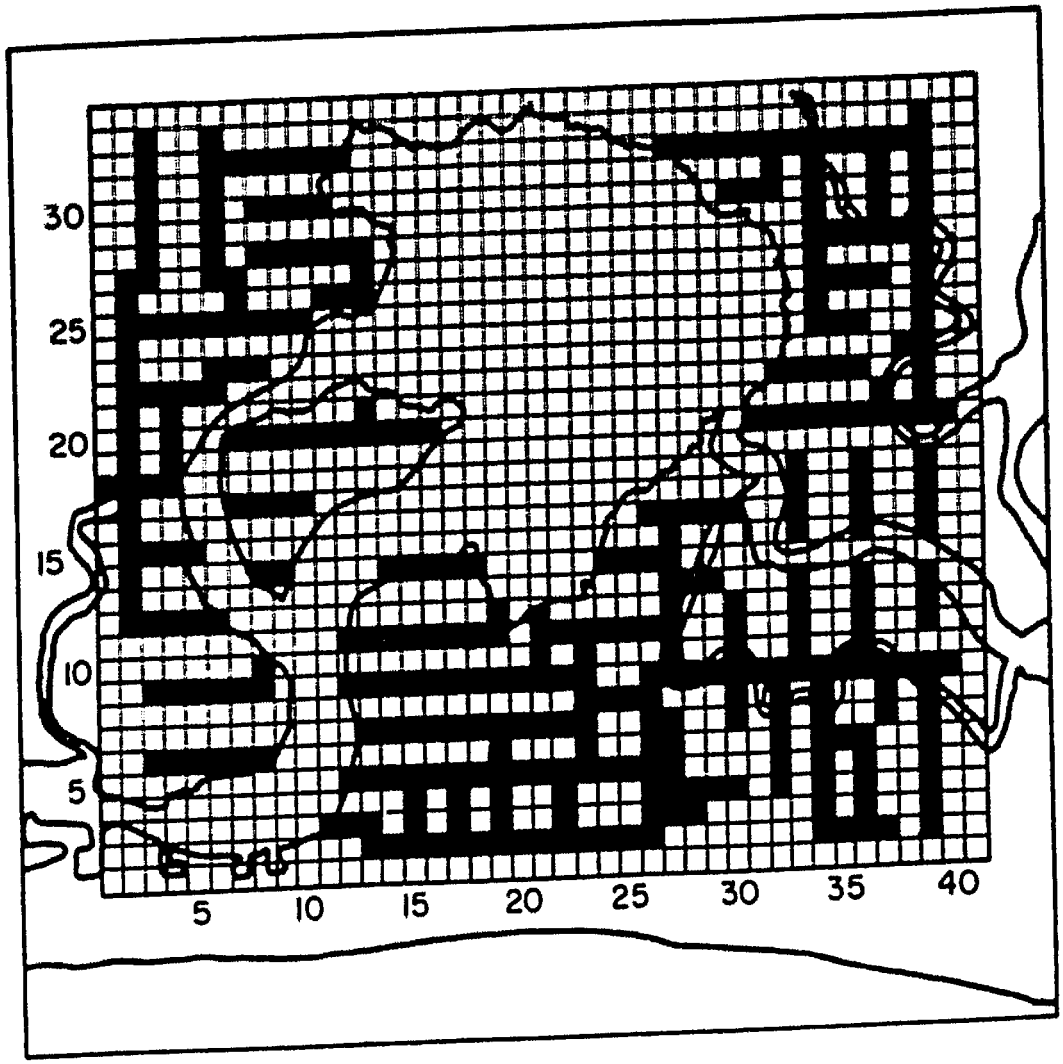

Figure 3-1: Feeder Channels in Great Sound

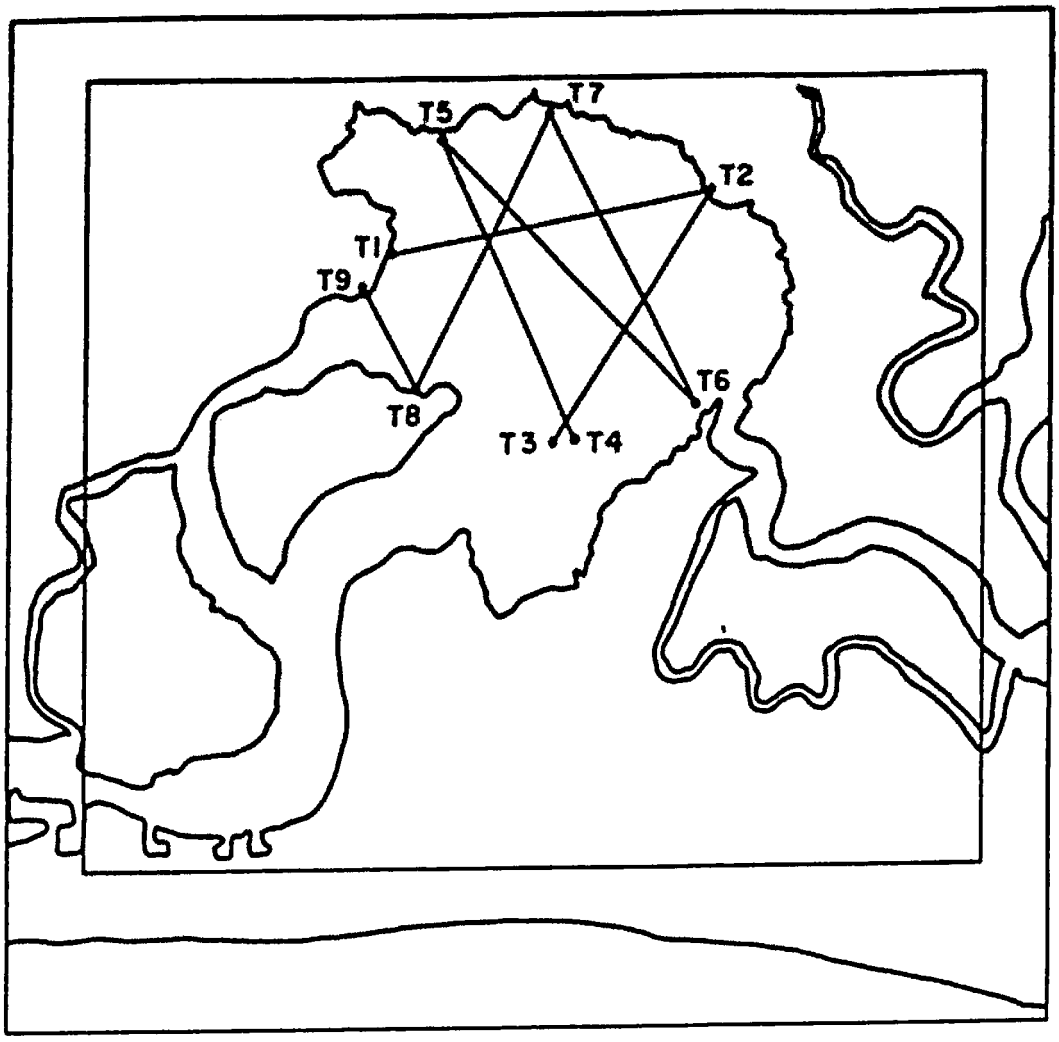

Figure 3-2: Bathymetric Traverses

The sound is quite shallow, with bottom elevations generally ranging from -0.76 m (-2.5 ft) to -0.15 m (-0.5 ft) Mean Low Water (MLW). The major exception is the Intracoastal Waterway, where bottom elevations are about -2.4 m (-8.0 ft) MLW. These bottom elevations were verified by comparison with NOAA's Nautical Chart of Great Sound and with USGS Quadrangles [24, 34, 35]. Bathymetry for Great Channel, Ingram Thorofare, and the feeder channels were obtained by surveying methods on three separate visits. These elevations were tied in to several USGS benchmarks [22].

Land elevations in the study area were determined by surveying methods and have little variation; although some upland (land greater than 1.68 m (5.5 ft) MLW) was found near Avalon and on Gull Island, most of the study area is inundated during spring high tide (elevation 1.52 m). Some intertidal mudflat elevations were also verified by bathymetry traverses since some of the traverses were taken near high tide when the boat could pass over mudflats.

3.4 Surface Roughness

Past applications of the HYDTID model used a set of linear equations to define Manning's n [21, 10]. These equations assumed n was directly proportional to elevation. This study included a field effort to collect discharge and water elevation data to determine the variation of Manning's n in Ingram Thorofare over a tidal cycle. From the one-dimensional equation of motion for unsteady non-uniform

flow [14] and using the Manning formula to define the friction slope:

$$n = 1.49\left(\frac{R^{4/3}}{V\cdot|V|}\left(\frac{\partial h}{\partial x} - \frac{V}{g}\frac{\partial V}{\partial x} - \frac{\partial V}{g\partial t}\right)\right)^{1/2} \qquad (2)$$

where R is the hydraulic radius, V is the velocity, and x is the horizontal direction. The discharge and water level data collected in May, 1984 were used to evaluate the right-hand side of Equation 2.

During ebb flow, Manning's n was calculated to be approximately 0.020 whereas during flood flow n was about 0.014 (see Fig. 3-3.) These results suggest that channel geometry rather than bedforms account for the variation of the roughness coefficient. Since flood flow tends to determine the orientation of the bedforms, one would expect higher Manning's n values during flood tide than during ebb tide. Because the reverse is true, it can be surmised that bedforms are not dominant in determining the roughness coefficient along Ingram Thorofare.

These results indicate that n is dependent on flow direction and only slightly dependent on elevation. Therefore, instead of using the linear equations relating n to z, the Manning's n values determined along Ingram Thorofare were used for Great Sound, Great Channel, and the feeder channels. Although bedforms and geometry

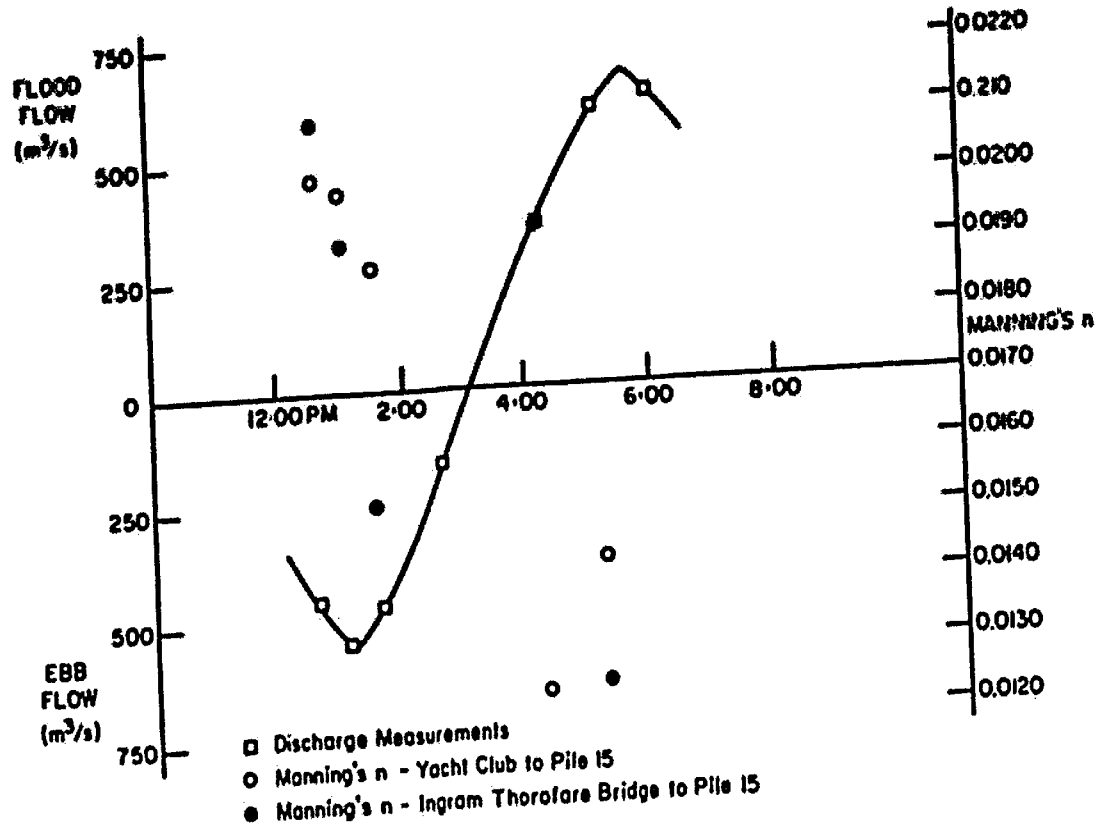

Figure 3-3: Variation in Manning's n for a Tidal Cycle, Spring Tide, May 31, 1984.

vary somewhat throughout the sound, it was felt that the roughness coefficients determined for Ingram Thorofare were more accurate than the linear equations relating n to elevation.

3.5 Tidal Data

Observed water levels at model boundaries were used as forcing functions. The model was calibrated against observed water levels in Great Sound and observed flows through the model boundaries.

Observed water level data were obtained at Ingram Thorofare Bridge, Great Channel Bridge, and Reuben's Wharf in Great Sound during both neap and spring tide events. The field water level data at Ingram Thorofare Bridge was used to excite the model at Ingram, Leonard, and Gravens Thorofares, and the collected water level data at Great Channel Bridge was used to excite the model at Great Channel Bridge and Scotch Bonnet (see Figs. 3-4 and 3-5). Water level data were collected both manually and with Leupold Stevens Type F and Type A water level recorders. Some portions of Fig. 3-5 were interpolated due to occasional malfunctioning of the recorders. From these observed data and data collected by the National Ocean Survey (NOS) [23], it can be seen that water levels in Great Sound approximate but do not reproduce a sinusoidal wave. Also, at several times the peak water levels at Reuben's Wharf equal or exceed those for Great Channel. This anomaly is verified by NOS data for neap and spring tidal cycles. Such a phenomena, where the

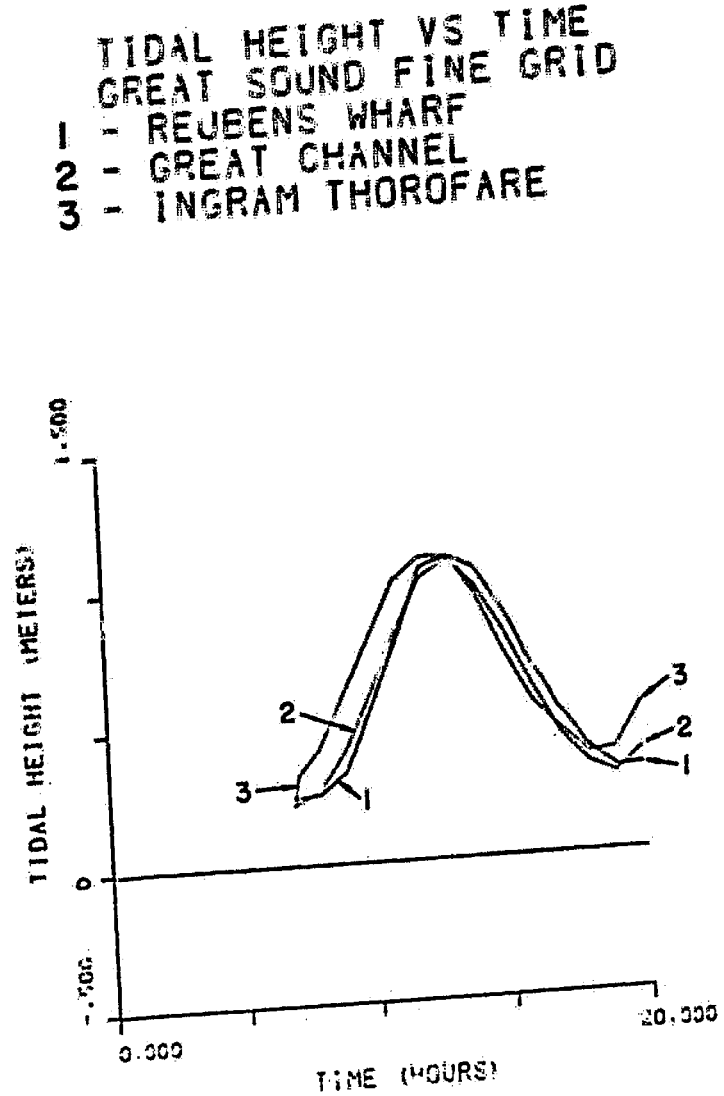

Figure 3-4: Neap Tide Water Level Measurements, June 1, 1983.

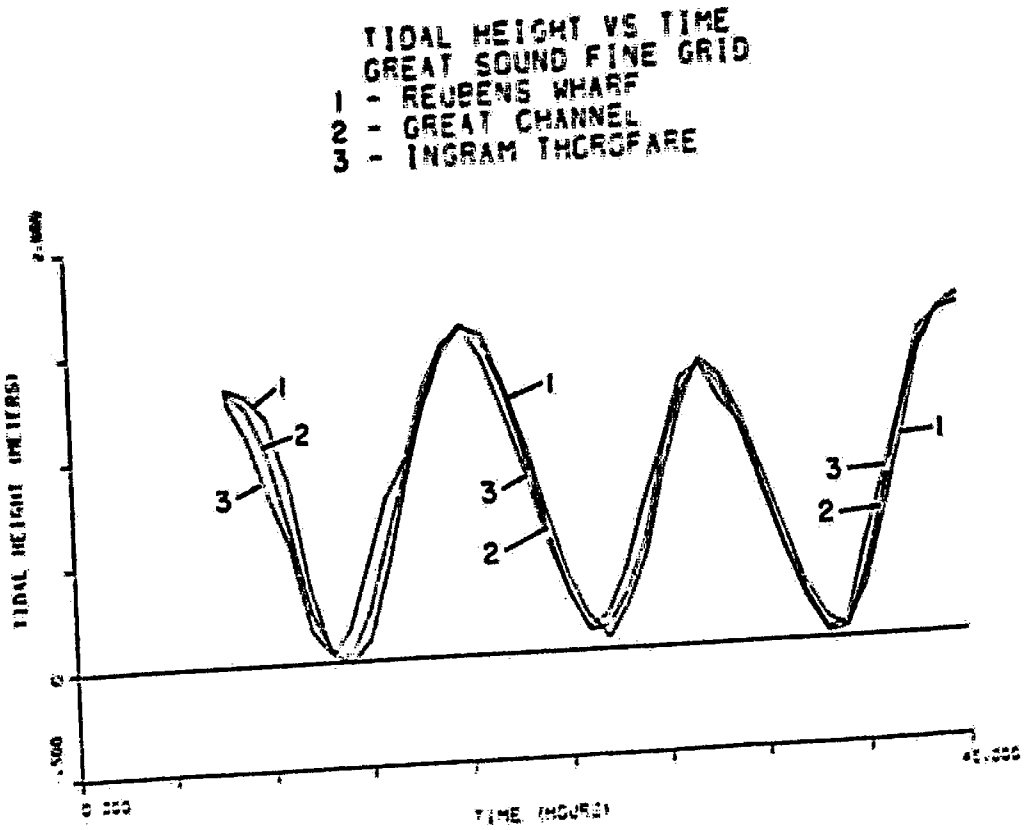

Figure 3-5: Spring Tide Water Level Measurements, May 24-25, 1983.

tidal range of the bay is greater than that of the adjoining channel, may be due to resonance or wind setup.

Discharge measurements and supplementary velocity profiles were taken in the two channels feeding Great Sound at various times in the tidal cycles. For each discharge measurement, the cross section was divided into several sections. In the center of each section, the depth and the velocity at sixth-tenths of the depth were determined. For an assumed logarithmic profile, six-tenths of the depth is the average velocity. Then, total discharge was calculated as the summation of the product of the cross-sectional area and average velocity for all of the sections. It should be emphasized that these measurements were time-averaged since a discharge measurement typically required about thirty minutes to perform.

Velocity profiles were taken to determine the vertical velocity distribution. Of the ten velocity profiles taken, six were not logarithmic over the upper half of the depth resulting in an estimated error of $\pm 20\%$ in the discharge measurements. Samples of observed logarithmic and non-logarithmic velocity profiles are shown in Figs. 3-6 and 3-7, respectively.

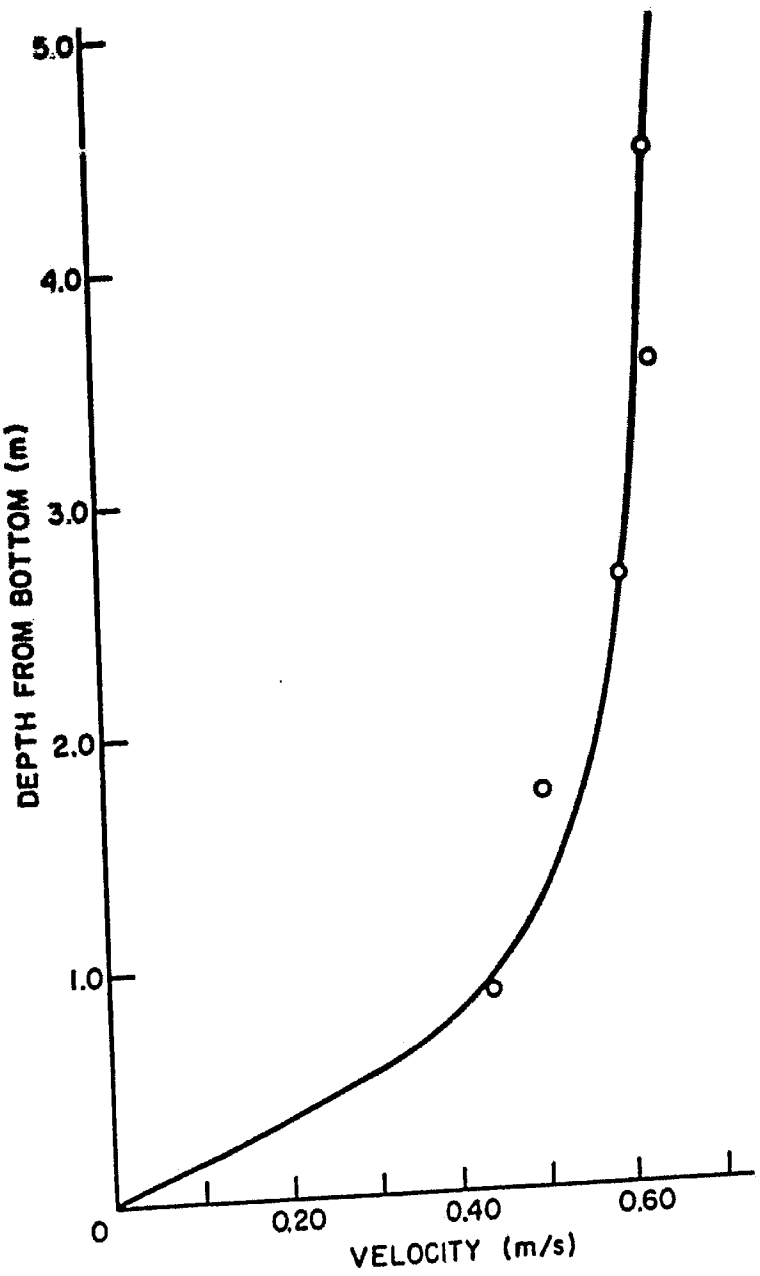

Figure 3-6: Velocity Profile at Ingram Thorofare, 9:10 to 9:30 am, May 24, 1983.

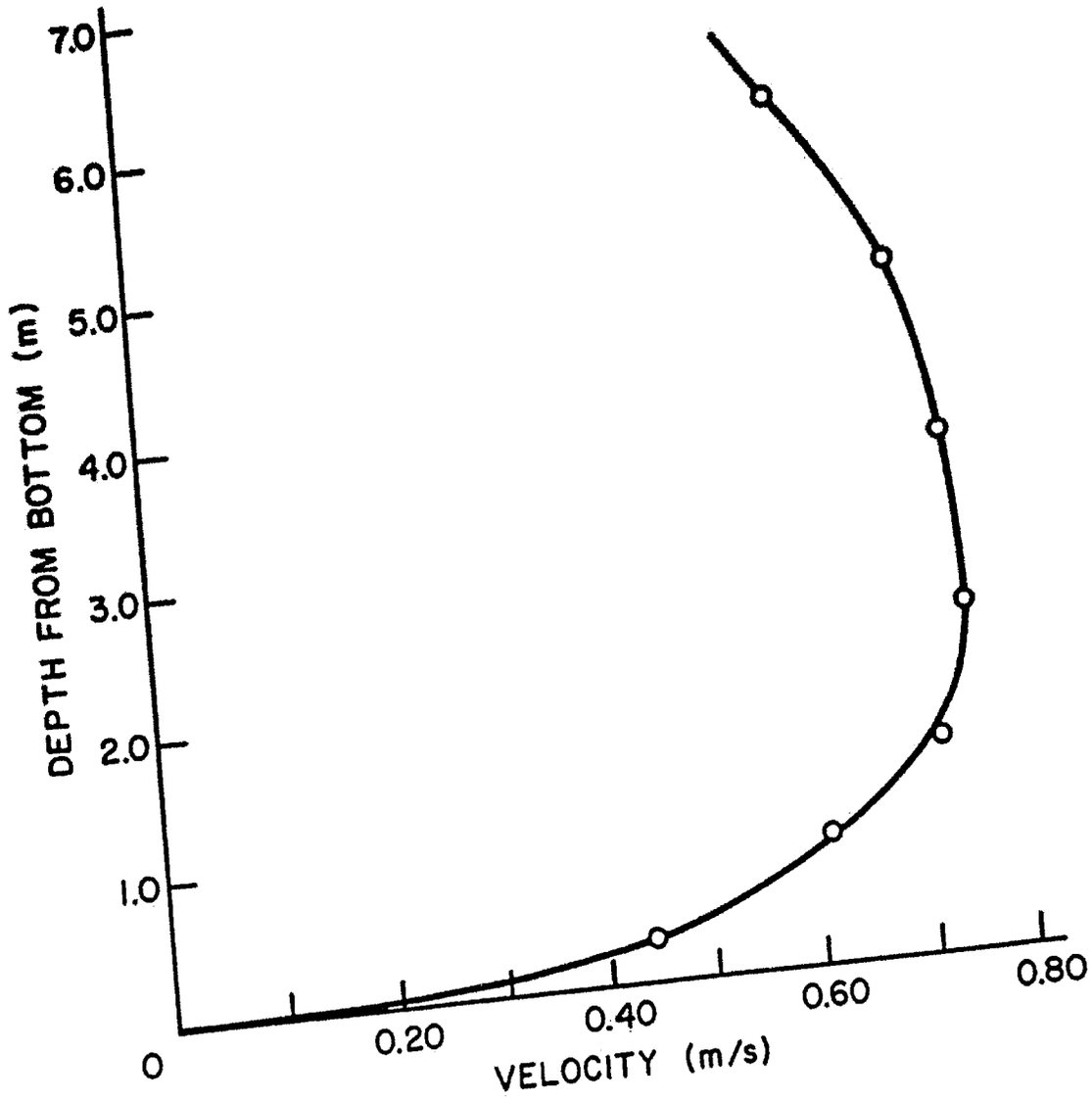

Figure 3-7: Velocity Profile at Ingram Thorofare, 5:27 to 5:34 pm, May 24, 1983.

3.6 Startup Technique

An initial, transient fluctuation may be caused by the incompatability between initial fluctuations and the forcing function [1]. The resulting erratic solution for discharges and elevations may persist for one or more tidal cycles. One way to manage initial transients is to allocate an initial interval of modeling time until the transients are dissipated by bottom friction. In shallow water, a single tidal cycle is considered to be sufficient [1, 10]. As an alternative, Gabriel et al. [10] began the simulation at a local low tide, filled water cells to the low water depth, set flows to zero, and used the data as the initial hydrodynamics.

Test runs with and without a startup interval revealed that the absence of a startup period did not significantly affect the elevations and discharges. Furthermore, for runs lacking the startup period no significant initial fluctuations in either water levels or flows were observed. Thus, for this effort it was decided to forego the use of startup intervals in order to economize on computer resources.

3.7 Remaining Inputs

Additional inputs to the HYDTID model include cell computation flags, convective acceleration flags, and wind, precipitation, and evaporation data.

Cell computation flags were assigned by matching the cell's top and right sides with one of the combinations in Figs. 2-2 and 2-3. Cells in marshland or intertidal mudflats were encoded as inundation cells to allow for flooding and draining throughout the tidal cycle. Forcing cells were defined by an offshore tidal boundary oriented towards the channel being forced; the remaining three sides of the forcing cell were made impermeable by using water-land boundaries. To insure computational stability, cells in the top row and right column of the grid were defined as land cells by using impermeable boundaries.

Convective acceleration flags were determined by classifying each cell side as "flow" or "non-flow". Then each cell was matched with one of the flow conditions in Fig. 3-8 and a flag number was assigned. For computational reasons, forcing cells must be considered closed cells and encoded as convective flag 22. Measures were taken to verify that the convective flags were consistent with cell computation flags (see Section 3.8). To attain consistency between computation and convective flags, cells representing

FLAG	REMARKS	FLOW CONDITION			
		TOP	BOTTOM	R SIDE	L SIDE
11		FLOW	FLOW	FLOW	FLOW
12		FLOW	FLOW	NO FLOW	NO FLOW
13		FLOW	FLOW	FLOW	NO FLOW
14		FLOW	FLOW	NO FLOW	FLOW
21		NO FLOW	NO FLOW	FLOW	FLOW
22		NO FLOW	NO FLOW	NO FLOW	NO FLOW
23		NO FLOW	NO FLOW	FLOW	NO FLOW
24		NO FLOW	NO FLOW	NO FLOW	FLOW
31		FLOW	NO FLOW	FLOW	FLOW
32		FLOW	NO FLOW	NO FLOW	NO FLOW
33		FLOW	NO FLOW	FLOW	NO FLOW
34		FLOW	NO FLOW	NO FLOW	FLOW
41		NO FLOW	FLOW	FLOW	FLOW
42		NO FLOW	FLOW	NO FLOW	NO FLOW
43		NO FLOW	FLOW	FLOW	NO FLOW
44		NO FLOW	FLOW	NO FLOW	FLOW

Figure 3-8: Convective Flagging Combinations (after Gabriel et al. [10])

mudflats or marshland were considered to be impermeable with respect to convective flags. These cells were accordingly defined as convective flag 22.

Wind, precipitation, and evaporation can be accounted for in the HYDTID model. During the data collection effort, these factors were negligible and were not included in the simulation. Experimental test runs including wind, precipitation, and evaporation were performed and insured these factors were negligible.

First, a simulation run was performed for a precipitation rate of 59.2 mm (2.33 in) per day on a small test grid. Compared to a similar run without precipitation, hourly water elevations varied by 4.1 mm (0.16 in) or less. When an evaporation rate of 6.4 mm/day (0.25 in/day) was used, hourly water elevations varied by no greater than 0.3 mm (0.012 in). To examine the effect of wind on hydrodynamics, a two-hour simulation was run on the Great Sound grid using a 24.1 km/hr (15.0 mph) west wind. Hourly elevations at Reuben's Wharf in Great Sound varied by 14.0 mm (0.55 in) or less compared to a similar run without wind. It is concluded that the effect of natural forces of the magnitudes tested is small and can be ignored.

Similarly, fresh-water inflow can be included in HYDRID. However, in the case of Great Sound such inflow was relatively small and was neglected.

After all of the inputs described in this chapter were prepared, calibration runs were undertaken. Accurate simulation of flows and water elevations were obtained by adjusting certain model parameters within realistic limits. These parameters include secondary channel arrangement, friction, marsh cell elevations and forcing cell distribution.

3.8 Test Runs

Before the model calibration was begun, several simple test cases were run in order to flush out errors in cell coding or other problems. These test runs included a zero test, a one-foot test, and a six-foot test.

In the zero test, zero-meter heights were assigned to the forcing cells for one time step. If all cells are properly coded, no flows should occur. By checking the ending hydrodynamics, miscoded cells were easily found by locating non-zero flows.

After any coding inconsistencies were corrected, a one-foot test was run. In this test all forcing cells are initialized at 0.0 m (0.0 ft) and raised to 0.30 m (1.0 ft), and held at that level for

one hour of simulation time (see Fig. 3-9.) This test verified that mudflat cells were properly inundated. To avoid instabilities during flooding, adjacent inundatable cells were always assigned different elevations.

In the six-foot test, forcing cells were raised from zero meters (0.0 ft) to 1.8 m (6.0 ft), held there for several hours, and reduced to zero meters. This test gauged the responsiveness of the grid to changes in forcing cell height, s. Also, the ability of the model to perform inundation and draining of an expanse of marshland was checked.

By using the six-foot test, unanticipated problems were discovered and solved. For example, an early grid configuration made no provision for feeder channels. During the six-foot test, marsh cells did not drain for many hours, and it became evident that feeder channels are important in draining the sound.

Another problem encountered was the occasional presence of "whirlpools", vortices caused by a computational anomaly. Possible direct causes of whirlpools which seem to correlate with whirlpool formation are: marsh/channel boundaries, adjacent water cells of markedly different depths, and grid configurations where water depths approach the maximum depth permitted by stability and

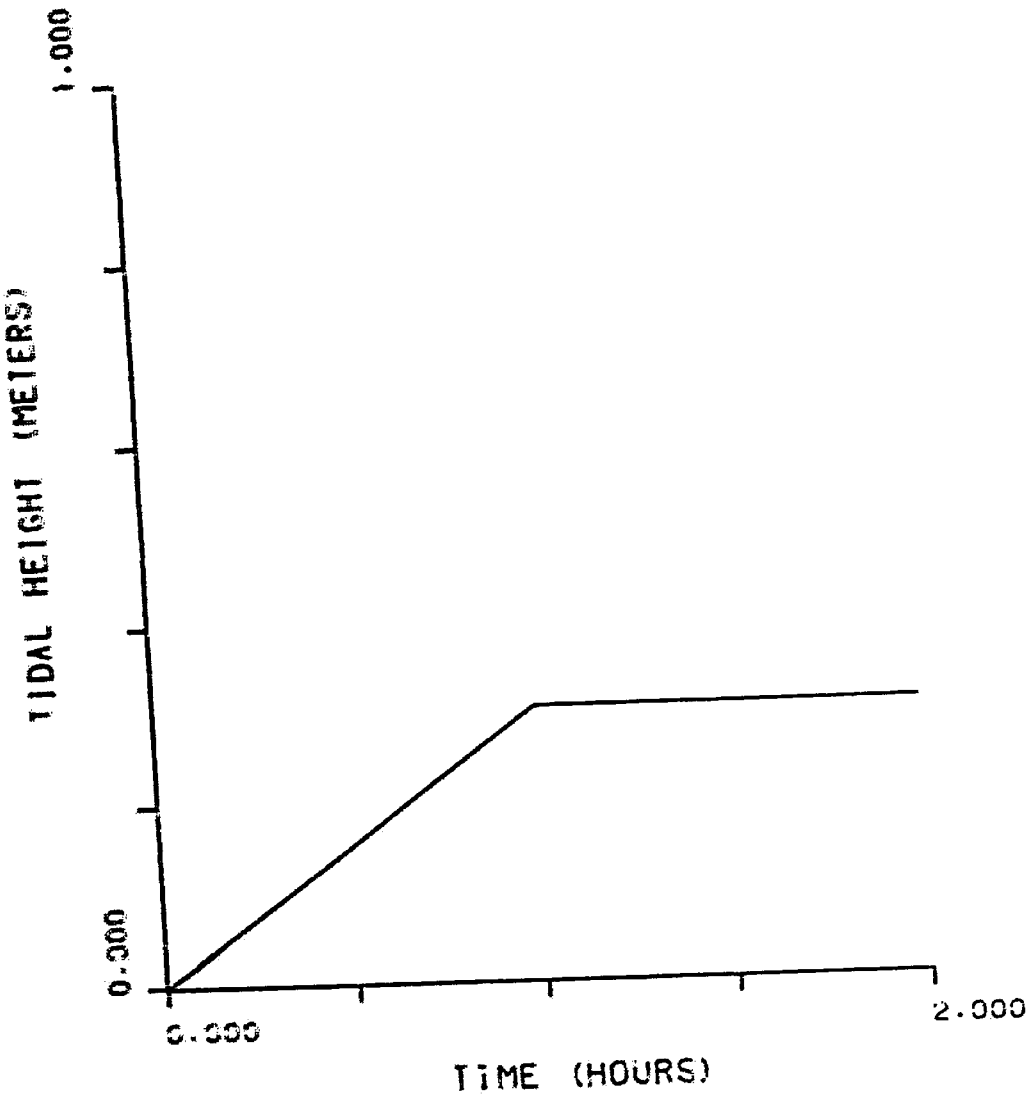

Figure 3-9: Forcing Function for the One-Foot Test

convergence criteria. Whirlpools were removed by adjustment of marsh and water cell elevations and by placement of impermeable barriers.

For the six-foot test, a water budget showed that the difference between the flood and ebb tidal prism was 4%. Ideally, this difference would be 0% and can be partially attributed to roundoff error in the computations.

3.9 Method of Presentation of the Results

The HYDTID program provides both flows and water elevations for twenty selected grid cells. Plots of observed and computed tidal elevations for these twenty cells can be obtained. Net flows and velocities may also be obtained.

However, a more sophisticated method was needed to conveniently present the voluminous amount of output data. Consequently Gabriel et al. [10] developed a graphical postprocessor to draw a picture of the overall flow pattern at any point in time using the instantaneous hydrodynamics (tidal heights and flows). In this study, instantaneous hydrodynamics were saved at ten-minute intervals.

The x flow on the right side of the cell and the y flow on the cell's top is plotted for each water cell. Each flow is signified

by an arrow scaled to represent the flow's magnitude. Forcing cells, impermeable boundaries, and dry cells (land or marshy area) are all indicated by special symbols defined in a legend included with the flow map. The moment in time the flow map represents and the scale of the flow vectors are also specified.

Instantaneous hydrodynamics were also used in plotting the temporal variation of flow rate, volume, and tidal height at selected locations.

4. RESULTS

4.1 Calibration for Spring Tide - Lehigh Data, May 24-25, 1983

To develop a model with a predictive capability specific to Great Sound, HYDTID was first calibrated for the spring tide event occurring on May 24 and 25, 1983. A grid overlay of 34 rows by 41 columns was used to discretize the study area (see Fig. 4-1). This calibration run was the most rigorous application of the model since most of the area is inundated and drained by spring tide. Also, in Great Sound the spring tide has a range of about 1.5 m (5.0 ft), the largest tidal range in the lunar cycle.

The model was calibrated against observed water levels at Reuben's Wharf in Great Sound and observed flows through Great Channel and Ingram Thorofare. The observed and computed tidal heights show satisfactory agreement despite a discernible phase lag of approximately 20 minutes throughout the two-day period (see Fig. 4-2). At the high and low extremes, calculated heights varied from observed heights by no more than 9.1 cm (0.3 ft). These disparities can be attributed to the nature of the observed water level data. At the high peaks, these data depict the water level in Great Sound as equaling or exceeding the water levels at Great Channel and Ingram Thorofare for the same time. Conversely, at the low peaks Great Sound water levels are lower than the water levels in the channels.

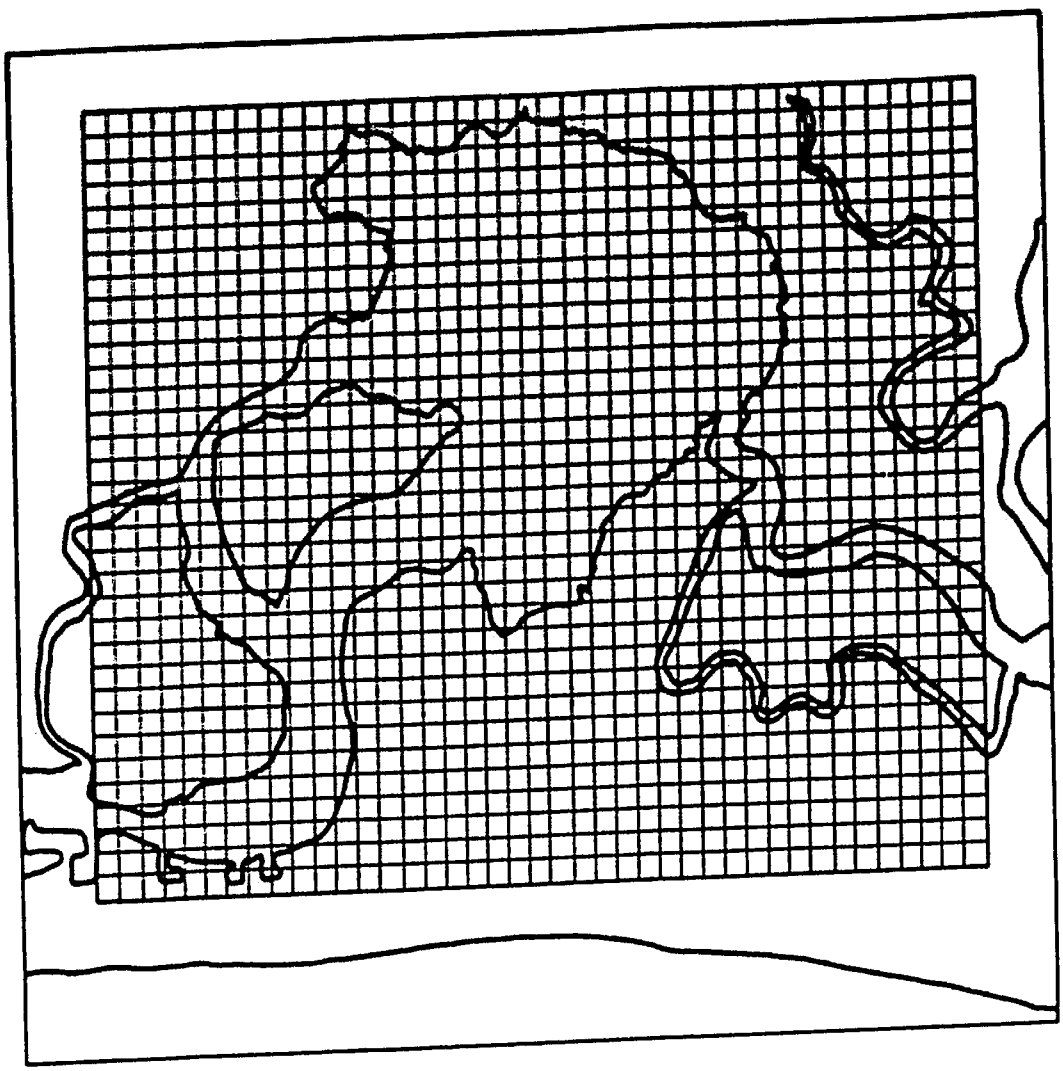

Figure 4-1: Great Sound Grid

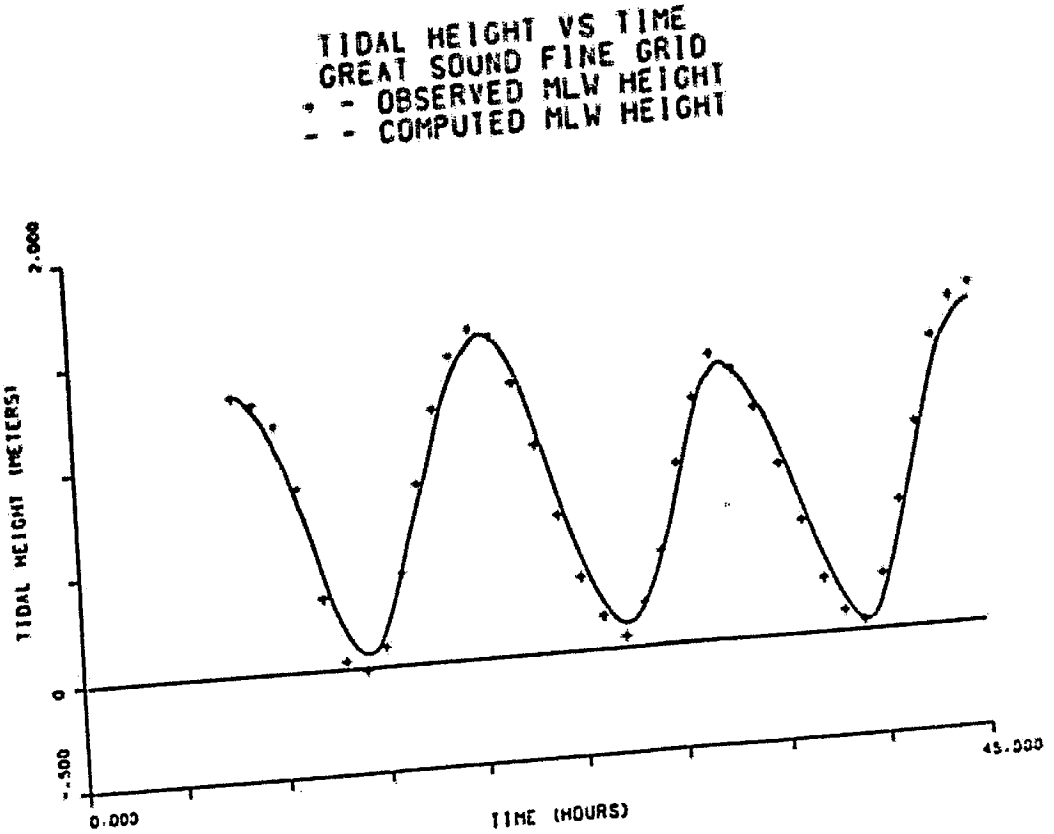

Figure 4-2: Tidal Height Versus Time - Spring Calibration

This phenomenon is also seen in data obtained by NOS [23] for other spring tide events. As mentioned in Section 3.5, such an anomaly may be due to resonance or wind. In any case, the HYDTID model will not predict such tidal behavior.

As shown in Figs. 4-3 and 4-4, flows in Great Channel and Ingram Thorofare were also predicted. For the most part, computed flows agree reasonably well with observed values at the field data stations. Discrepancies between observed and computed flows are partially introduced by the flow-measuring procedure. Specifically, these inaccuracies include:

1. Cable measurement of depths. The flow tends to push the cable downstream so that it curves instead of hanging vertically. Depths could not be corrected because corrections available in the literature [7] were not always appropriate for the computed discharges. Consequently, soundings with the cable and weight overestimated true depths, especially at high flows.

2. Non-logarithmic velocity profiles. Since the assumption of logarithmic velocity profiles was often invalid, inaccuracies were introduced in the flow measurement calculations.

3. Division of the cross-section into a limited number of subsections. Also, only one sounding was taken for each subsection.

Also, computed flows were highly sensitive to small errors in forcing functions. During the calibration process, it was found that flows in the channels were quite sensitive to the relative

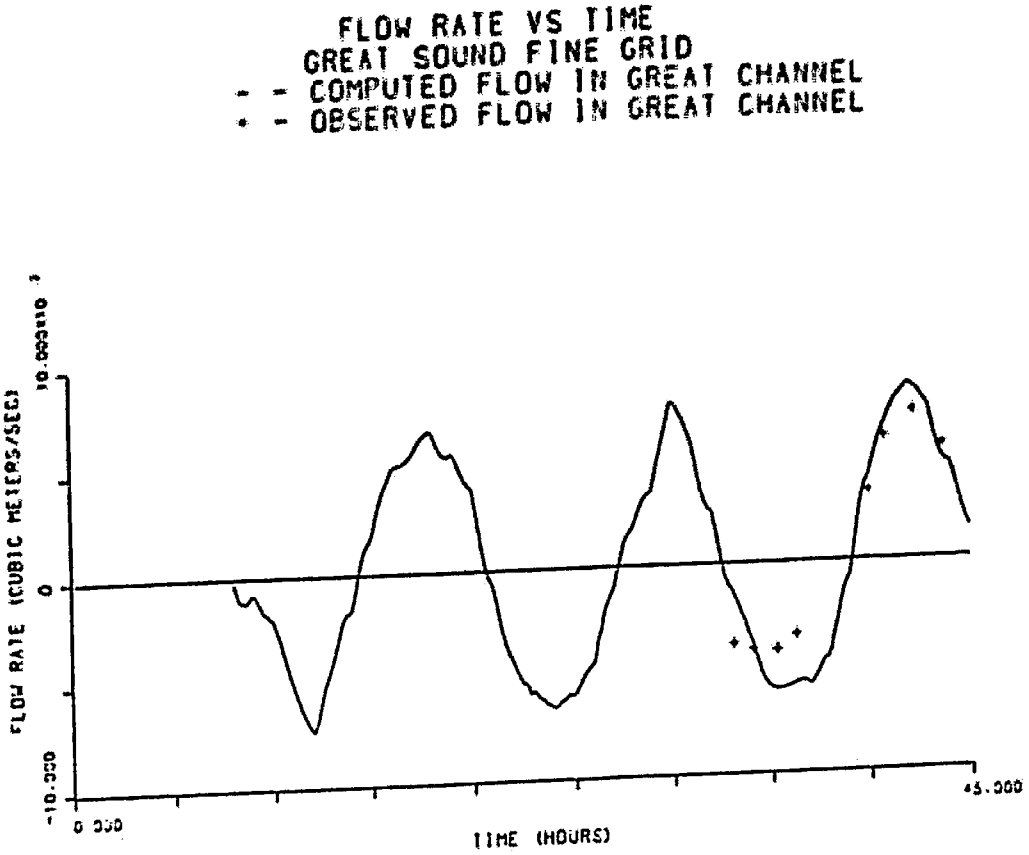

Figure 4-3: Flow Rate Versus Time in Great Channel - Spring Calibration

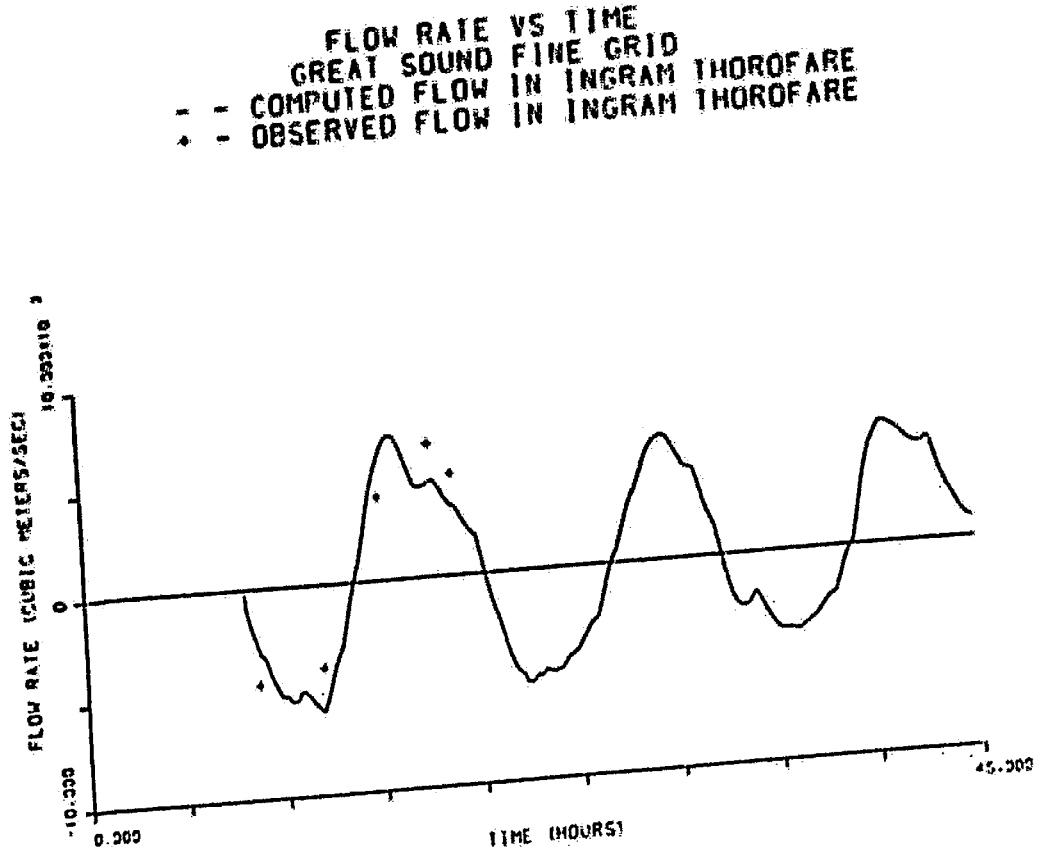

Figure 4-4: Flow Rate Versus Time in Ingram Thorofare - Spring Calibration

strengths of "driving head" (the difference in water levels between the forcing cell and Great Sound) for the two main channels. For instance, when the driving head at Ingram Thorofare was much stronger than that at Great Channel, large flows passed through Ingram Thorofare and smaller flows through Great Channel. Hence, small errors in observed water levels tended to produce large fluctuations in flows.

A plot of cumulative volume versus time yields useful information regarding the water budget. The cumulative volumes for Townsends Inlet (the channel into which Ingram, Gravens, and Leonard Thorofare drain), for Great Channel (including flow from Scotch Bonnet), and for the entire study area are shown in Fig. 4-5. The cumulative volume should equal zero at each time when the elevations in the sound are the same as at startup. This is indeed the case for spring calibration: at times of 18.7, 22.3, and 43.2 hours, cumulative volume equals zero. At these times, elevations in Great Sound approximately equal the initial water elevations, showing that the model is accurate in calculating flowrates.

The tidal prism for an ebb or flood tide equals the volume at the beginning minus the volume at the end of the tide. For instance, for Great Channel during spring tide calibration at 8.00 hours the cumulative volume is 0.0 m^3 (0.0 ft^3) and at 14.00 hours the

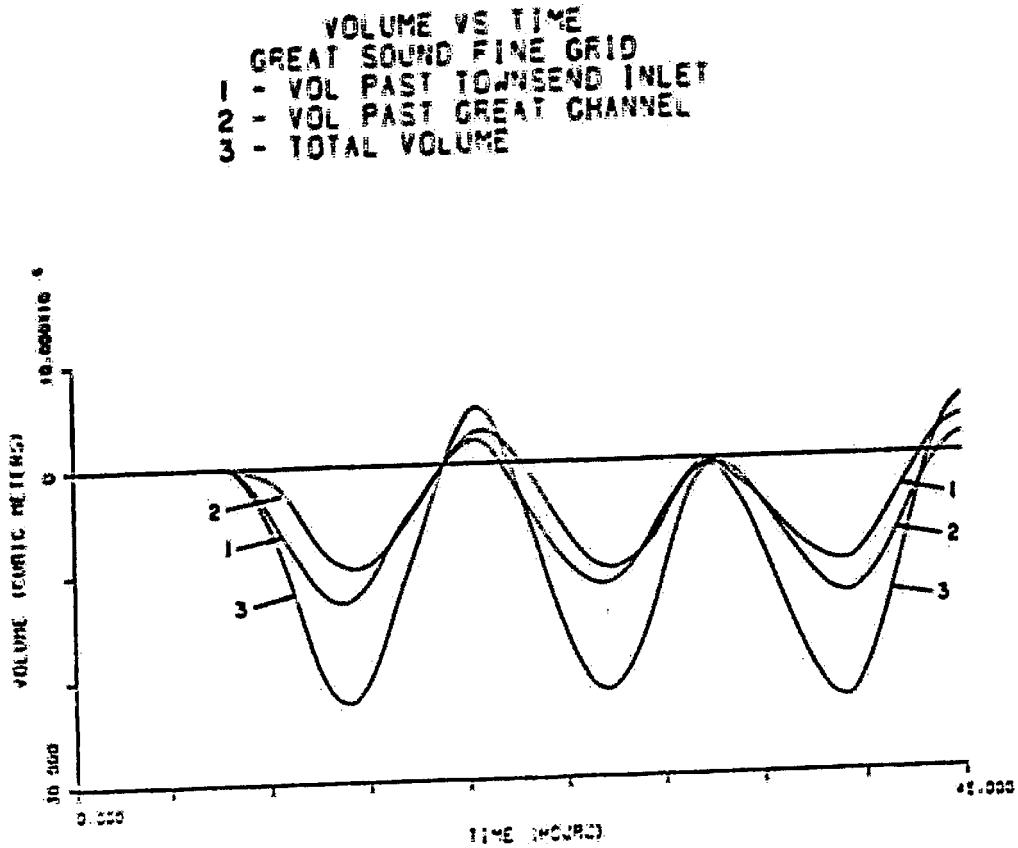

Figure 4-5: Cumulative Volume Versus Time - Spring Calibration

cumulative volume is 9.90×10^6 m^3 (34.97×10^7 ft^3). Therefore, the flood tidal prism is 9.90×10^6 m^3 (34.97×10^7 ft^3). Tidal prisms calculated from Fig. 4-5 are shown in Tables 4-1 and 4-2 for Great Channel and Ingram Thorofare, respectively.

There is no clearly discernible flow through Great Sound; the cumulative volume curves for Townsends Inlet and Great Channel cross repeatedly, indicating that there is no consistent net flow-through in one direction.

Hourly flow maps for spring tide calibration are presented in Appendix I.2. At 0800 hours, May 24, 1983, the simulation is beginning and flows are zero throughout the sound. From 0900 hours to 1300 hours, water is exiting the sound. As expected, most of the flow passes through Great Channel and Ingram Thorofare. The magnitude of flows through Scotch Bonnet, Leonard Thorofare, and Gravens Thorofare is smaller: about 25% of the total flow passes through these three channels. Flows in channels of order 1 and 2 are even smaller, and the arrows representing flows in these channels can be seen only as dots.

At 1400 hours, the tide is beginning to turn, and water begins to enter the sound via Ingram Thorofare. Because the driving head at Great Channel is weaker (lower) than the head at Ingram

Ebb/Flood	Start Time	Tidal Prism	
		(m^3)	(ft^3)
E	0800	9.90×10^6	34.97×10^7
F	1400	1.31×10^7	46.15×10^7
E	2030	1.35×10^7	47.60×10^7
F	2730	9.62×10^6	33.96×10^7
E	3230	1.40×10^7	49.35×10^7
F	3900	1.61×10^7	56.90×10^7

Table 4-1: Tidal Prisms for Great Channel - Spring Calibration

Ebb/Flood	Start Time	Tidal Prism	
		(m^3)	(ft^3)
E	0800	1.32×10^7	46.57×10^7
F	1400	1.53×10^7	54.04×10^7
E	2100	1.38×10^7	48.83×10^7
F	2700	1.15×10^7	40.78×10^7
E	3200	9.90×10^6	34.97×10^7
F	3900	1.38×10^7	48.77×10^7

Table 4-2: Tidal Prisms for Townsends Inlet - Spring Calibration

Thorofare, water is still flowing out through Great Channel. An hour later, flow through Great Channel has reversed direction, although the strong driving head at Ingram Thorofare still has primary influence over most of the sound. At this time, the nodal point (at which the net flow is zero) is between Gull and Sturgeon Islands. The nodal point occurs because the two main channels are in opposition.

Between 1600 hours and 2000 hours, the sound continues to fill. As the driving head at Great Channel increases, the nodal point gradually moves to the northeast along the Intracoastal Waterway. As the water level rises, the inundation cells are flooded and become water cells. Between 2000 hours and 2100 hours, the higher high tide in the semi-diurnal cycle has been reached, and the entire sound is submerged except for part of Gull Island.

From 2100 hours, May 24, until 0300 hours, May 25, the sound is draining. Marsh cells reappear as they become dry.

For the remainder of the simulation, from 0400 hours to 0800 hours, the sound fills and drains in a similar manner. Generally, Ingram Thorofare dominates the filling of the sound compared to Great Channel. After a few hours of inundation, Great Channel attains approximate parity with Ingram Thorofare in terms of filling

Great Sound.

4.2 Calibration for Neap Tide - Lehigh Data, June 1, 1983

In order to predict the hydrodynamics for two considerably different events in the lunar cycle, HYDTID was also calibrated for neap tide conditions. As with spring tide, the computed and observed neap tide elevations at Reuben's Wharf were in close agreement, never varying by more than 9.1 cm (0.3 ft). However, the observed forcing function data for Great Channel was questionable for two reasons.

First, on plots of water elevation versus time, water levels for Great Channel almost always appear between the levels for Ingram Thorofare and Great Sound. This characteristic exists in all available data, including neap, mean, and spring tide, for NOS data as well as for 1983 Lehigh data. Great Channel is usually not as strong a forcing function as Ingram Thorofare yet still definitely excites the water levels in Great Sound. However, the rising limb of Great Channel for neap tide (see Fig. 3-4) violates this pattern. Instead of lying between the water level curves for Ingram Thorofare and Great Sound, the Great Channel curve is almost coincident with the Great Sound curve.

Second, computed discharges during the flood tide for Great Channel do not agree well with the observed discharges (see Fig.

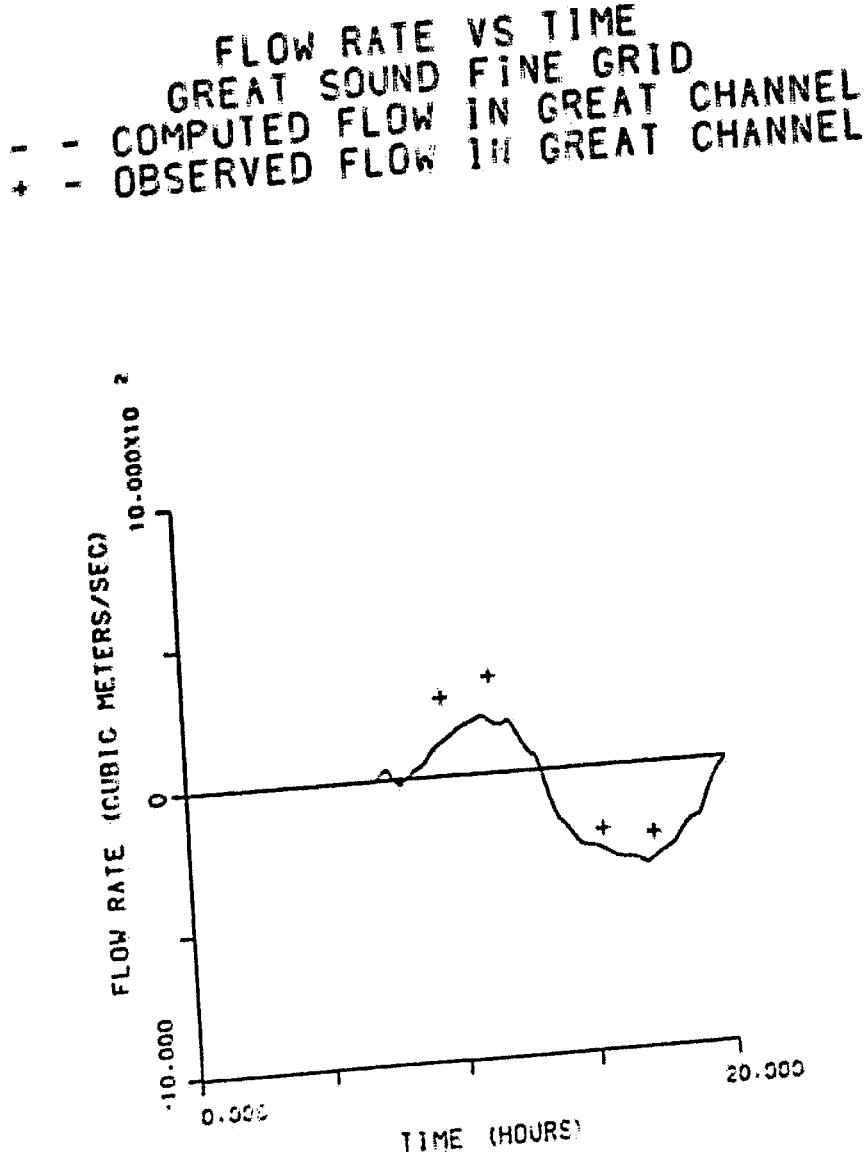

Figure 4-6: Flow Rate Versus Time in Great Channel - Neap Calibration, First Attempt

4-6.) This disparity is most evident at approximately 7:45 a.m., when flows become negative, an occurence not supported by observed data. Also, the plot of cumulative volume versus time (Fig. 4-7) shows a relatively small influx through Great Channel as compared to Townsend Inlet.

For these two reasons, it was believed that the collected data for the rising limb (flood tide) of Great Channel were erroneous. Hence, this forcing function was shifted forward by 15 minutes. This shift effectively alleviated the two problems described above: the water level curve for Great Channel was moved to between the curves for Ingram Thorofare and Great Sound, and computed and observed flows through Great Channel agreed more closely (see Fig. 4-8). Computed discharges through Ingram Thorofare (Fig. 4-9) and elevations at Reuben's Wharf (Fig. 4-10) were also in good agreement with observed values.

Tidal prisms for neap tide were computed in a manner similar to spring tide from a plot of cumulative volume versus time (see Fig. 4-11). Tidal prisms for Great Channel were 5.5×10^7 m^3 (18.0×10^7 $ft.^3$) for flood tide and 8.2×10^7 m^3 (26.85×10^7 ft^3) for ebb tide. At Townsends Inlet, tidal prisms were 1.0×10^8 m^3 (3.60×10^8 ft^3) for flood and 6.9×10^7 m^3 (2.25×10^8 ft^3) for ebb. As expected, these values are smaller than comparable tidal prisms for spring tide.

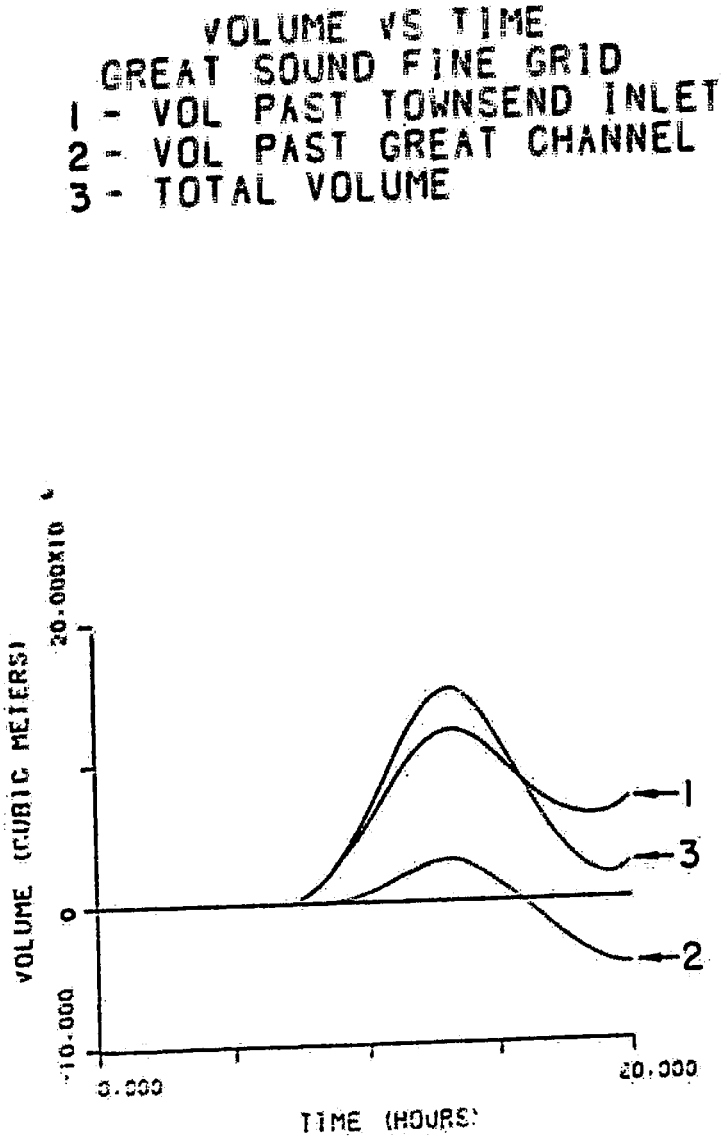

Figure 4-7: Cumulative Volume Versus Time - Neap Calibration, First Attempt

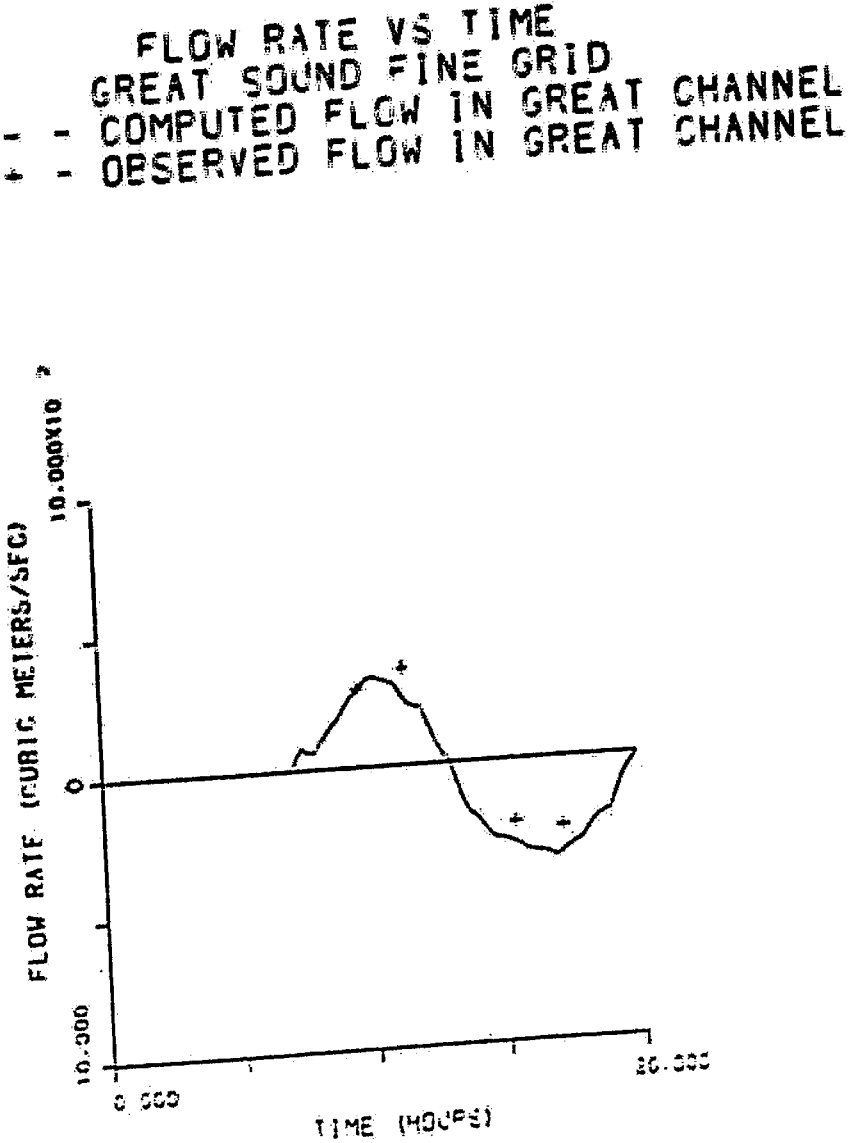

Figure 4-8: Flow Rate in Great Channel - Neap Calibration, Second Attempt

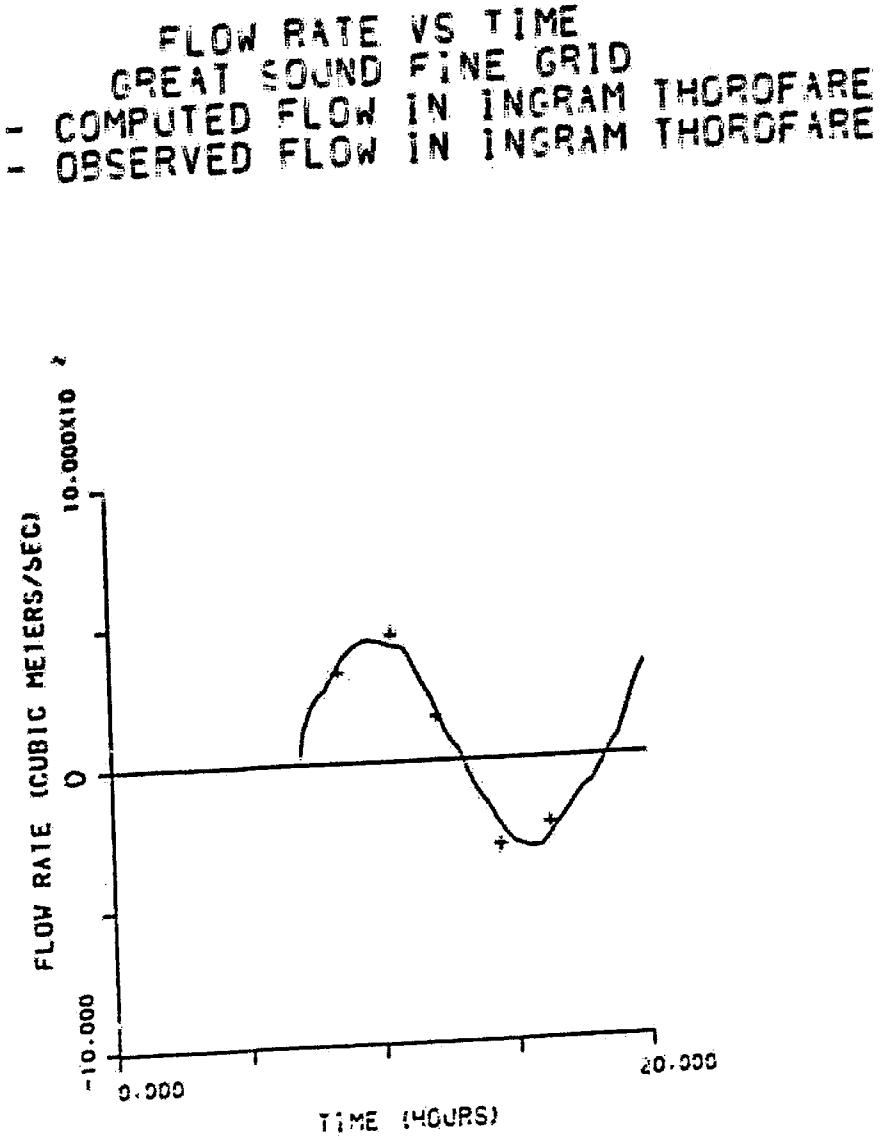

Figure 4-9: Flow Rate in Ingram Thorofare - Neap Calibration, Second Attempt

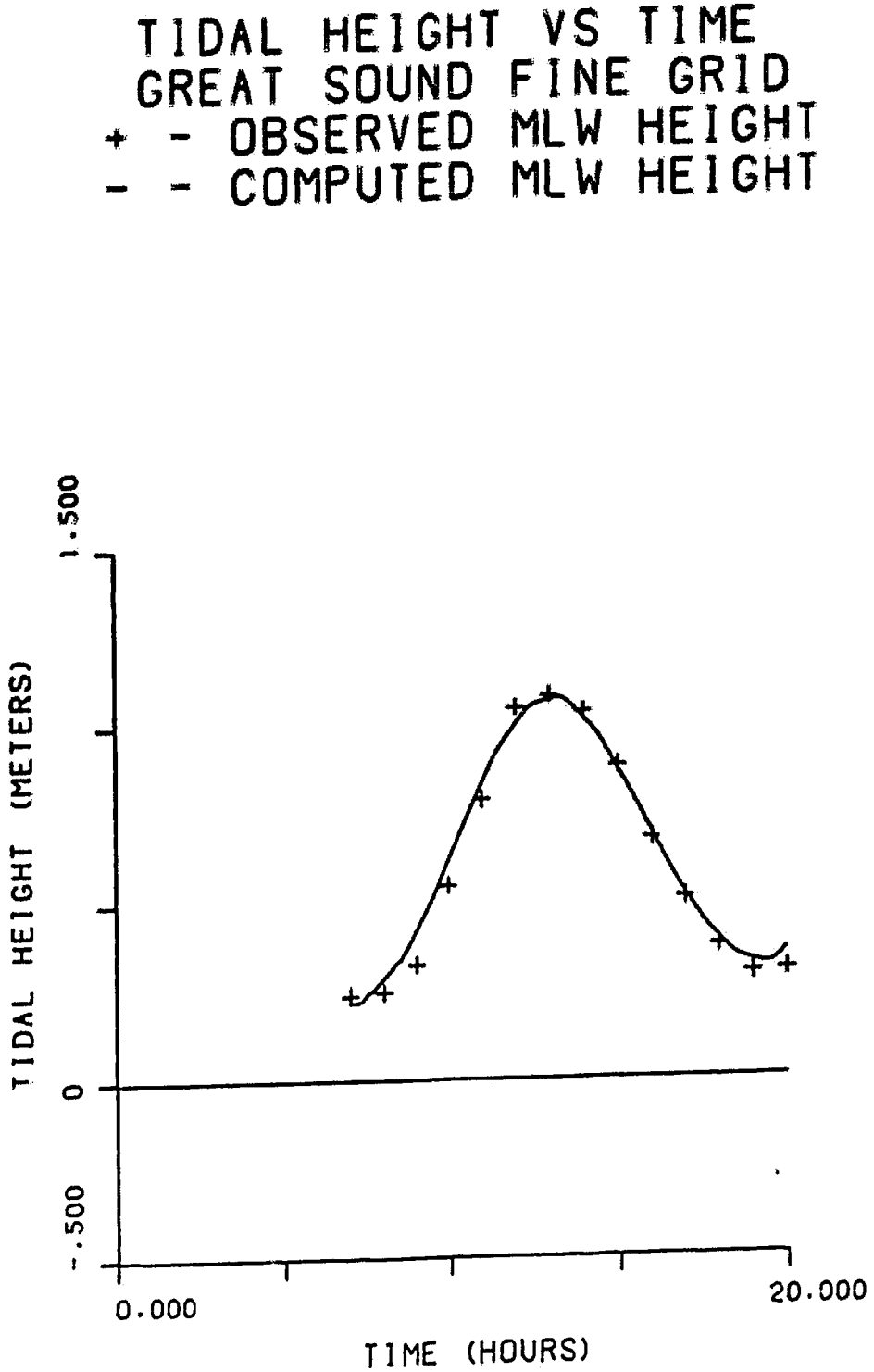

Figure 4-10: Tidal Height Versus Time - Neap Calibration, Second Attempt

Calculation of net flow through the sound is most meaningful when the elevations in Great Sound are approximately the same at the beginning and ending of the period over which the calculation is performed. Because the neap calibration run is only 13 hours long, the elevations do not return to their initial levels. Since it was believed that the calculation should be done over at least one tidal cycle to be representative, the calculation was not performed for neap tide. Nevertheless, from Fig. 4-11 a general influx through Townsends Inlet and an outflow through Great Channel can be discerned. However, due to deficiencies in the observed Great Channel elevation curve the results for neap tide are not as reliable as the results for spring tide.

Hourly flow maps for neap tide calibration are presented in Appendix I.3. The process of filling and draining is similar to spring tide, except that during neap tide most of the marshland has not become flooded. Between 0800 hours and 0900 hours, cells representing mudflat areas have become flooded, but at the high-water mark occurring near 1300 hours most of the marsh cells are still visible.

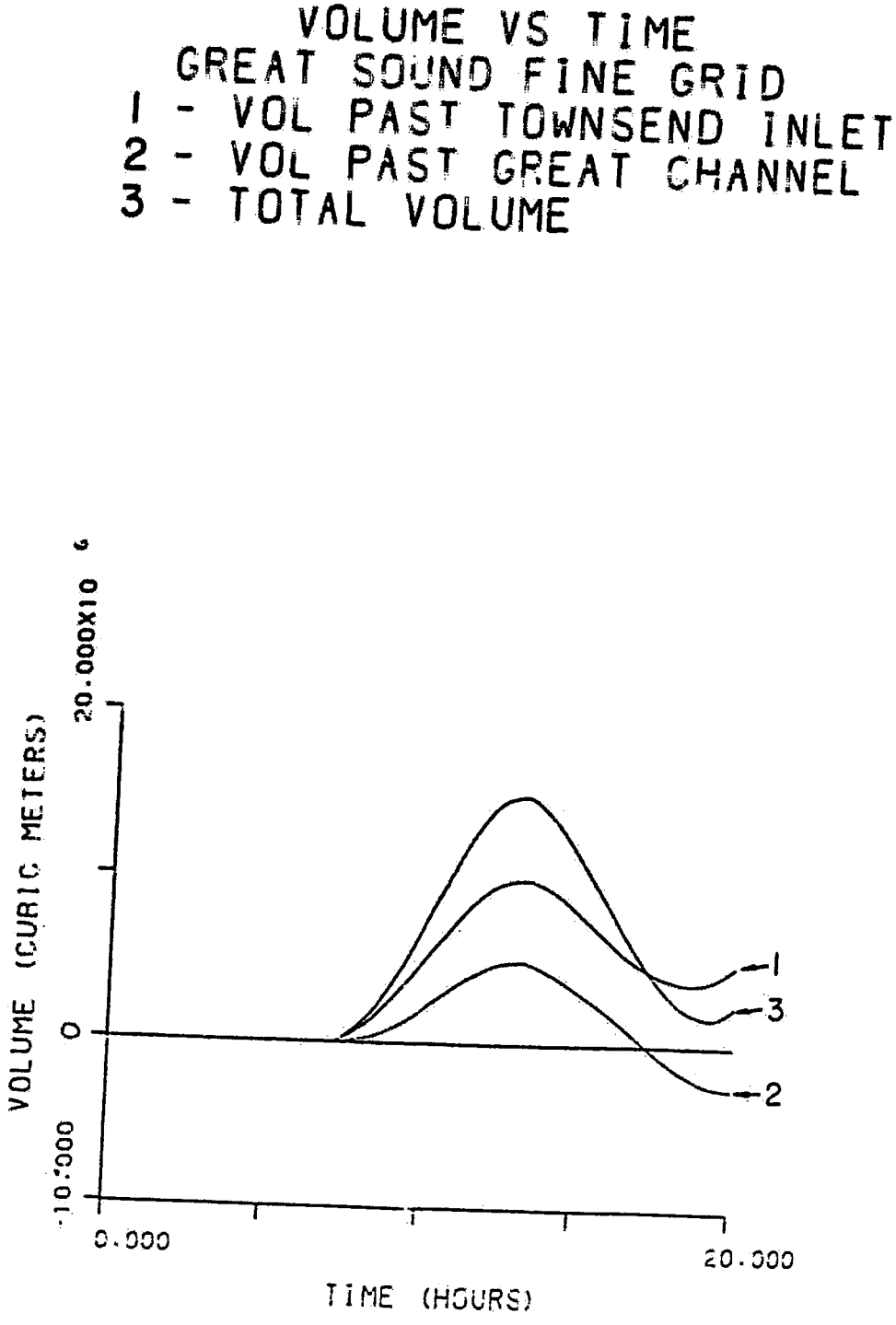

Figure 4-11: Cumulative Volume Versus Time - Neap Calibration, Second Attempt

4.3 Verification for Mean Tide - NOS Data, August 8-9, 1978

To further assure the model's reliability, an independent set of tidal data collected by NOS [23] was used in a verification run. The observed NOS data for Great Sound contained no data below 0.30 m (1.0 ft) MLW. To supplement these, water levels for the lower low water period were derived by taking Sandy Hook data for the same time and applying a correction factor found in the NOS Tide Tables [25] (See Fig. 4-12). As with spring and neap tide calibration, observed and computed values show satisfactory agreement and never varied by more than 9.1 cm (0.3 ft).

Discharges for Great Channel and Ingram Thorofare are presented in Figs. 4-13 and 4-14. Although observed flows were unavailable, the discharges for mean tide appear to be fairly smooth and sinusoidal, as would be expected.

Cumulative volume versus time is plotted in Fig. 4-15. Tidal prisms calculated from this graph are shown in Tables 4-3 and 4-4. Generally, calculated tidal prisms for mean tide were smaller than for spring tide and larger than for neap tide, as expected.

According to Fig. 4-15, a definite flow-through exists in the sound for mean tide. Inflow or outflow for each channel was calculated by dividing the change in cumulative volume by the

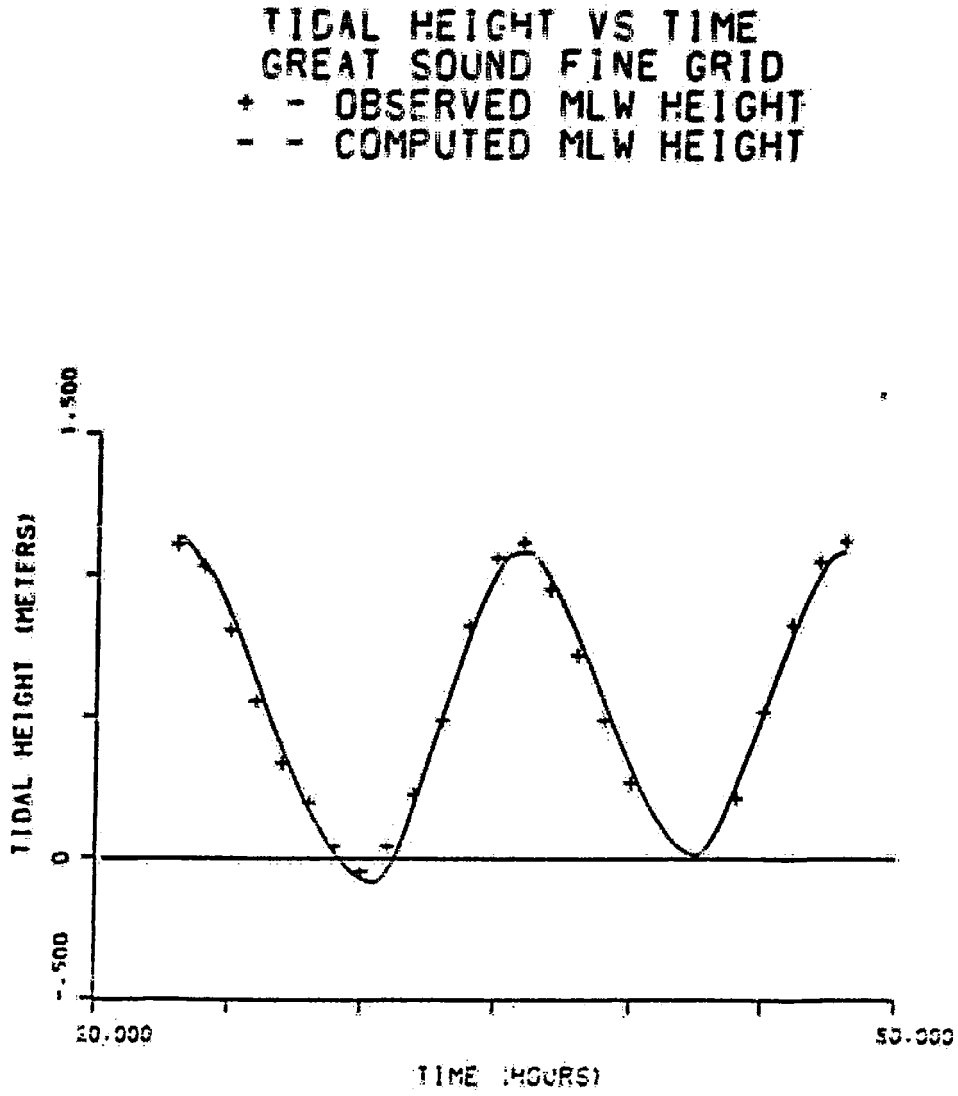

Figure 4-12: Tidal Height Versus Time - Mean Verification

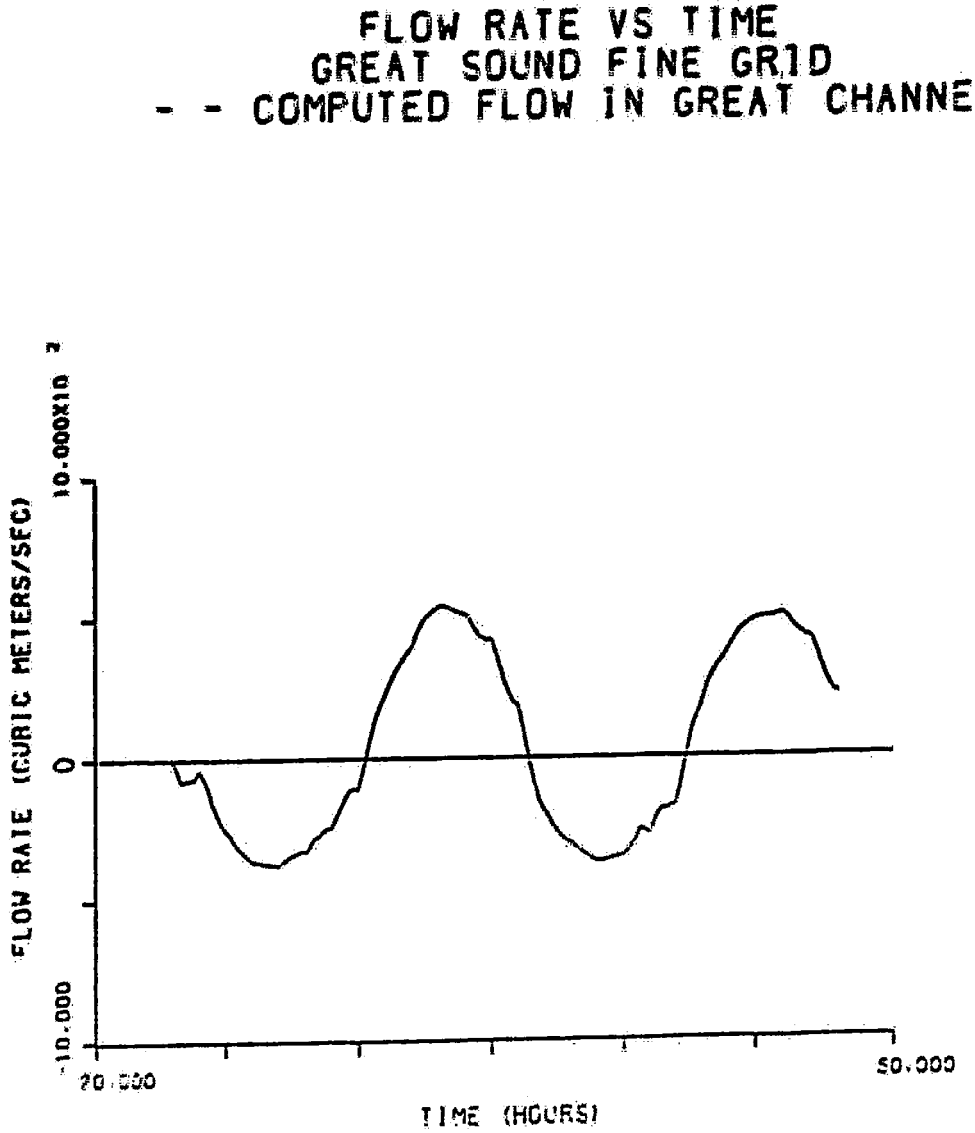

Figure 4-13: Flow Rate Versus Time in Great Channel - Mean Verification

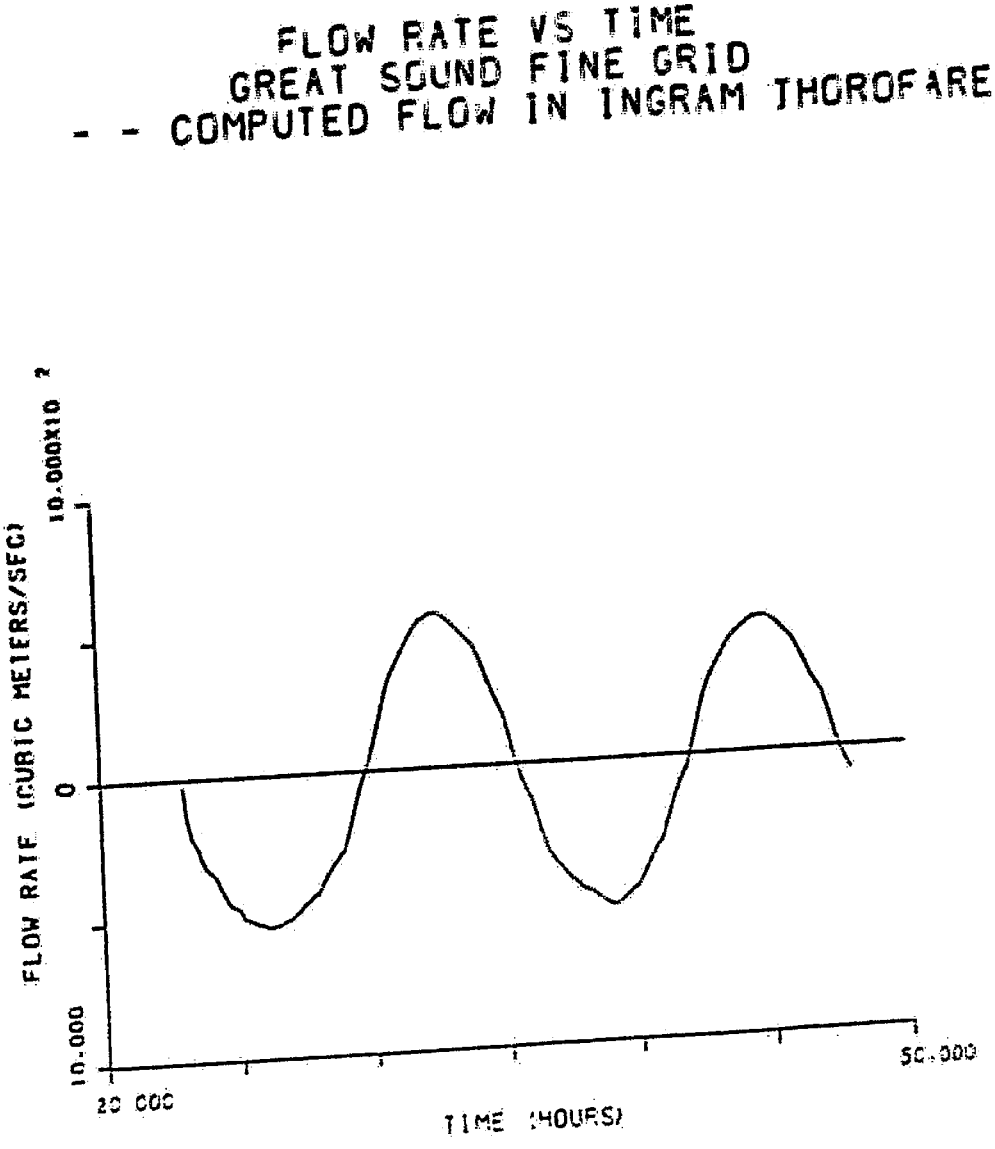

Figure 4-14: Flow Rate Versus Time in Ingram Thorofare - Mean Verification

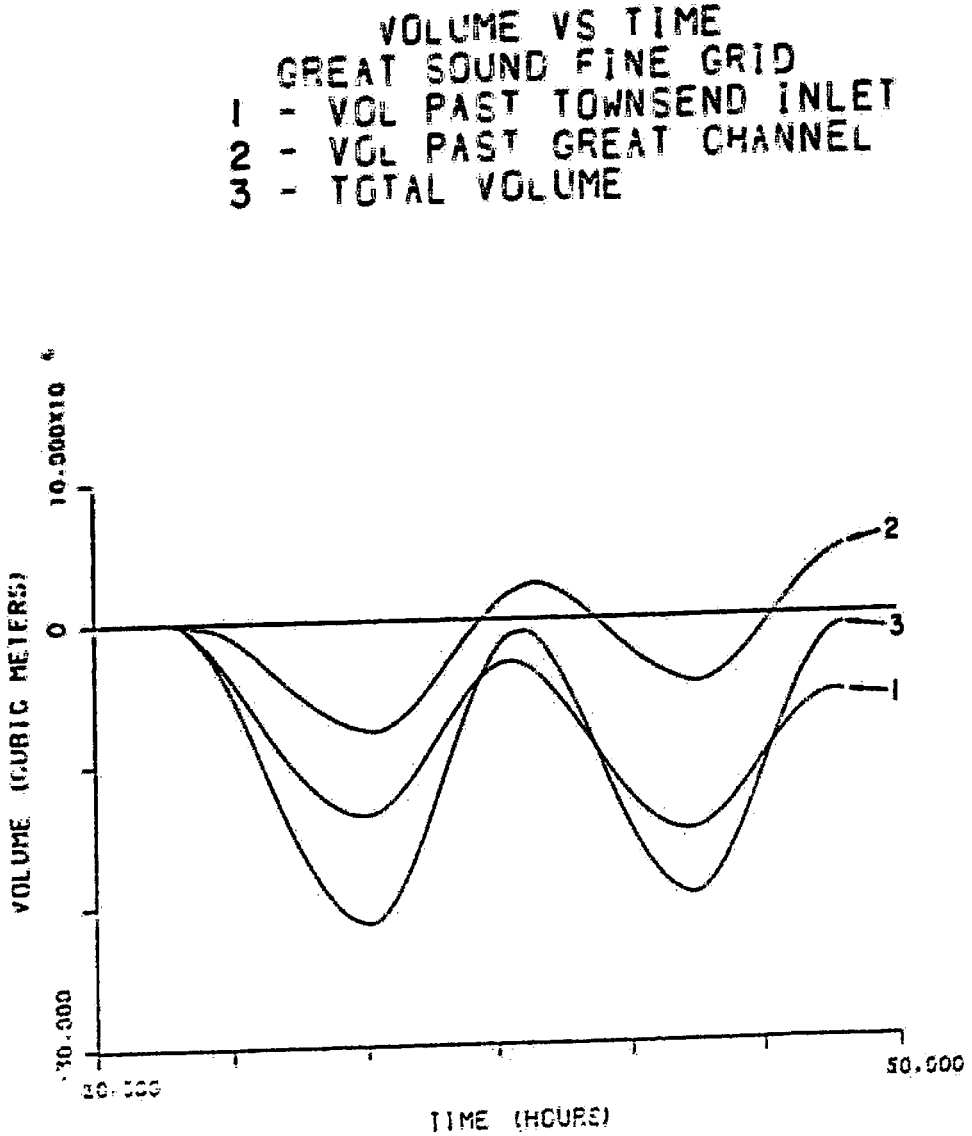

Figure 4-15: Cumulative Volume Versus Time - Mean Verification

Ebb/Flood	Start Time	Tidal Prism	
		(m^3)	(ft^3)
E	2300	8.00×10^6	28.26×10^7
F	3030	1.03×10^7	36.38×10^7
E	3630	7.01×10^6	24.77×10^7
F	4225	9.15×10^6	32.33×10^7

Table 4-3: Tidal Prisms for Great Channel - Mean Verification

Ebb/Flood	Start Time	Tidal Prism	
		(m^3)	(ft^3)
E	2300	1.38×10^7	48.71×10^7
F	2950	1.09×10^7	38.45×10^7
E	3530	1.28×10^7	45.03×10^7
F	4220	1.04×10^7	36.61×10^7

Table 4-4: Tidal Prisms for Townsends Inlet - Mean Verification

duration of the run. For Townsends Inlet, a net outflow of 60.6 m^3/s (2140 ft^3/s) was calculated; in Great Channel, there was a net inflow of 50.1 m^3/s (1770 ft^3/s). Inflow did not equal outflow because the water elevations throughout the sound were not exactly the same as at initial conditions. These results indicate that the net flow-through exits via Townsends Inlet. The results of neap tide calibration, where the net flow entered through Townsends Inlet and exited through Great Sound, do not support this conclusion.

Flow maps for mean tide verification are on file at Lehigh University [32]. These maps reveal that the flow dynamics are quite similar to spring and neap calibration flow fields, except that a significant net outflow through Townsends Inlet occurs during mean tide.

4.4 Hypothetical Scenarios

To demonstrate the model's predictive capability, two additional simulations were run. In the first simulation, the channel geometries before the existence of the Intracoastal Waterway were modeled. In the second simulation, a sea level rise was modeled corresponding to a 0.61 m (2.0 ft) increase in the elevations at Great Channel and Ingram Thorofare.

For the pre-dredging simulation, bathymetric data were obtained

for circa 1906, before the dredging of Great Sound and the main channels was undertaken [11]. These data were limited in that the 1906 survey consisted of a single line of soundings extending through the main channels and the sound; no cross sections are available. Furthermore, it was clear that the line of soundings did not always follow the thalweg through the sound and channels. Consequently, the question of how representative the line of soundings was to the main channel remains. In spite of these doubts, the bathymetric data were used to develop a pre-dredging configuration of the study area. The channel connecting Long Reach and Great Channel just inland from Avalon was also modified in accordance with the map accompanying these data. Finally, mudflat areas in Great Sound created by dredge spoil deposition were removed. Elevation changes to specific cells are listed in Tables 4-5, 4-6, and 4-7.

For the purpose of comparison, this simulation was run using the same tidal forcing data as in the spring tide calibration run. From Figs. 4-16, 4-17, 4-18, and 4-19, it can be seen that elevations, flows and tidal prisms for the pre-dredging simulation and the present-day simulation (i.e, spring tide calibration) were very similar. This similarity is further established by comparing flow maps from the pre-dredging scenario to flow maps at the same times for spring calibration (see Figs. 4-20, 4-21, and 4-22, and

X Coordinate	Y Coordinate	Present-Day Elevation		Pre-Dredging Elevation	
		(m)	(ft)	(m)	(ft)
13	2	-3.66	-12.0	-0.27	-0.9
13	3	-4.27	-14.0	-0.27	-0.9
14	2	-3.05	-10.0	-0.27	-0.9
14	22	0.30	1.0	-0.30	-1.0
15	2	-3.05	-10.0	-0.27	-0.9
15	21	0.24	0.8	-0.30	-1.0
16	2	-3.05	-10.0	-0.27	-0.9
16	22	0.03	0.1	-0.30	-1.0
17	2	-3.05	-10.0	-0.27	-0.9
17	22	0.15	0.5	-0.30	-1.0
18	2	-3.05	-10.0	-0.27	-0.9
18	22	0.24	0.8	-0.30	-1.0
19	2	-3.05	-10.0	-0.27	-0.9
19	21	0.24	0.8	-0.30	-1.0
20	2	-3.05	-10.0	-0.27	-0.9
20	20	0.24	0.8	-0.30	-1.0
20	21	0.30	1.0	-0.30	-1.0
21	2	-3.05	-10.0	-0.27	-0.9

Table 4-5: Cell Elevation Corrections for Pre-Dredging Scenario

X Coordinate	Y Coordinate	Present-Day Elevation		Pre-Dredging Elevation	
		(m)	(ft)	(m)	(ft)
21	20	0.30	1.0	-0.30	-1.0
22	2	-3.05	-10.0	-0.27	-0.9
22	25	0.30	1.0	-0.61	-2.0
23	2	-3.05	-10.0	-0.27	-0.9
23	19	-2.59	-8.5	-2.44	-8.0
23	25	0.15	0.5	-0.61	-2.0
24	2	-3.05	-10.0	-0.27	-0.9
24	19	-2.59	-8.5	-1.83	-6.0
24	20	-2.59	-8.5	-1.22	-4.0
24	23	0.03	0.1	-0.30	-1.0
25	2	-3.05	-10.0	-0.27	-0.9
25	20	-2.59	-8.5	-0.61	-2.0
25	25	0.34	1.1	-0.61	-2.0
26	2	3.05	-10.0	-0.27	-0.9
26	3	-2.74	-9.0	-1.22	-4.0
26	4	-2.44	-8.0	-1.22	-4.0
26	5	-2.44	-8.0	-1.22	-4.0
26	6	-2.13	-7.0	-1.22	-4.0

Table 4-6: Cell Elevation Corrections for Pre-Dredging Scenario, Continued

X Coordinate	Y Coordinate	Present-Day Elevation		Pre-Dredging Elevation	
		(m)	(ft)	(m)	(ft)
26	7	-1.83	-6.0	-1.22	-4.0
26	21	0.24	0.8	-0.30	-1.0
26	25	0.06	0.2	-0.30	-1.0
27	20	-2.59	-8.5	-1.83	-6.0
27	21	0.30	1.0	-0.30	-1.0
27	25	0.24	0.8	-0.30	-1.0
28	20	-2.59	-8.5	-2.44	-8.0
28	21	-2.59	-8.5	-1.83	-6.0
29	21	-2.74	-9.0	-2.44	-8.0
29	24	1.22	4.0	-1.22	-4.0
30	18	-5.49	-18.0	-4.88	-16.0
30	19	-5.18	-17.0	-4.27	-14.0
30	20	-5.18	-17.0	-3.66	-12.0
30	21	-5.18	-17.0	-3.05	-10.0

Table 4-7: Cell Elevation Corrections for Pre-Dredging Scenario, Continued

Appendix I.2). Except for an increase in flow along row 16 for columns 25 to 30 at 1800 hours, and the formation of a small whirlpool near the confluence of Cresse and Gull Island Thorofares at 1900 hours, the overall flow pattern during the pre-dredging run appears remarkably similar to the flow field during the present-day simulation.

Apparently, the creation of the Intracoastal Waterway did little to alter the overall flushing characteristics of Great Sound. There are two probable reasons for this effect: (1) due to the presence of two major, opposing channels filling and draining the sound there is a nodal point that moves back and forth through the sound regardless of the channel's depth; and (2) the main channel depths are naturally deep in both pre-dredging and recently-dredged cases.

In the sea-level rise simulation, a rise in the ocean level was modeled corresponding to a 0.61 m (2.0 ft) rise in water elevations at Great Channel and Ingram Thorofare. It was assumed that no additional vertical accretion of the marsh and no shoaling of channels occurred. With these assumptions, it was possible to use the same grid configuration used in spring tide calibration. Hourly spring tidal forcing functions in the two channels were incremented by 0.61 m (2.0 ft). If desired, a sea-level rise for the Atlantic

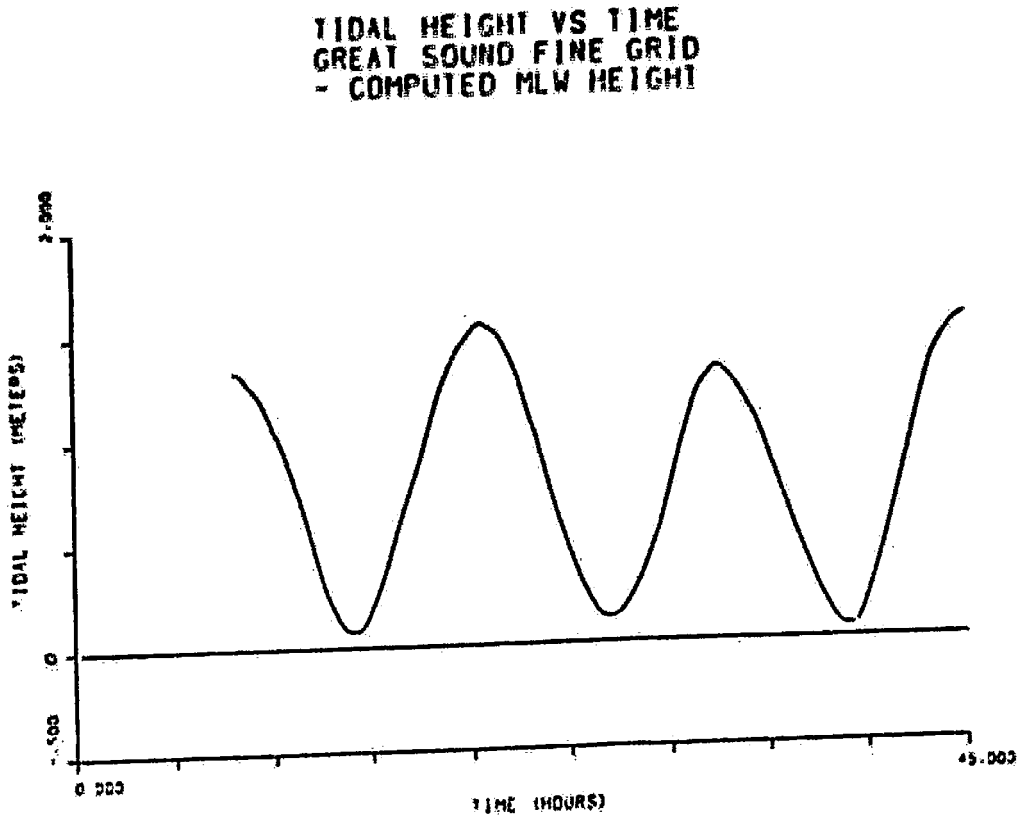

Figure 4-16: Tidal Height Versus Time - Pre-Dredging Scenario

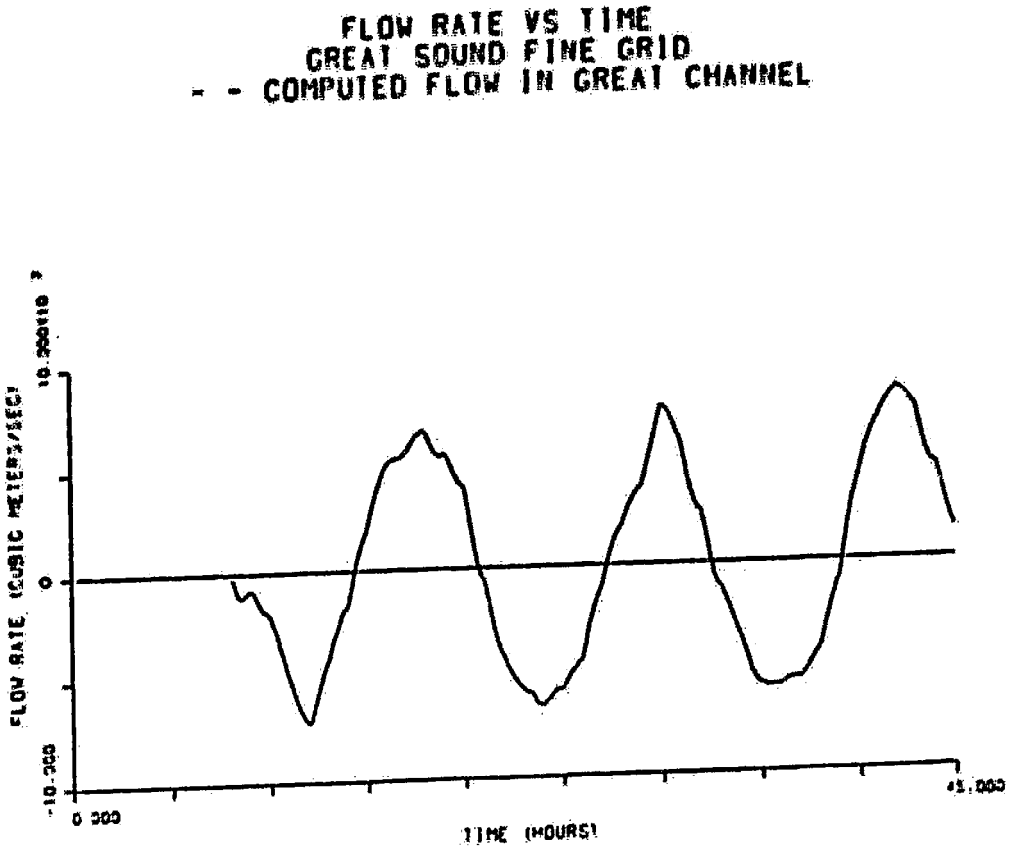

Figure 4-17: Flow Rate Versus Time in Great Channel - Pre-Dredging Scenario

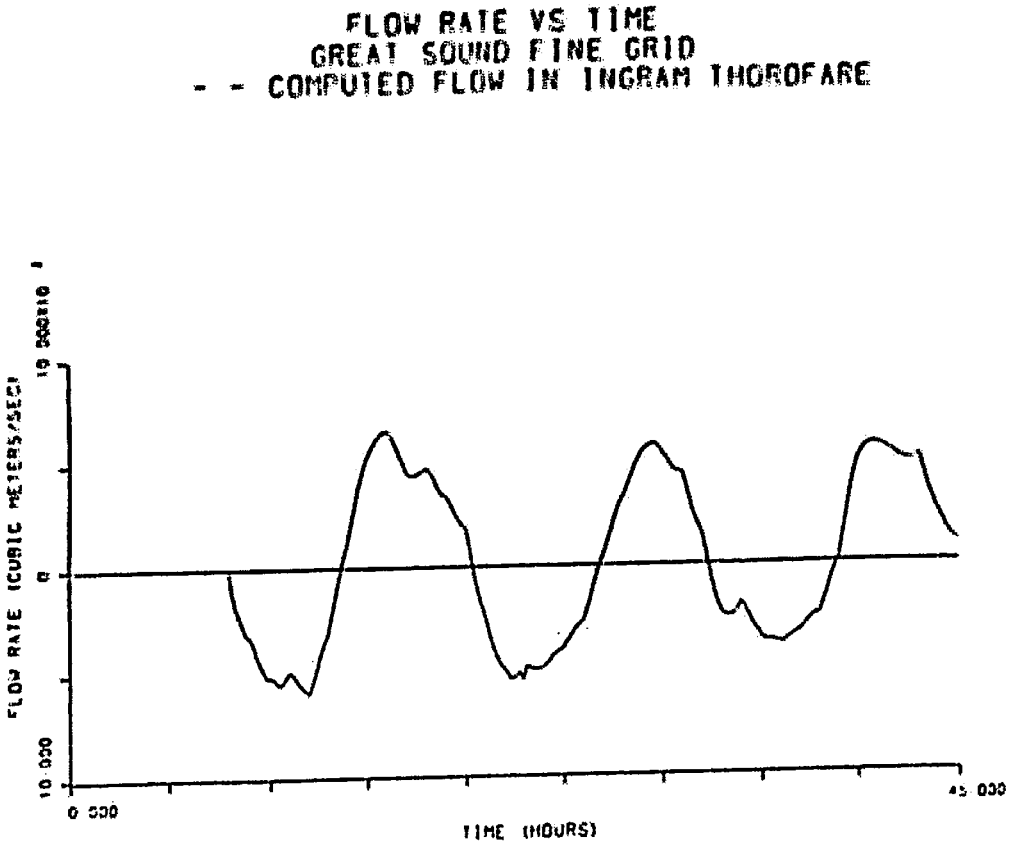

Figure 4-18: Flow Rate Versus Time in Ingram Thorofare - Pre-Dredging Scenario

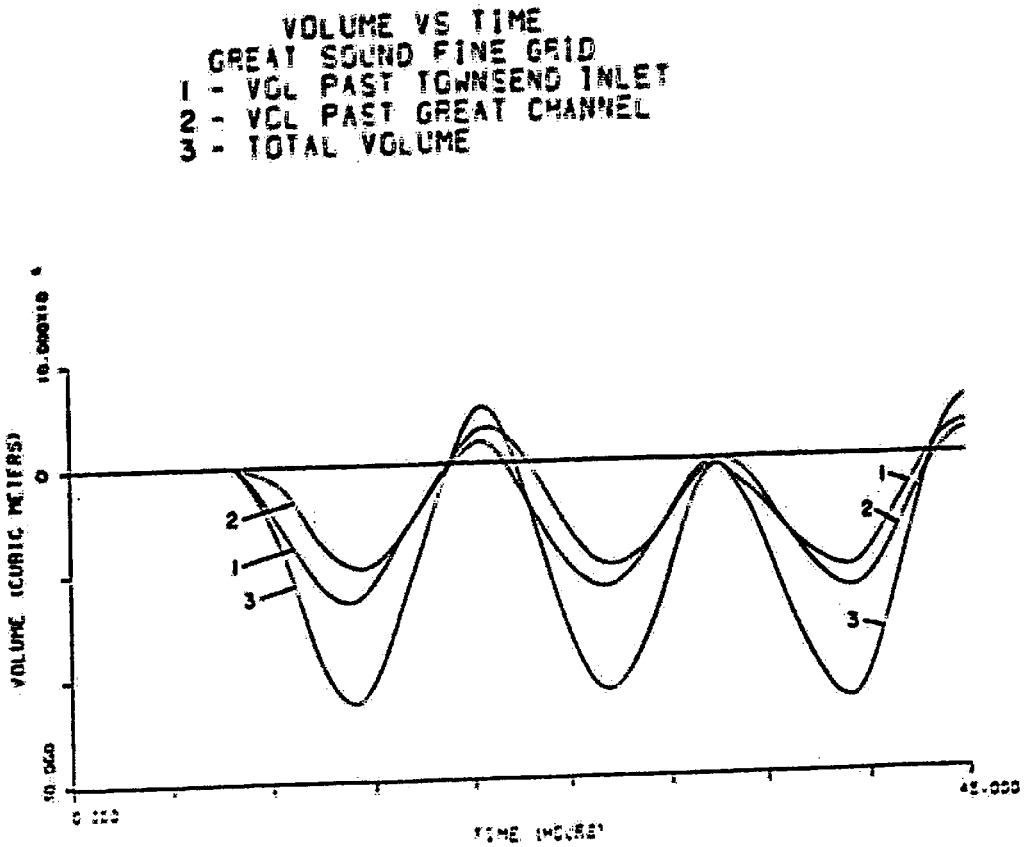

Figure 4-19: Cumulative Volume Versus Time - Pre-Dredging Scenario

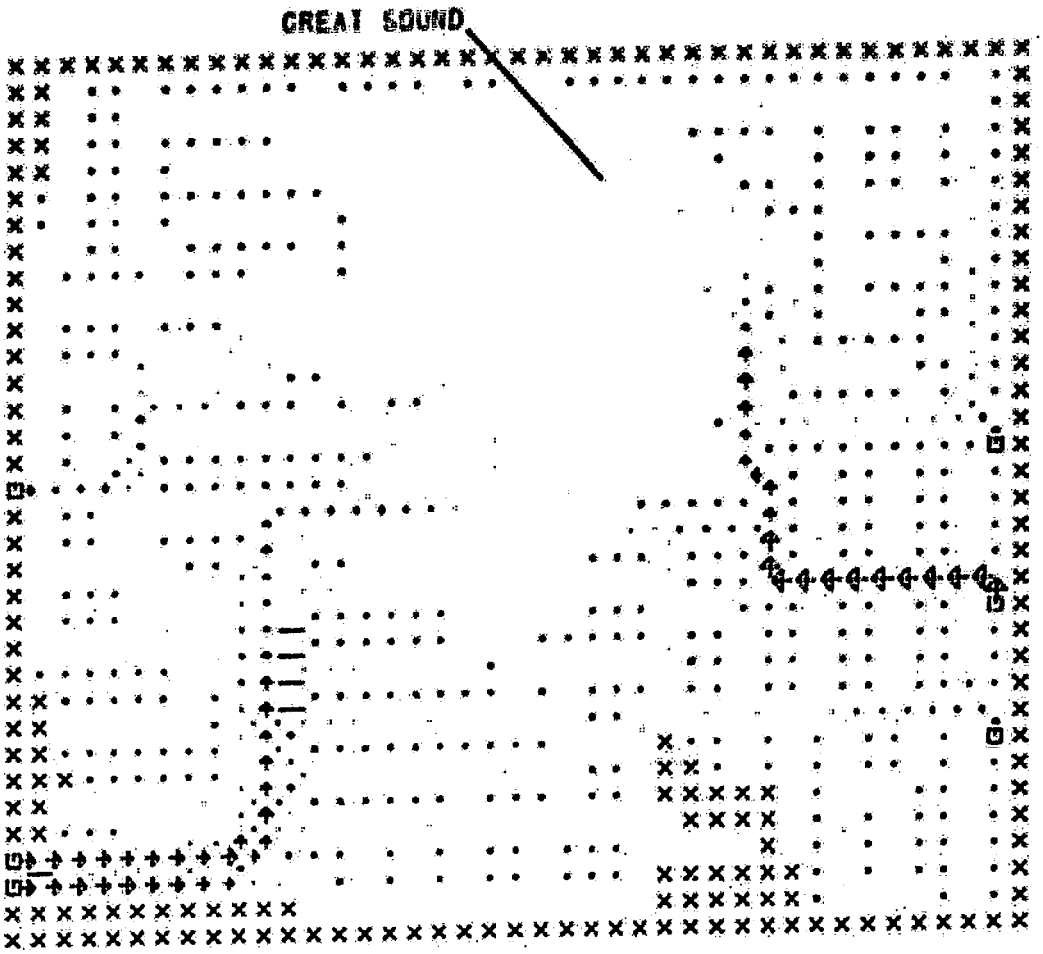

Figure 4-20: Flow Map for Pre-Dredging Scenario - 1800 Hours

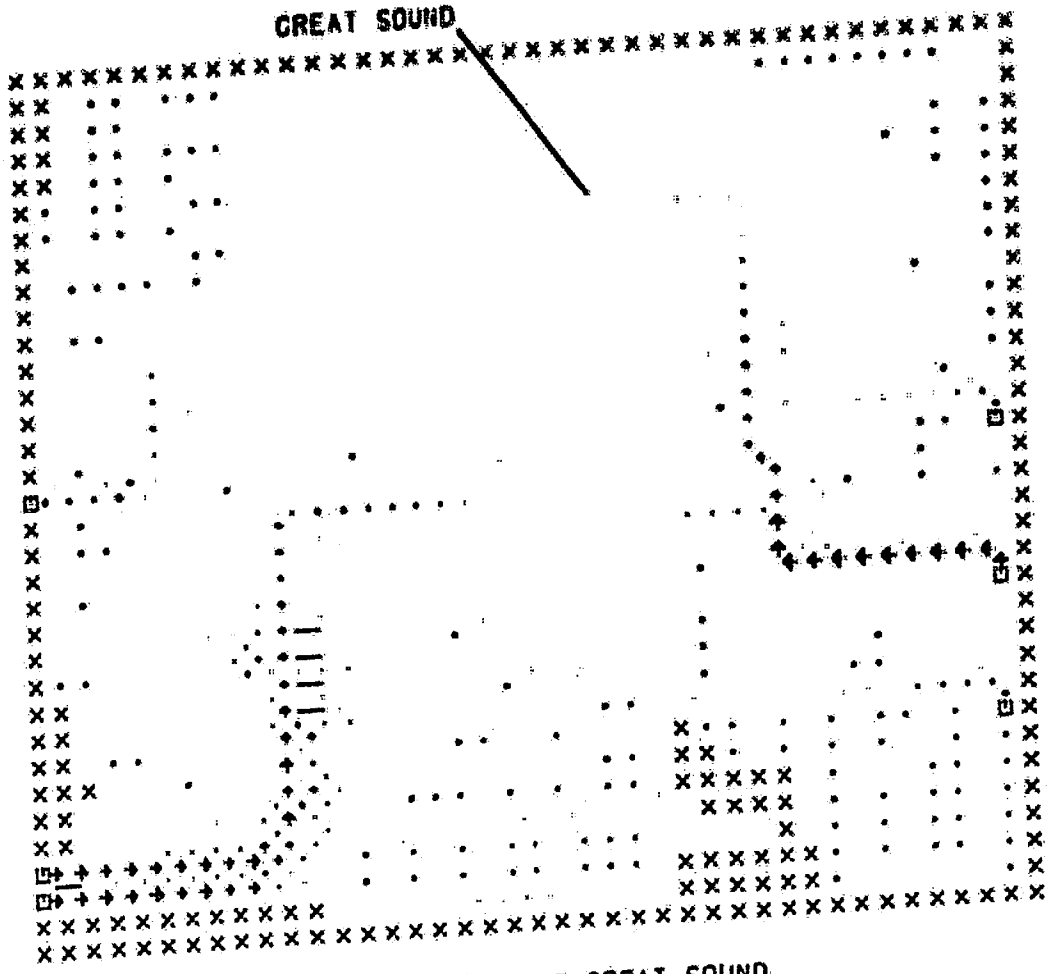

FLOW PATTERN FOR GREAT SOUND
1900 HRS CIRCA 1906
X - LAND CELL
* - INUNDATION CELL
⊡ - FORCING CELL
— - NO FLOW BOUNDARY
SCALE - 74000. CFS / INCH

Figure 4-21: Flow Map for Pre-Dredging Scenario - 1900 Hours

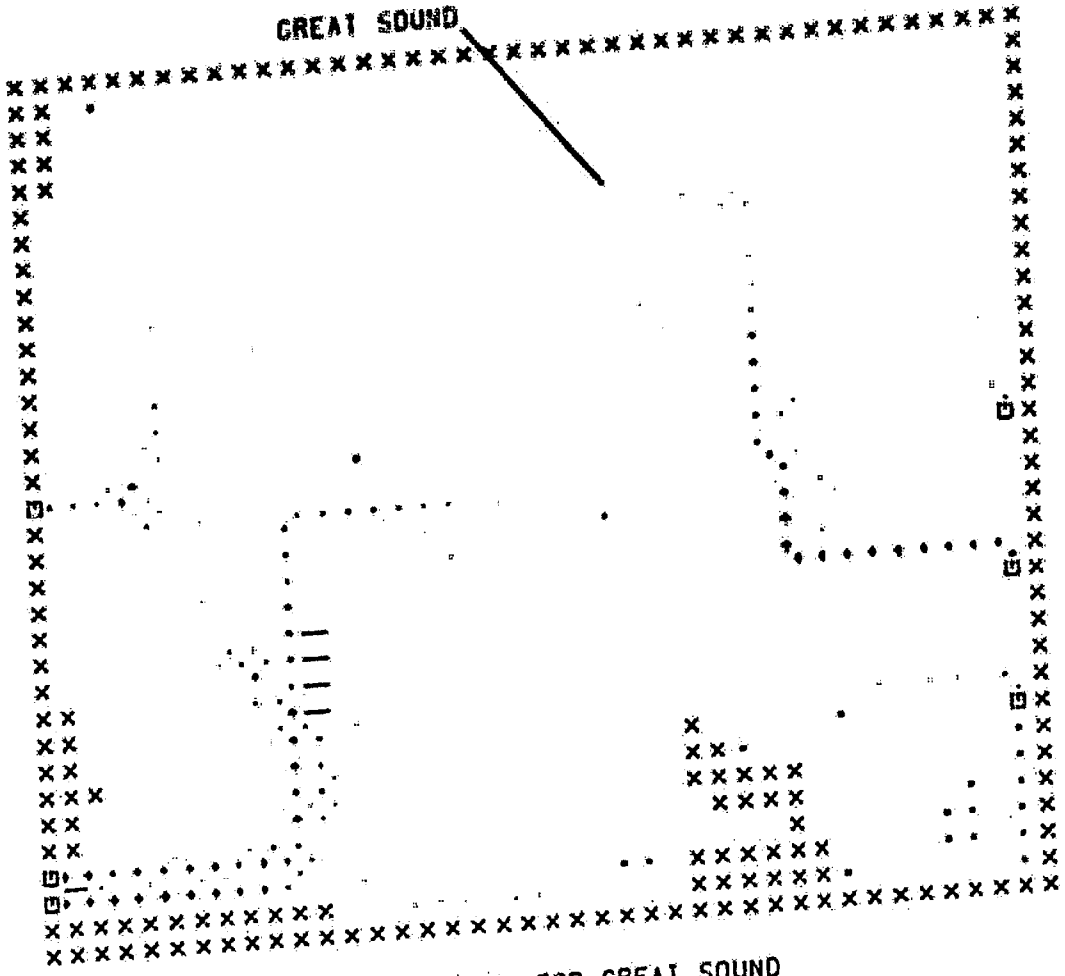

Figure 4-22: Flow Map for Pre-Dredging Scenario - 2000 Hours

Ocean could be modeled by using the coarse grid model developed by Gabriel et al. [10]. Forcing functions at Great Channel and Ingram Thorofare could be obtained by using the coarse grid model with the ocean-based forcing functions as input.

Elevations versus time at Reuben's Wharf are shown in Fig. 4-23. The elevation at which 50% of the marsh is submerged is 1.3 m (4.3 ft). The duration over which 50% of the marsh is submerged is approximately 6.7 hours. The duration for 50% marsh submergence is only 3.17 hours for present tidal conditions. Such an increase in submerged duration could change the ecological and sediment transport characteristics of Great Sound [28].

Flows for both main channels are considerably higher than for the corresponding flows for spring calibration (see Figs. 4-24 and 4-25). This increase is due to the marshland being completely flooded for a longer duration than it was for spring tide calibration. To raise the elevation by a unit when the marsh is completely submerged requires more water than when it is partly submerged.

Correspondingly, plots of cumulative volumes for the two main channels reveal substantially higher tidal prisms (see Fig. 4-26). Tidal prisms are presented in Tables 4-8 and 4-9.

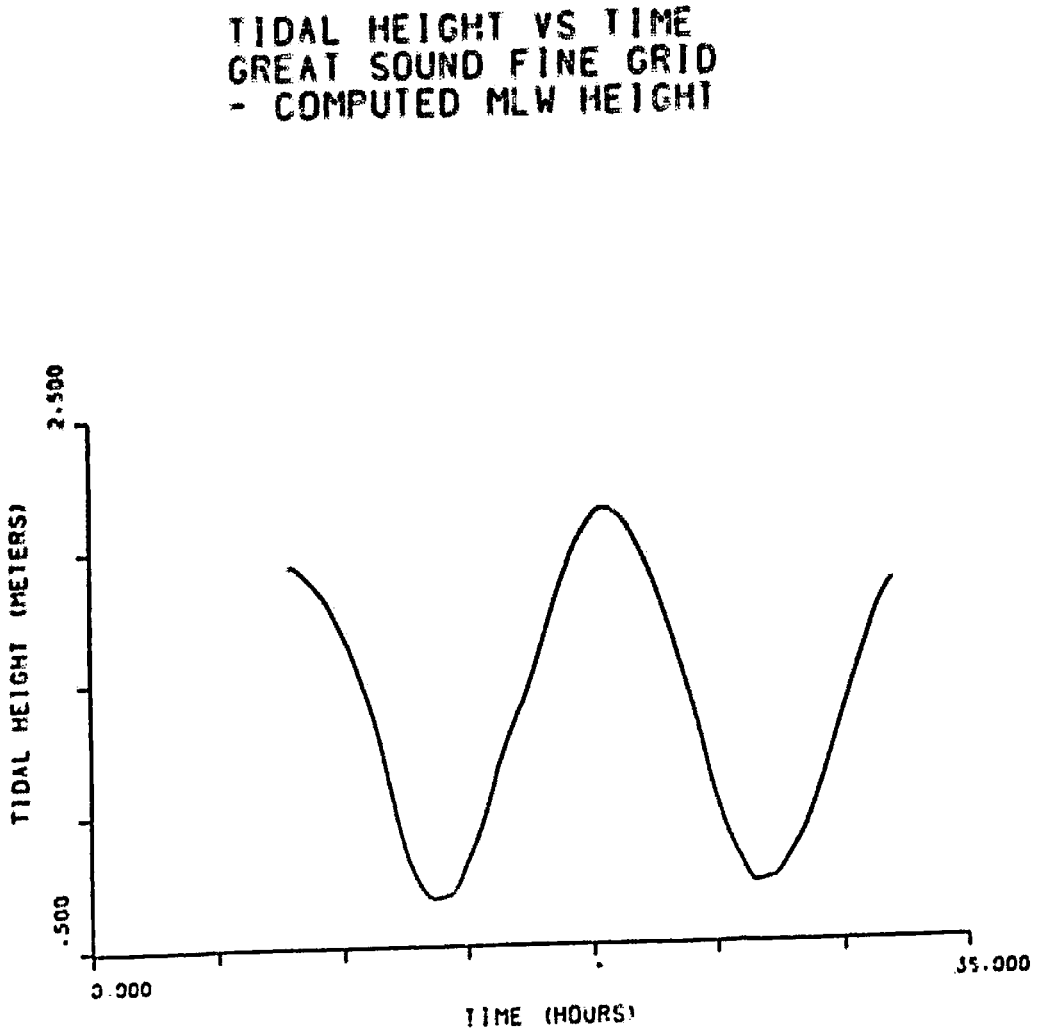

Figure 4-23: Tidal Height Versus Time - Sea Level Rise Scenario

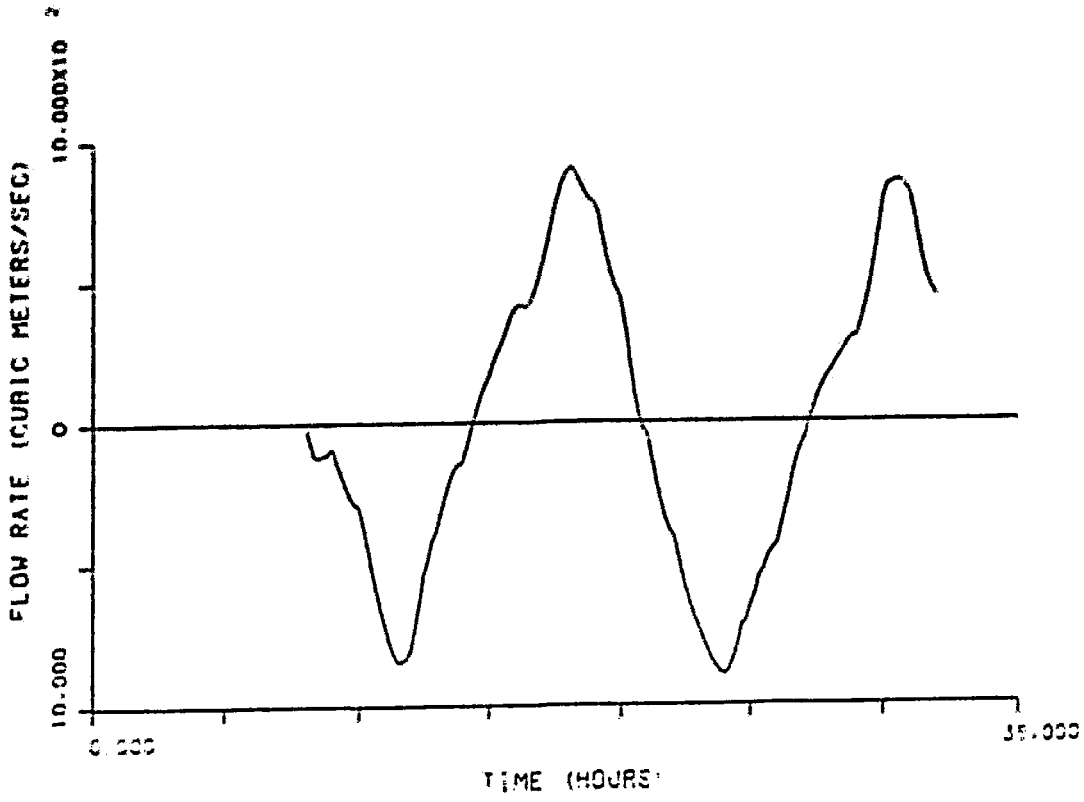

Figure 4-24: Flow Rate Versus Time in Great Channel - Sea Level Rise Scenario

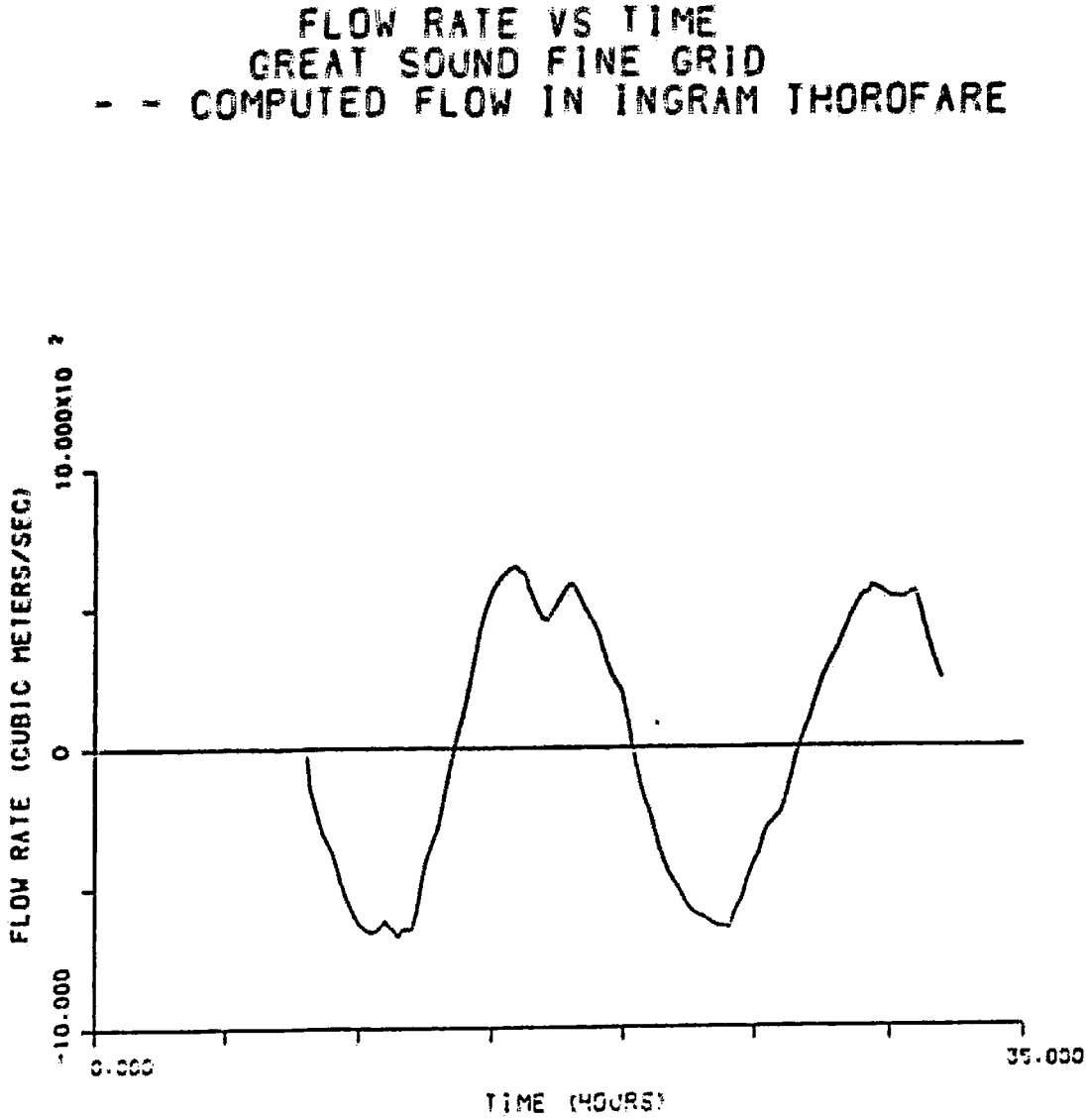

Figure 4-25: Flow Rate Versus Time in Ingram Thorofare - Sea Level Rise Scenario

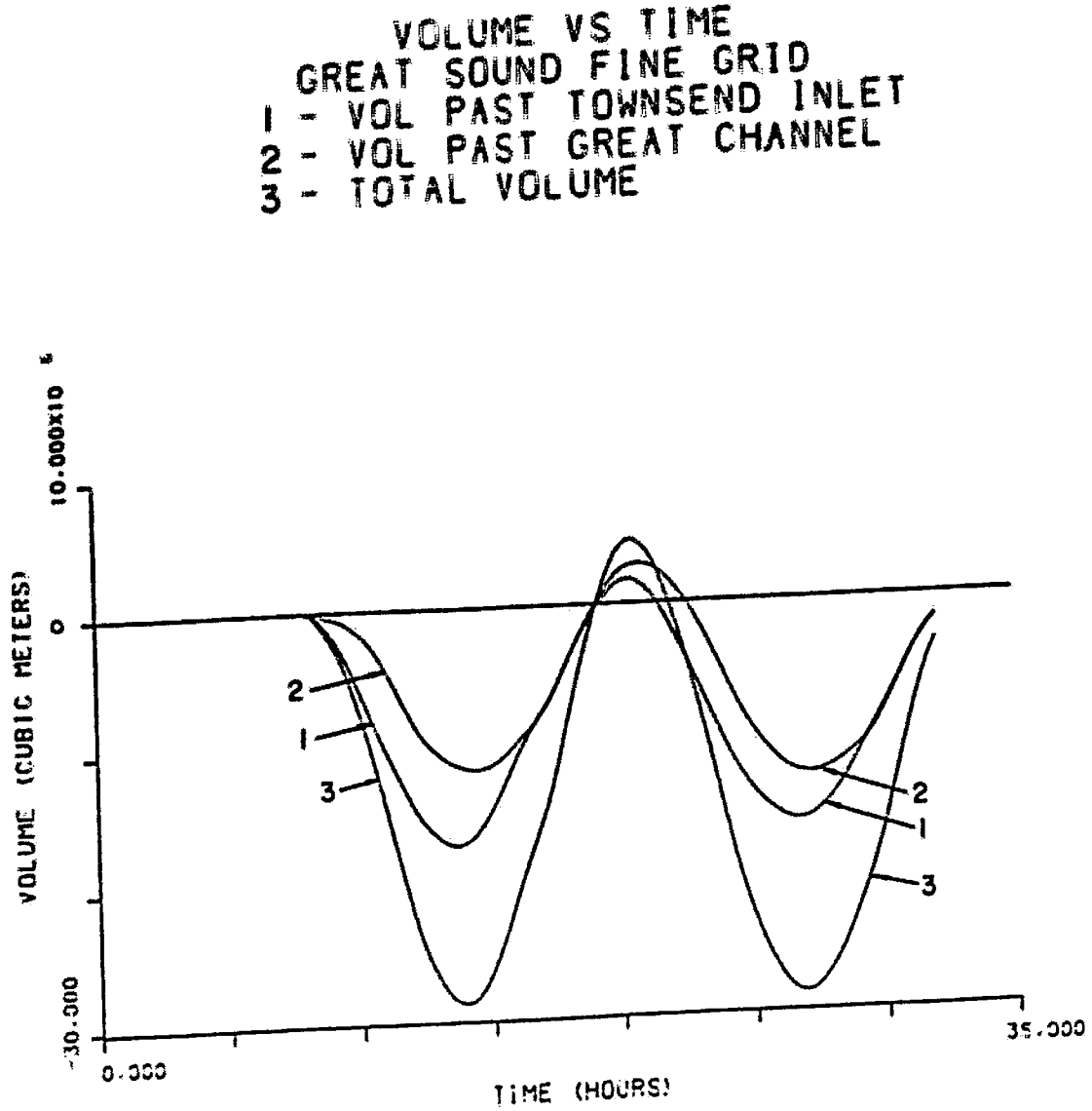

Figure 4-26: Cumulative Volume Versus Time - Sea Level Rise Scenario

Ebb/Flood	Start Time	Tidal Prism	
		(m^3)	(ft^3)
E	0800	1.16×10^7	40.92×10^7
F	1425	1.44×10^7	50.94×10^7
E	2040	1.59×10^7	56.31×10^7

Table 4-8: Tidal Prisms for Great Channel - Sea Level Rise Scenario

Ebb/Flood	Start Time	Tidal Prism	
		(m^3)	(ft^3)
E	0800	1.73×10^7	60.95×10^7
F	1330	1.89×10^7	66.91×10^7
E	2025	1.78×10^7	62.99×10^7

Table 4-9: Tidal Prisms for Townsends Inlet - Sea Level Rise Scenario

Generally, the distribution of flows throughout the sound did not seem to be significantly affected by sea level rise. Flow maps at times of 1200, 1400, and 2000 hours are shown in Figs. 4-27, 4-28, and 4-29.

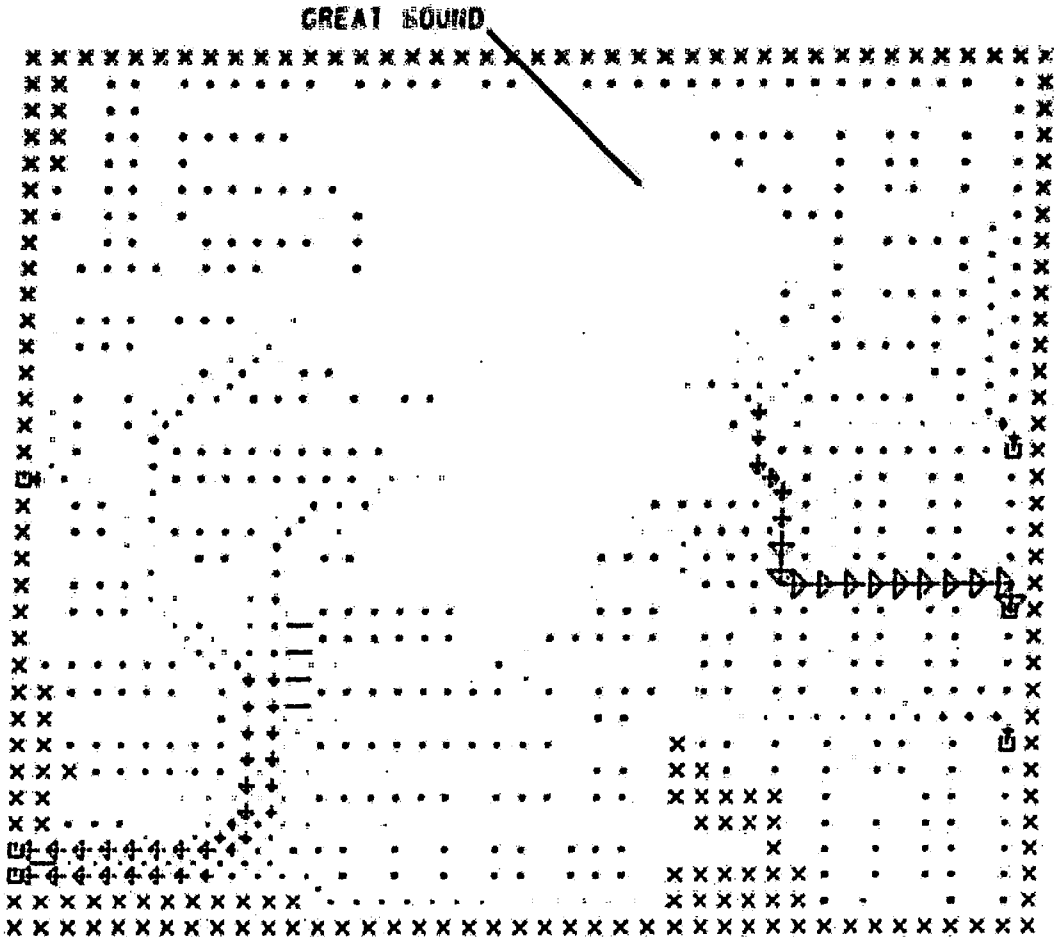

Figure 4-27: Flow Map for Sea Level Rise Scenario - 1200 Hours

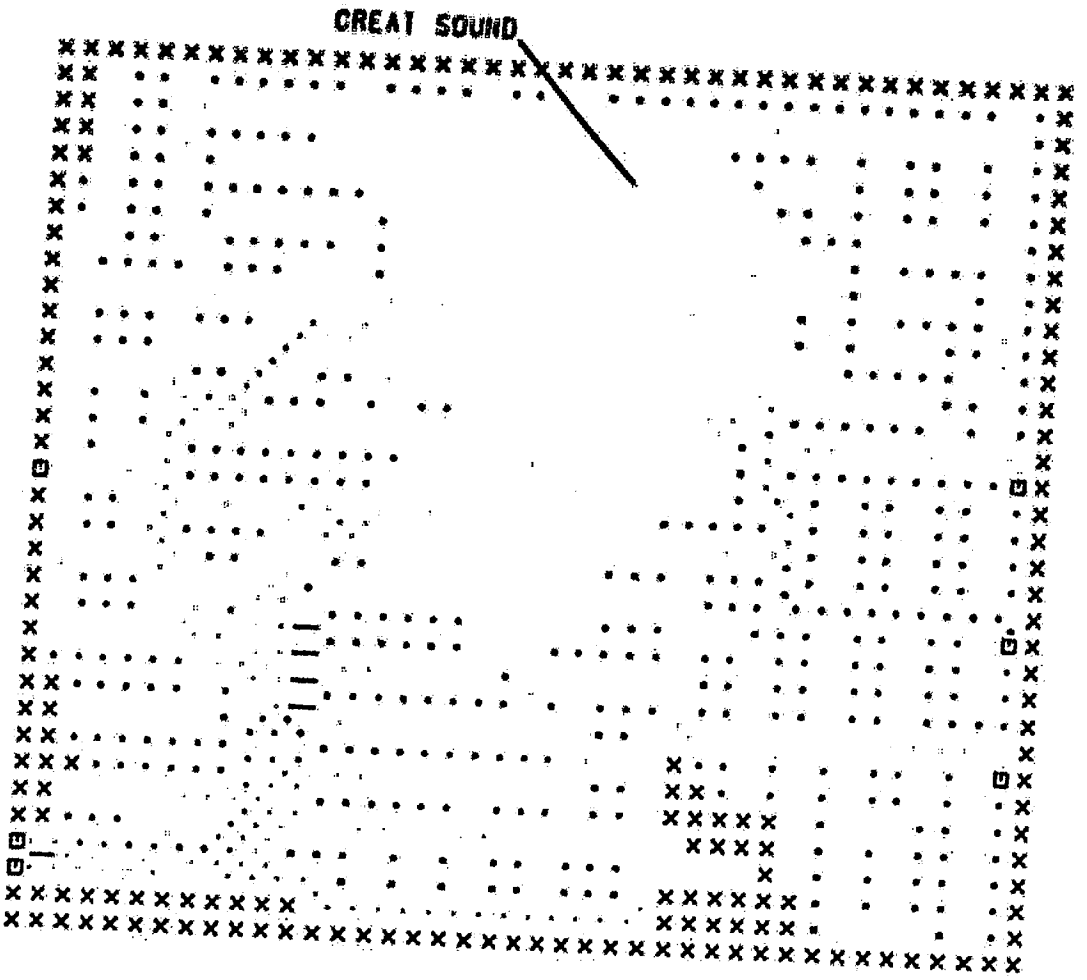

Figure 4-28: Flow Map for Sea Level Rise Scenario - 1400 Hours

Figure 4-29: Flow Map for Sea Level Rise Scenario - 2000 Hours

5. SUMMARY, CONCLUSIONS, AND RECOMMENDATIONS

5.1 Summary

The two-dimensional, hydrodynamic model HYDTID was applied to Great Sound in southern New Jersey and was used to predict flows and tidal heights for three selected tidal conditions. The model explicitly solves the vertically and time averaged momentum and continuity equations for a specific set of initial and boundary conditions.

The model was implemented by first discretizing the area into cells and choosing the cell size, time step, and study area boundaries. Data gathered in the field included bathymetry, topography, tidal elevations, and discharges. Forcing functions were applied at Great Channel and Ingram Thorofare. The model was calibrated for both spring and neap tide events using observed flows at Great Channel and Ingram Thorofare and tidal elevations at Reuben's Wharf. The calibration process consisted of varying friction values, barrier characteristics, cell elevations, feeder channel arrangement, and allocation of forcing cells. Additionally, the model was verified using an independent set of mean tide data collected by NOS.

As calibrated, the model is a satisfactory predictor of tidal heights and elevations in Great Sound. Additional fine tuning could

further enhance the model's accuracy.

To demonstrate the model's predictive capability, two additional simulation runs were performed. In the first simulation, the study area was modeled as it existed before the creation of the Intracoastal Waterway. The hydrodynamics in this simulation proved to be remarkably similar to present-day hydrodynamics in Great Sound, probably due in part to the balancing effect of the two main channels. A second simulation modeled a sea-level rise corresponding to a 0.61 m (2.0 ft) rise in forcing functions at Great Channel and Ingram Thorofare. As anticipated, flows were substantially higher than in the spring tide calibration run, and the marsh was submerged for longer durations.

5.2 Conclusions

Based on the results of this study, the following can be concluded:

1. The model accurately simulates the depth averaged flow field and tidal elevations throughout Great Sound for selected spring, mean, and neap tide events;

2. The model can be used to assess the qualitative effects of introducing certain changes to the Great Sound area, such as dredging or sea-level rise;

3. Feeder channels can be modeled by using one wide channel to represent several feeder channels to give an accurate circulation model of the system;

4. Linear relationships relating Manning's n to elevation are inappropriate for Great Sound based on the 1984

Lehigh data collection effort.

5.3 Recommendations for Future Work

The results of this study should be further verified and enhanced by additional work in several areas. As the application of this model was part of an ongoing, interdisciplinary effort, further improvement would make the model more useful in studying geology, ecology, sediment and contaminant transport, and commerce in Great Sound.

Another set of neap tide data should be taken to check the set used in model calibration. Specifically, the relative positions of the rising limbs of the Great Channel, Ingram Thorofare, and Reuben's Wharf water elevation curves need to be verified.

Discharge measurements of greater accuracy would also improve the calibration process. A better method of measuring depths, perhaps by using a heavier weight on the cable, should be used to control the cable's downstream drift. Also, velocity profiles taken at the time of the discharge measurements were not always logarithmic. More velocity profiles should be taken and integrated to obtain average velocities for each discharge measurement.

Manning's n should be calculated specifically for Great Sound, Great Channel, and the small feeder channels. In this study,

Manning's n values determined along Ingram Thorofare were used for Great Sound, Great Channel, and the feeder channels. Since bedforms and geometry vary somewhat throughout the study area, Manning's n values should be obtained at various locations.

The linear equation relating Manning's n to elevation for elevations greater than zero MLW should be verified empirically. The results of this study indicate that for Ingram Thorofare Manning's n is only slightly dependent on elevation. Therefore, a field study of Manning's n for flow over marshland should be undertaken to further determine the sensitivity of Manning's n to discharge and elevation.

Other potential simulation runs include modeling a third inlet between Avalon and Stone Harbor, simulating construction that converts marshland into upland, and modeling increased dredging. As the need for these or other simulation runs develop, pertinent topographic, bathymetric, and hydraulic data should be collected.

The prediction of hydrodynamics and sediment transport is essential to managing and planning the back-bay environment. Therefore, the hydrodynamic model should be used in conjunction with a sediment transport model of Great Sound.

REFERENCES

[1] Bode, L. E., and Sobey, R. J.
"Initial Transients in Long Wave Computations".
Journal of the Hydraulics Division, ASCE 110:1371-1397, 1984.

[2] Brown, E. I.
Inlets on Sandy Coasts.
In Proceedings of the American Society of Civil Engineers, pages 505-553. ASCE, New York, 1928.

[3] Burke, R. W., and Stolzenbach, K. D.
Free Surface Flow Through Marsh Grass.
Technical Report, Massachusetts Institute of Technology, 1983.

[4] Butler, H. L.
"Evolution of a Numerical Model for Simulating Long-Period Wave Behavior in Ocean-Estuarine Systems".
In Estuarine and Wetland Processes with Emphasis on Modeling, pages 147-182. Plenum Press, New York, 1980.

[5] Butler, H. L., and Raney, D. C.
"Finite Difference Schemes for Simulating Flow in an Inlet-Wetlands System".
In Proceedings of the Army Numerical Analysis and Computers Conference, pages 131-148. Department of the Army, Durham, North Carolina, 1976.

[6] Chu, W. S. and Yeh, W. G.
"Two-Dimensional Tidally Averaged Estuarine Model".
Journal of the Hydraulics Division, ASCE 106:501-515, 1980.

[7] Corbett, Don M.
Stream-Gaging Procedure.
Technical Report Water Supply Paper 888, U. S. Geological Survey, 1943.

[8] Dronkers, J. J.
Tidal Computations in Rivers and Coastal Waters.
John Wiley and Sons, Inc., New York, 1964.

[9] Dronkers, J. J.
"Tidal Computations for Rivers, Coastal Areas, and Seas".
Journal of the Hydraulics Division, ASCE 95:29-77, 1969.

[10] Gabriel, R. J., Lennon, G. P., and Weisman, R. N.
The Hydraulics of the Hereford Inlet-Bay System.
Technical Report, No. 477.1, Fritz Engineering Laboratory, Lehigh University, 1983.

[11] Geological Survey of New Jersey.
Annual Report of the State Geologist,1907.

[12] Hall, J., and Nadeau, J.
Personal Correspondence, June 12, 1984.

[13] Harris, D. L. and Bodine, B. R.
Comparison of Numerical and Physical Hydraulic Models.
Technical Report, U. S. Army Corps of Engineers, Coastal Engineering Research Center, and U. S. Army Engineer Waterways Experimental Station, 1977.

[14] Henderson, F. M.
Open Channel Flow.
MacMillan Publishing Co., Inc., New York, 1966.

[15] Hinwood, J. B. and Wallis, I. G.
"Classification of Models of Tidal Waters".
Journal of the Hydraulics Division, ASCE 101:1315-1331, 1975.

[16] Horton, R. E.
"Erosional Development of Streams and Their Drainage Basins: Hydrophysical Approach to Qualitative Morphology".
Bulletin of the Geological Society of America 56:275-370, 1945.

[17] Huval, C. J. and Wintergerst, G. L.
Simplified Numerical (Lumped Parameter) Simulation.
Technical Report, U. S. Army Corps of Engineers, Coastal Engineering Research Center, 1977.

[18] Keulegan, G. H.
Tidal Flow in Entrances: Water Level Fluctuations of Basins in Communication with Seas.
Technical Report, Technical Bulletin No. 14, Committee on Tidal Hydraulics, U. S. Army Corps of Engineers, 1967.

[19] Kouwen, N., Unny, T. E., and Hill, H. M.
"Flow Retardance in Vegetated Channels".
Journal of the Irrigation and Drainage Division, ASCE 95:329-342, 1969.

[20] Lamb, H.
Hydrodynamics.
Dover Publications, Dover, New Jersey, 1932.

[21] Masch, F. D.,Brandes, R. J., and Reagan, J. D.
Numerical Simulation of Hydrodynamics, Vol. 1, App. 2.
Technical Report, U. S. Army Corps of Engineers, Coastal Engineering Research Center, and U. S. Army Engineer Waterways Experimental Station, 1977.

[22] National Geodetic Survey.
Vertical Geodetic Control Data, Quad No. 390743.

[23] National Ocean Survey.
Hourly Tidal Heights for Hereford Inlet, Great Sound, and Townsend's Inlet.
1978.

[24] National Ocean Survey.
Nautical Chart 12316: Little Egg Harbor to Cape May, New Jersey.
Washington, D. C.

[25] National Ocean Survey.
Tide Tables 1978: High and Low Water Predictions for the East Coast of North and South America.
Washington, D. C.

[26] National Ocean Survey.
Tide Tables 1983: High and Low Water Predictions for the East Coast of North and South America.
Washington, D. C.

[27] Oliveira, I. B.
"Natural Flushing Ability in Tidal Inlets".
In Proceedings of the Twelth Conference on Coastal Engineering, pages 1827-1845. ASCE, New York, 1970.

[28] Orson R., Panageoutou, W., and Leatherman, S.
"Response of Tidal Salt Marshes of the U. S. Atlantic and Gulf Coasts to Rising Sea Levels".
Journal of Coastal Research 1:29-37, 1985.

[29] Petryk, S. and Basmajian, G.
"Analysis of Flow Through Vegetation".
Journal of the Hydraulics Division, ASCE 101:871-884, 1975.

[30] Pomeroy, L. R. and Wiegert, R. C.
The Ecology of a Salt Marsh.
Springer-Verlag, New York, 1981.

[31] Ree, W. O.
"Retardance Coefficients for Row Crops in Diversion Terraces".
Transactions of the American Society of Agricultural Engineers
1:78-80, 1958.

[32] Schuepfer, F.
Project Log for Hydrodynamic Model of an Inlet-Sound System in Southern New Jersey.
Technical Report, Center for Marine and Environmental Studies, Report No. 113, 1985.

[33] Snyder, R. M.
"Tidal Hydraulics in Estuarine Channels".
Journal of the Hydraulics Division, ASCE 106:237-245, 1980.

[34] U. S. Coast and Geodetic Survey.
Avalon Quadrangle, 7.5 Minute Series (Topographic).
U. S. Geological Survey, Washington D. C.

[35] U. S. Coast and Geodetic Survey.
Stone Harbor Quadrangle, 7.5 Minute Series (Topographic).
U. S. Geological Survey, Washington D. C.

I. APPENDIX

I.1 TIDAL HYDRODYNAMIC EQUATIONS

In order to describe the tidal hydrodynamics of a tidal system, the equations of motion and the unsteady continuity equation must be solved simultaneously. Specifically, for viscous Newtonian fluids Harris and Bodine [13] modified the equations into a form better suited for tidal computations. The assumptions made in deriving the equations were that water is incompressible and that each important variable (depth, x-direction flow and y-direction flow) is averaged over a finite volume and time interval. The governing momentum equations are:

x and y momentum:

$$\underbrace{\frac{\partial q_x}{\partial t}}_{A} = \underbrace{\frac{-q_x}{d}\cdot\frac{\partial q_x}{\partial x} - \frac{q_y}{d}\frac{\partial q_x}{\partial y}}_{B} + \underbrace{\Omega q_y}_{C} - \underbrace{gd\frac{\partial h}{\partial x}}_{D} - \underbrace{gd\,S_{ex}}_{E} + \underbrace{K\,V_w^2\cos\psi}_{F} \quad (1)$$

$$\underbrace{\frac{\partial q_y}{\partial t}}_{A} = \underbrace{\frac{-q_x}{d}\cdot\frac{\partial q_y}{\partial x} - \frac{q_y}{d}\frac{\partial q_y}{\partial y}}_{B} - \underbrace{\Omega q_x}_{C} - \underbrace{gd\frac{\partial h}{\partial y}}_{D} - \underbrace{gd\,S_{ey}}_{E} + \underbrace{K\,V_w^2\sin\psi}_{F} \quad (2)$$

Correspondingly, the continuity equation is

$$\underbrace{\frac{\partial h}{\partial t}}_{G} = \underbrace{-\frac{\partial q_x}{\partial x} - \frac{\partial q_y}{\partial y}}_{H} + \underbrace{(r - e)}_{I} \quad (3)$$

where Ω is the Coriolis parameter, S_{ex} and S_{ey} represent the bottom friction, K is a wind stress coefficient, V_w is the wind speed at an elevation above the water surface, ψ is the angle between the wind

velocity vector and the x-axis, and all other parameters are as defined in Section 2.1.

In Eqs. (1) and (2), the terms labeled A describe the change in flow as a function of time. Terms B express convective acceleration and depend on the motion of the particle in space. Terms C are the Coriolis acceleration terms and are due to the use of a rotating coordinate system fixed to the earth. Terms D, the gravity terms, represent the surface gradient which drives the flow. Terms E describe the change in momentum due to bottom friction, and terms F account for wind stresses. In the continuity equation, term G expresses the temporal variation of the water surface, terms H describe the horizontal flow of water as a function of space, and terms I represent precipitation and evaporation.

In the explicit solution method used to solve the equations, computations of flows and water levels are performed at alternate time levels. The following superscripts are used to describe particular time levels:

t-1 : previous time level

t : current time level

t+1 : next time level

t+2 : two subsequent levels

Centered finite difference approximations can be used to approximate the derivatives in Eqs. (1), (2), and (3). The terms in the equation of motion for the x direction can be written as follows:

term A:

$$\frac{\partial q_x}{\partial t} = \frac{q_x^{t+1}(i,j) - q_x^{t-1}(i,j)}{\Delta t} \qquad (4)$$

terms B:

$$\frac{q_x}{d}\frac{\partial q_x}{\partial x} = \frac{q_x^{t+1}(i,j)}{d_x} \cdot \frac{q_x^{t-1}(i+1,j) - q_x^{t-1}(i-1,j)}{2\,\Delta x} \qquad (5)$$

where

$$d_x = \frac{d^t(i,j) + d^t(i+1,j)}{2} \qquad (6)$$

$$\frac{q_y}{d} \cdot \frac{\partial q_x}{\partial y} = \frac{\bar{q}_y}{d_x} \cdot \frac{q_x^{t-1}(i,j+1) - q_x^{t-1}(i,j-1)}{2\,\Delta y} \qquad (7)$$

where

$$\bar{q}_y = \frac{1}{4}\left[q_y^{t-1}(i,j) + q_y^{t-1}(i+1,j) + q_y^{t-1}(i,j-1) + q_y^{t-1}(i+1,j-1)\right] \qquad (8)$$

term C:

$$-\Omega q_y = -\Omega \bar{q}_y \qquad (9)$$

term D:

$$-gd\frac{\partial h}{\partial x} = -gd_x \cdot \frac{[h^t(i+1,j) - h^t(i,j)]}{\Delta x} \qquad (10)$$

term E:

$$gd\,S_{ex} = \frac{g \cdot n_x^2}{(2.21) \cdot d_x^{4/3}} \cdot [q_x^{t+1}(i,j) \cdot \overline{q/d}] \qquad (11)$$

where

$$n_x = \frac{n(i,j) + n(i+1,j)}{2} \tag{12}$$

and

$$\overline{q/d} = \frac{[(q_x^{t-1}(i,j))^2 + (\bar{q}_y)^2]^{1/2}}{d_x} \tag{13}.$$

In these relations, the only unknown is q_x^{t+1}, the x-direction flow at the next time step. By combining the terms as in Eq. (1) and solving for q_x^{t+1}, the following explicit relation is obtained:

$$\begin{aligned} q_x^{t+1}(i,j) = [q_x^{t-1}(i,j) &- \Delta t \cdot \frac{\bar{q}_y}{d_x} \cdot \frac{q_x^{t-1}(i,j+1) - q_x^{t-1}(i,j-1)}{2\,\Delta y} \\ &+ \Delta t\, \Omega \bar{q}_y - \Delta t\, g d_x \frac{h^t(i+1,j) - h^t(i,j)}{\Delta x} \\ &+ \Delta t\, K\, V_w^2 \cos\psi\,]/C_{fx} \end{aligned} \tag{14}$$

where

$$C_{fx} = 1 + \frac{\Delta t}{d_x} \cdot \frac{q_x^{t-1}(i+1,j) - q_x^{t-1}(i-1,j)}{2\,\Delta x} + \frac{g n_x^2\, \Delta t}{2.21\, d_x^{4/3}} [\overline{q/d}] \tag{15}$$

Similarly, application of finite differences to the y momentum equation produces

$$q_y^{t+1}(i,j) = [q_y^{t-1}(i,j) - \Delta t \frac{\bar{q}_x}{d_y} \cdot \frac{q_y^{t-1}(i+1,j) - q_y^{t-1}(i-1,j)}{2\,\Delta x}$$

$$- \Delta t\, g\, \overline{q/d}\, n_y - \Delta t\, g\, d_y \frac{h^t(i,j+1) - h^t(i,j)}{\Delta y}$$

$$+ \Delta t\, K\, v_w^2 \sin\psi]/C_{fy} \qquad (16)$$

where

$$C_{fy} = 1 + \frac{\Delta t}{d_y} \cdot \frac{q_y^{t-1}(i,j+1) - q_y^{t-1}(i,j-1)}{2\,\Delta y} + \frac{g n_y^2\, \Delta t}{2.21 \cdot d_y^{4/3}} \overline{[q/d]} \qquad (17)$$

$$d_y = \frac{d^t(i,j) + d^t(i,j+1)}{2} \qquad (18)$$

$$\bar{q}_x = \frac{1}{4}[q_x^{t-1}(i,j) + q_x^{t-1}(i,j+1) + q_x^{t-1}(i-1,j) + q_x^{t-1}(i-1,j+1)] \qquad (19)$$

$$n_y = \frac{n(i,j) + n(i,j+1)}{2} \qquad (20)$$

$$\overline{q/d} = \frac{[(\bar{q}_x)^2 + (q_y^{t-1}(i,j))^2]^{1/2}}{d_y} \qquad (21)$$

The third unknown, the water level h at time t+2, can be

calculated from the continuity equation and from the flows q_x^{t+1} and q_y^{t+1} just computed. For Eq. (3), the derivatives are approximated as follows:

$$\frac{\partial h}{\partial t} = \frac{h^{t+2}(i,j) - h^{t}(i,j)}{\Delta t} \tag{22}$$

$$\frac{\partial q_x}{\partial x} = \frac{q_x^{t+1}(i,j) - q_x^{t+1}(i-1, j)}{\Delta x} \tag{23}$$

$$\frac{\partial q_y}{\partial y} = \frac{q_y^{t+1}(i,j) - q_y^{t+1}(i,j-1)}{\Delta y} \tag{24}$$

By combining these difference terms and solving for h^{t+2}, the following expression is obtained:

$$h(i,j)^{t+2} = h^{t}(i,j) - \Delta t \frac{q_x^{t+1}(i,j) - q_x^{t+1}(i-1,j)}{\Delta x} - \Delta t \frac{q_y^{t+1}(i,j) - q_y^{t+1}(i,j-1)}{\Delta y} + \Delta t\,(r - e) \tag{25}$$

Thus it can be seen that Eqs. (14) and (16) are used to obtain q_x and q_y at time level t+1. Then Eq. (25) is solved for h at the next time level, t+2. Using h^{t+2}, q_x^{t+3} and q_y^{t+3} are then obtained, and so on. Consequently, the flows and water levels are always determined one time step apart, although results are presented only at even time levels. As long as time steps are small, determining flows and time levels one time step apart will not cause significant error.

Eqs. (14), (16), and (25) were formulated for an open water cell that was free to communicate with its neighbors. For situations where flow between cells is prohibited, such as at impermeable barriers, the convective acceleration terms must be reformulatd to provide a more accurate expression for the flow gradients. For instance, the expression used in Eq. (5), $[q_x^{t-1}(i+1,j) - q_x^{t-1}(i-1,j)]$, would be incorrect at a vertical impermeable boundary, since the cells (i+1,j) and (i-1,j) would not be linked by a continuous water surface. For the cell on the left side of the boundary, a more meaningful approximation of the gradient would be $[q_x(i,j) - q_x(i,j-1)]/\Delta y$.

The reformulation of the convective terms is done by the convective flagging scheme shown in Fig. 3-8. The two digits vary from 1 to 4, the first digit representing the x direction and the second the y direction. The flags are as follows:

Flag Value	Type of Approximation
1	Centered Difference
2	Zero
3	Forward Difference
4	Backward Difference

The following modified finite differences are used:

Flag — Computation

1: $$\frac{q_y}{d} \cdot \frac{\partial q_x}{\partial y} = \frac{\bar{q}_y}{d_x} \cdot \frac{q_x^{t-1}(i,j+1) - q_x^{t-1}(i,j-1)}{2\,\Delta y} \qquad (26)$$

2: $$\frac{q_y}{d} \cdot \frac{\partial q_x}{\partial y} = 0. \qquad (27)$$

3: $$\frac{q_y}{d} \cdot \frac{\partial q_x}{\partial y} = \frac{\bar{q}_y}{d_x} \cdot \frac{q_x^{t-1}(i,j+1) - q_x^{t-1}(i,j)}{\Delta y} \qquad (28)$$

4: $$\frac{q_y}{d} \cdot \frac{\partial q_x}{\partial y} = \frac{\bar{q}_y}{d_x} \cdot \frac{q_x^{t-1}(i,j) - q_x^{t-1}(i,j-1)}{\Delta y} \qquad (29)$$

y direction

Flag — Computation

1: $$\frac{q_x}{d} \cdot \frac{\partial q_y}{\partial x} = \frac{\bar{q}_x}{d_y} \cdot \frac{q_y^{t-1}(i+1,j) - q_y^{t-1}(i-1,j)}{2\,\Delta x} \qquad (30)$$

2: $$\frac{q_x}{d} \cdot \frac{\partial q_y}{\partial x} = 0. \qquad (31)$$

3: $$\frac{q_x}{d} \cdot \frac{\partial q_y}{\partial x} = \frac{\bar{q}_x}{d_y} \cdot \frac{q_y^{t-1}(i+1,j) - q_y^{t-1}(i,j)}{\Delta x} \qquad (32)$$

4: $$\frac{q_x}{d} \cdot \frac{\partial q_y}{\partial x} = \frac{\bar{q}_x}{d_y} \cdot \frac{q_y^{t-1}(i,j) - q_y^{t-1}(i,j-1)}{\Delta x} \qquad (33)$$

I.2 FLOW MAPS FOR SPRING TIDE CALIBRATION

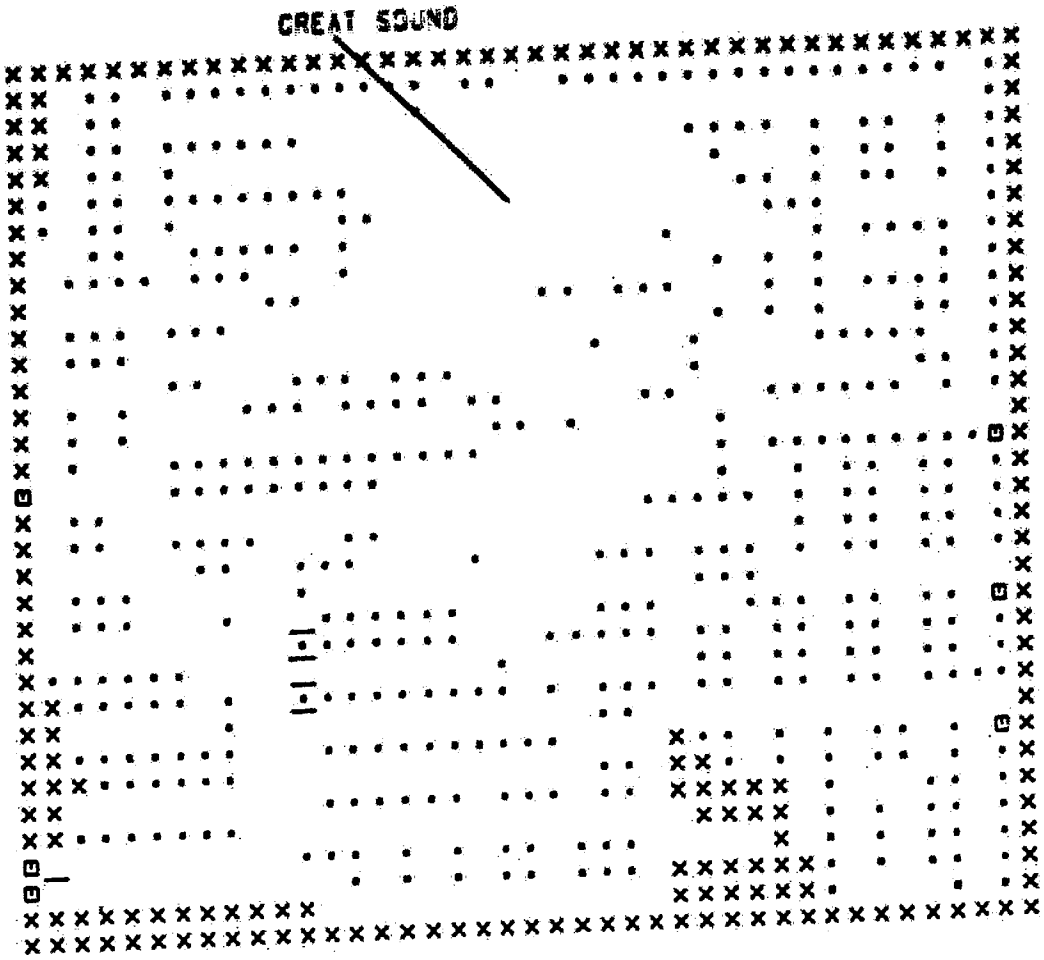

FLOW PATTERN FOR GREAT SOUND
0800 HRS 24 MAY 1982
X - LAND CELL
* - INUNDATION CELL
⊡ - FORCING CELL
— - NO FLOW BOUNDARY
SCALE - 74000. CFS / INCH

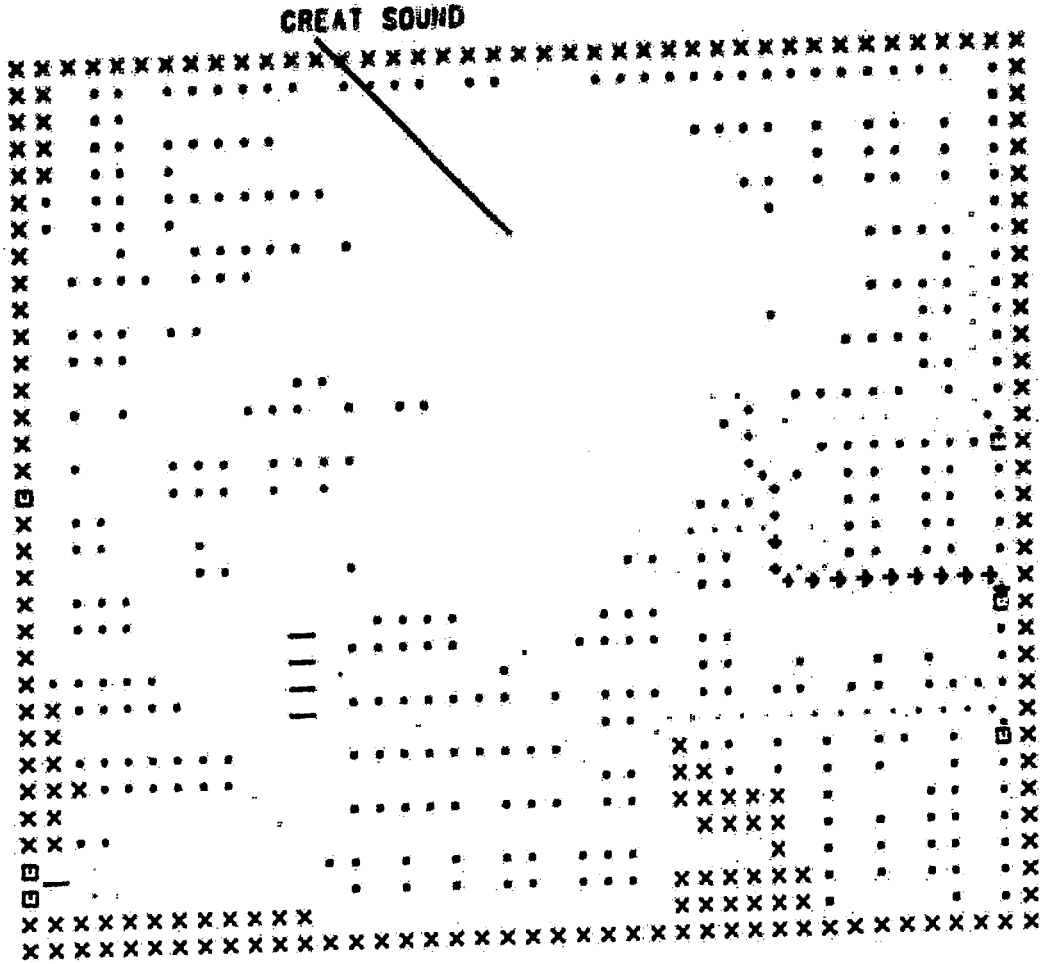

FLOW PATTERN FOR GREAT SOUND
0900 HRS 24 MAY 1983
X - LAND CELL
* - INUNDATION CELL
⊡ - FORCING CELL
— - NO FLOW BOUNDARY
SCALE - 74000. CFS / INCH

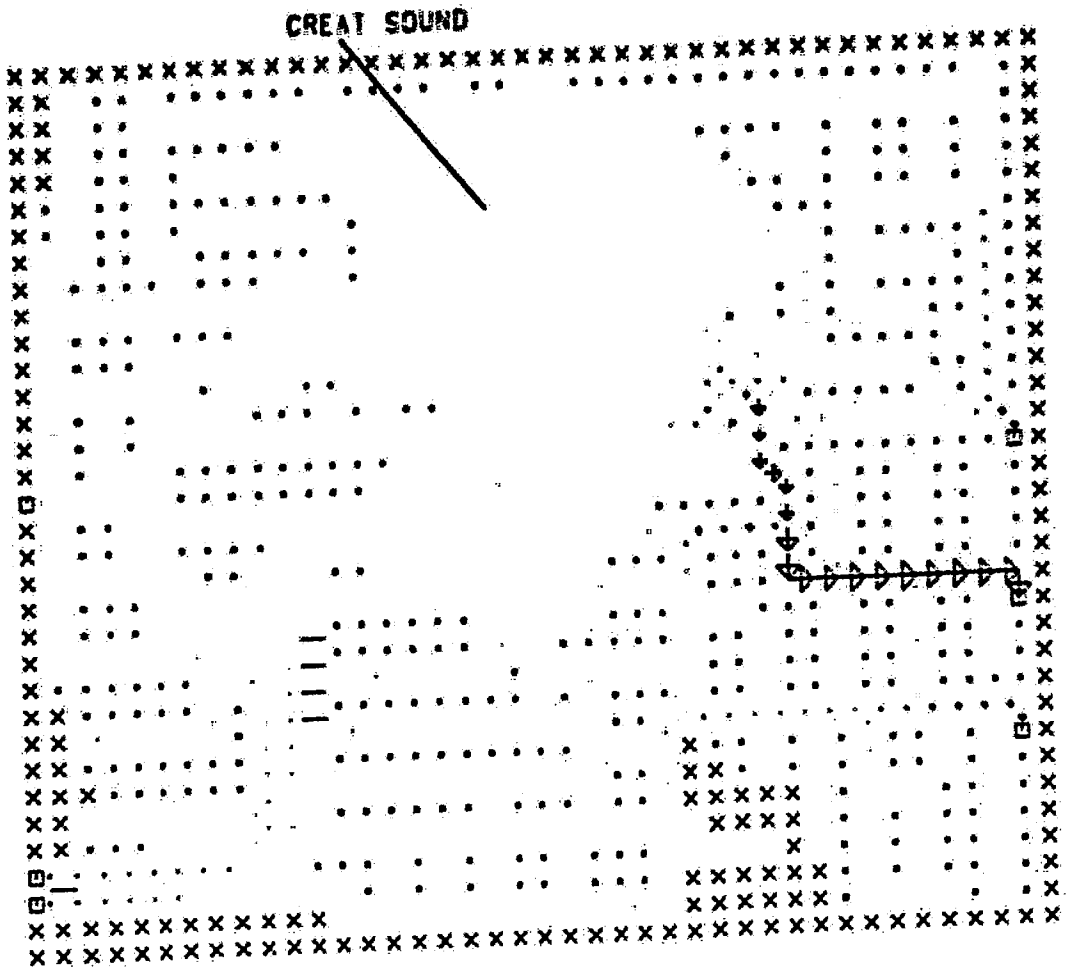

FLOW PATTERN FOR GREAT SOUND
1000 HRS 24 MAY 1983
X - LAND CELL
* - INUNDATION CELL
E - FORCING CELL
— - NO FLOW BOUNDARY
SCALE - 74000. CFS / INCH

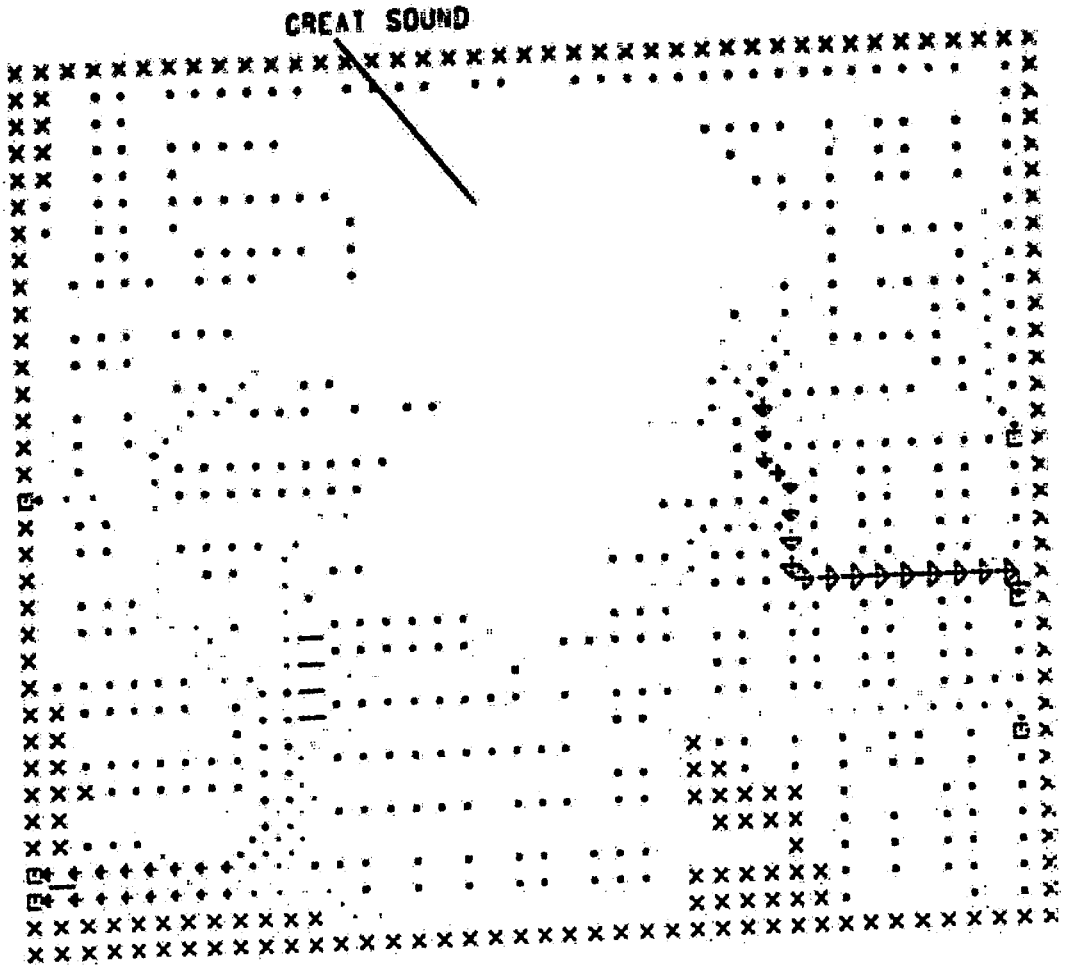

FLOW PATTERN FOR GREAT SOUND
1100 HRS 24 MAY 1983
X - LAND CELL
⁂ - INUNDATION CELL
⊟ - FORCING CELL
— - NO FLOW BOUNDARY
SCALE - 74000. CFS / INCH

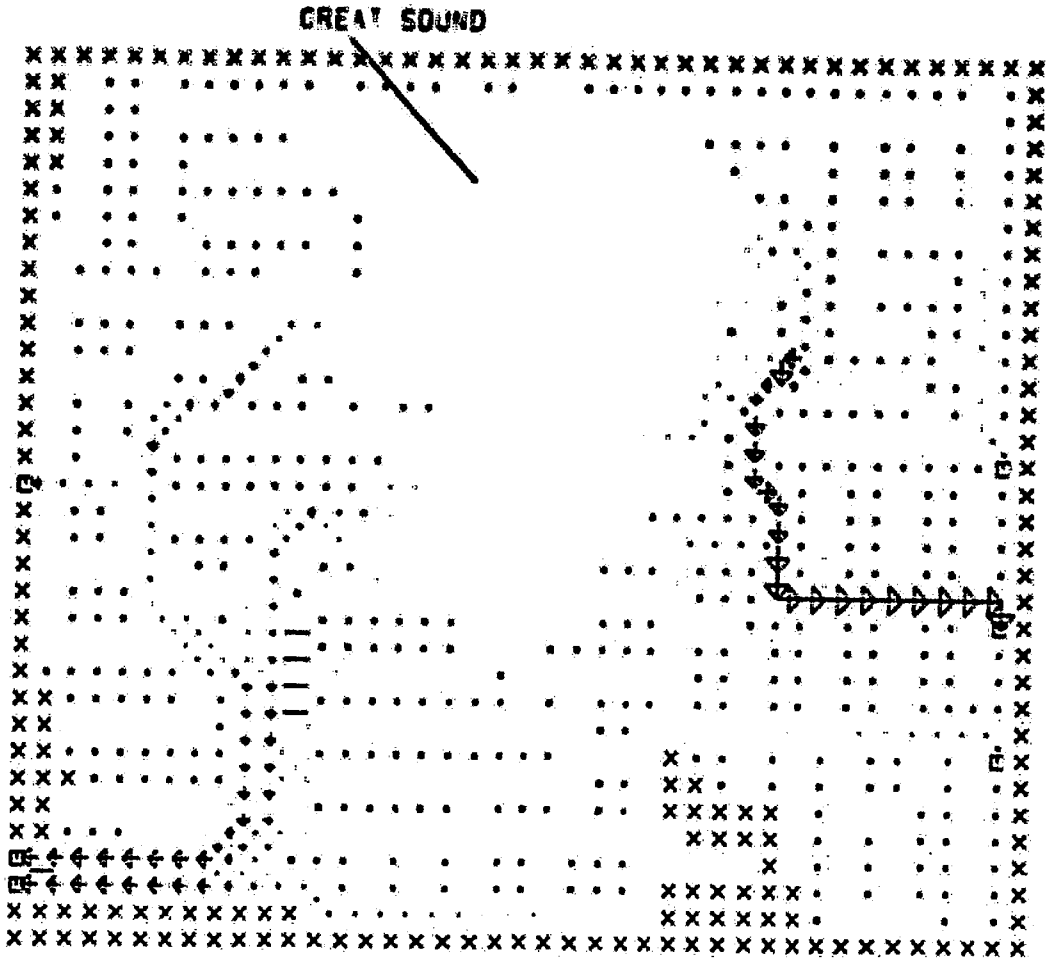

FLOW PATTERN FOR GREAT SOUND
1200 HRS 24 MAY 1983
X - LAND CELL
X - INUNDATION CELL
⊞ - FORCING CELL
– - NO FLOW BOUNDARY
SCALE - 74000. CFS / INCH

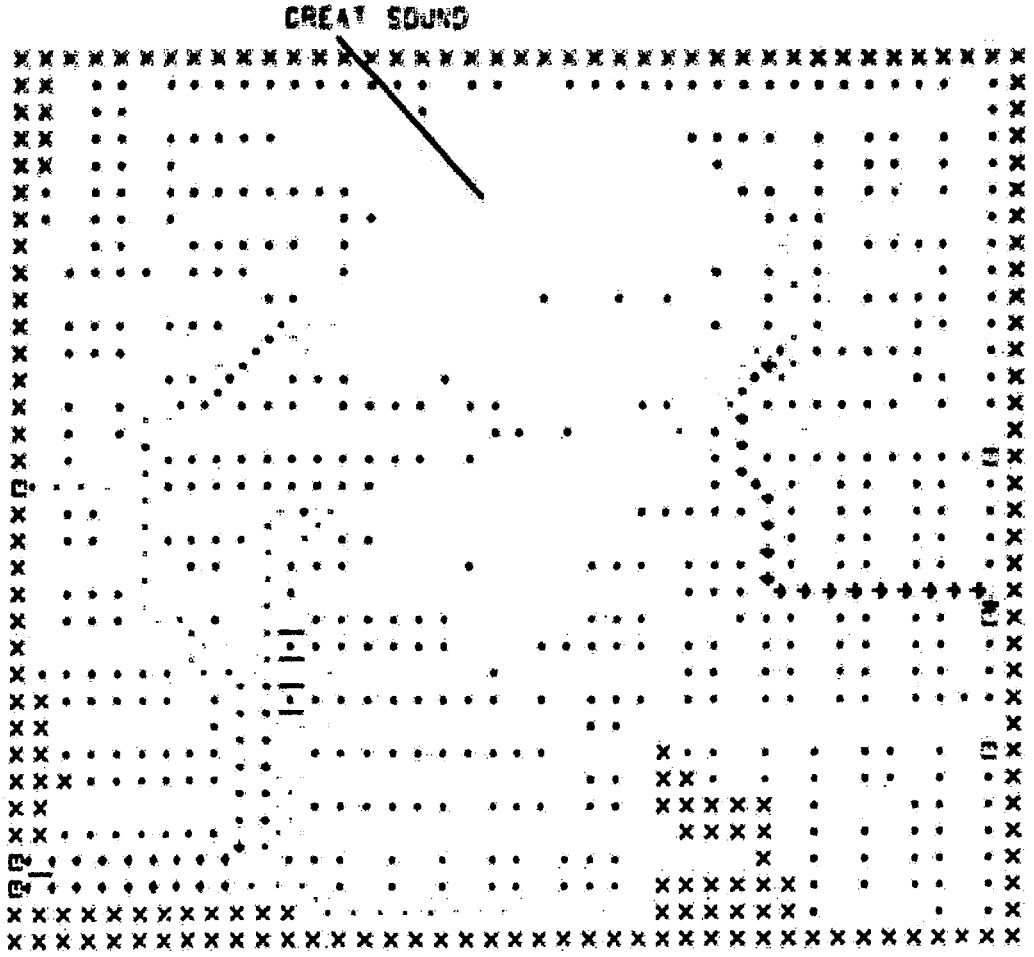

FLOW PATTERN FOR GREAT SOUND
1300 HRS 24 MAY 1983
X - LAND CELL
* - INUNDATION CELL
□ - FORCING CELL
— - NO FLOW BOUNDARY
SCALE - 74000. CFS / INCH

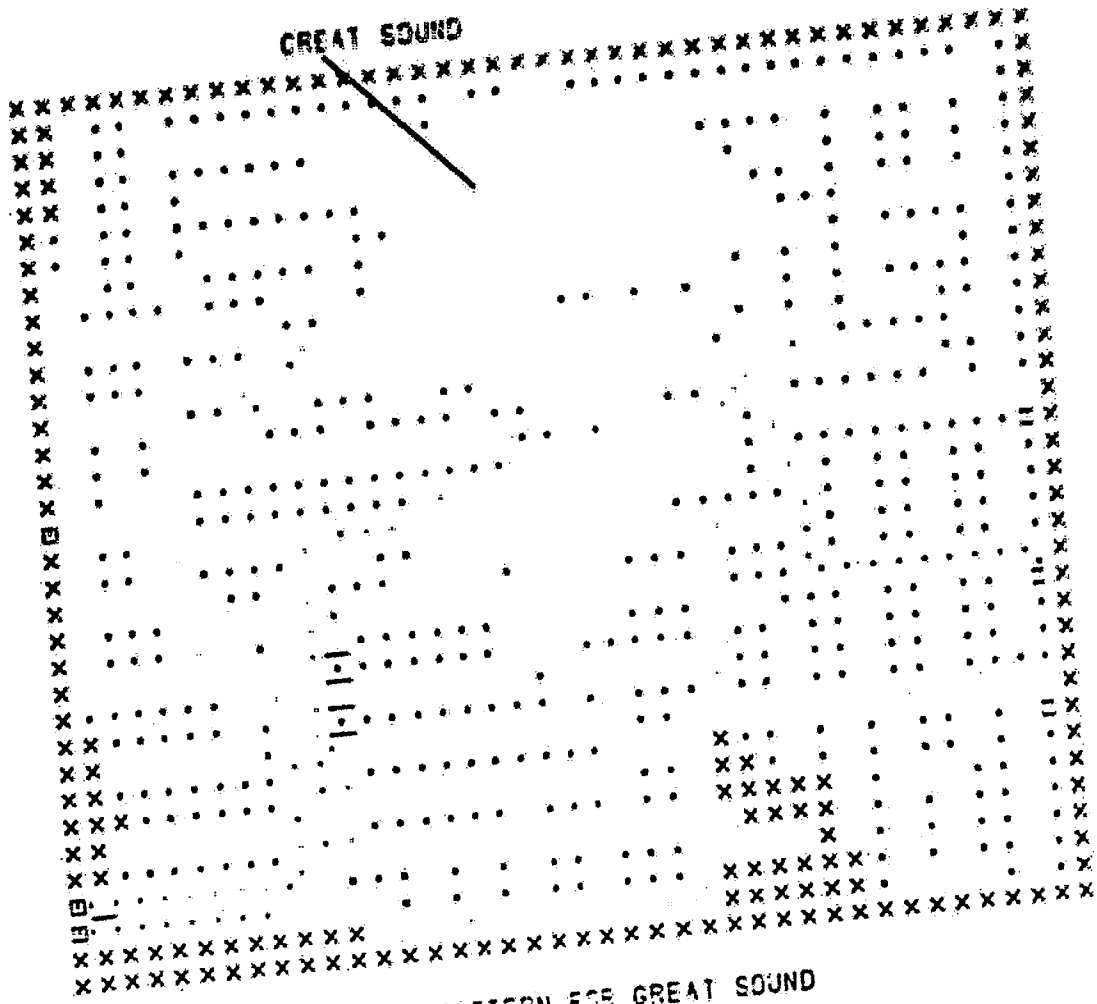

FLOW PATTERN FOR GREAT SOUND
1400 HRS 24 MAY 1963
X - LAND CELL
⋇ - INUNDATION CELL
E - FORCING CELL
— - NO FLOW BOUNDARY
SCALE - 74000. CFS / INCH

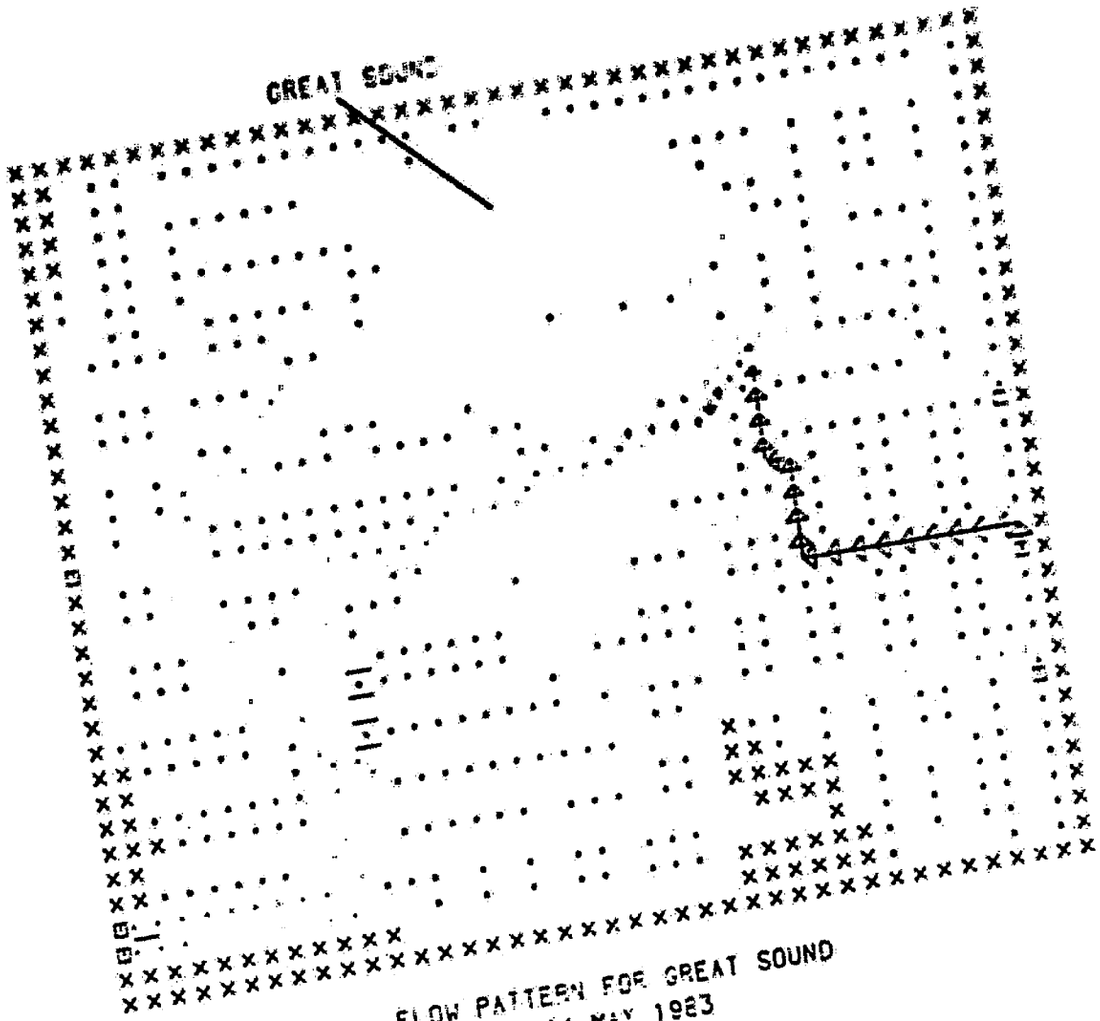

FLOW PATTERN FOR GREAT SOUND
1500 HRS 24 MAY 1983
X - LAND CELL
X - INUNDATION CELL
□ - FORCING CELL
— - NO FLOW BOUNDARY
SCALE - 74000. CFS / INCH

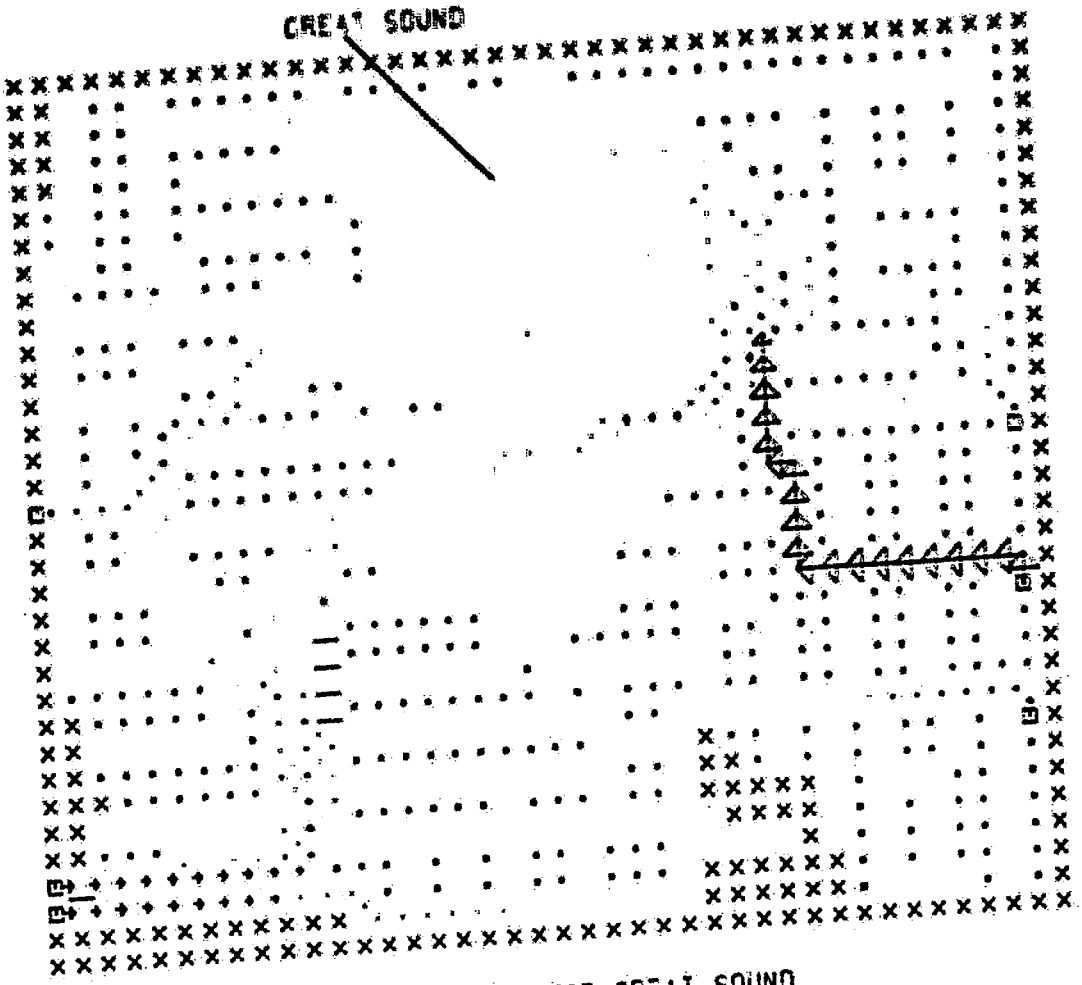

FLOW PATTERN FOR GREAT SOUND
1600 HRS 24 MAY 1953
X - LAND CELL
X - INUNDATION CELL
⊡ - FORCING CELL
— - NO FLOW BOUNDARY
SCALE - 74000. CFS / INCH

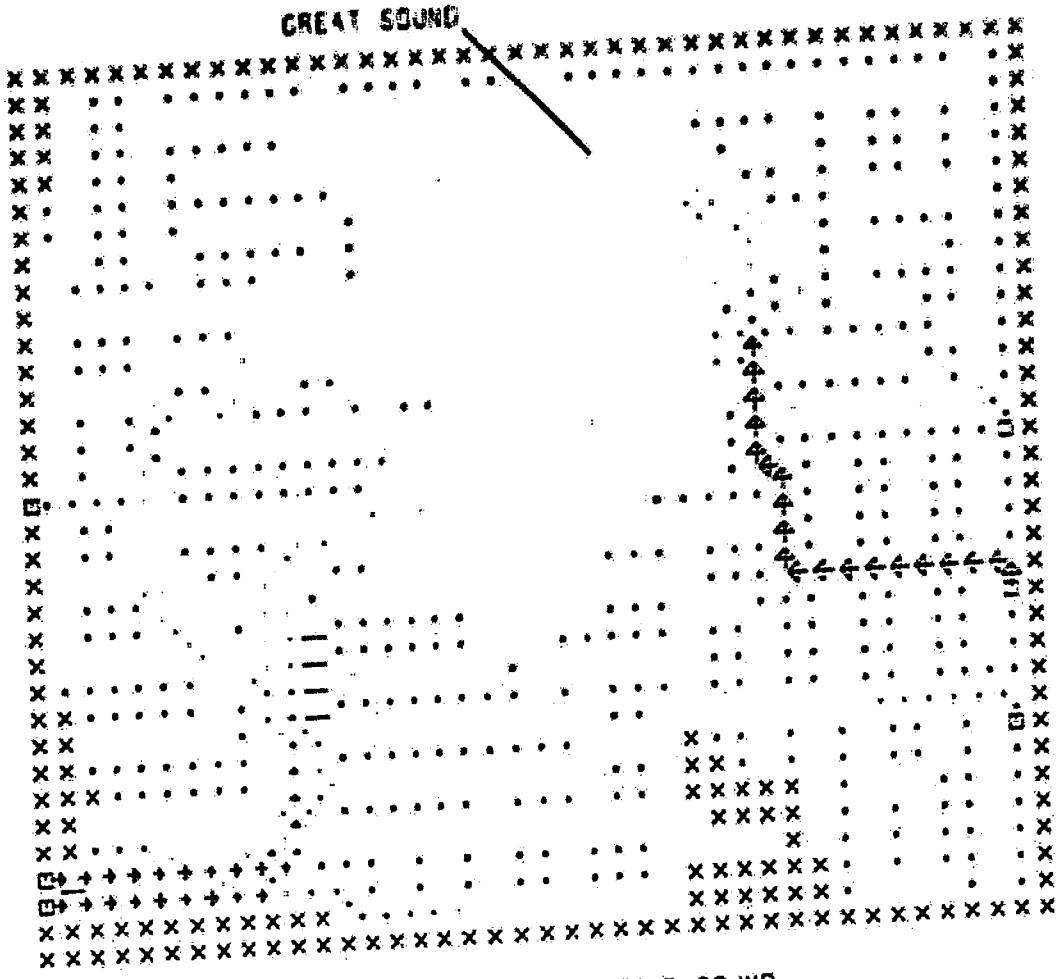

FLOW PATTERN FOR GREAT SOUND
1700 HRS 24 MAY 1983
X - LAND CELL
* - INUNDATION CELL
□ - FORCING CELL
— - NO FLOW BOUNDARY
SCALE - 74000. CFS / INCH

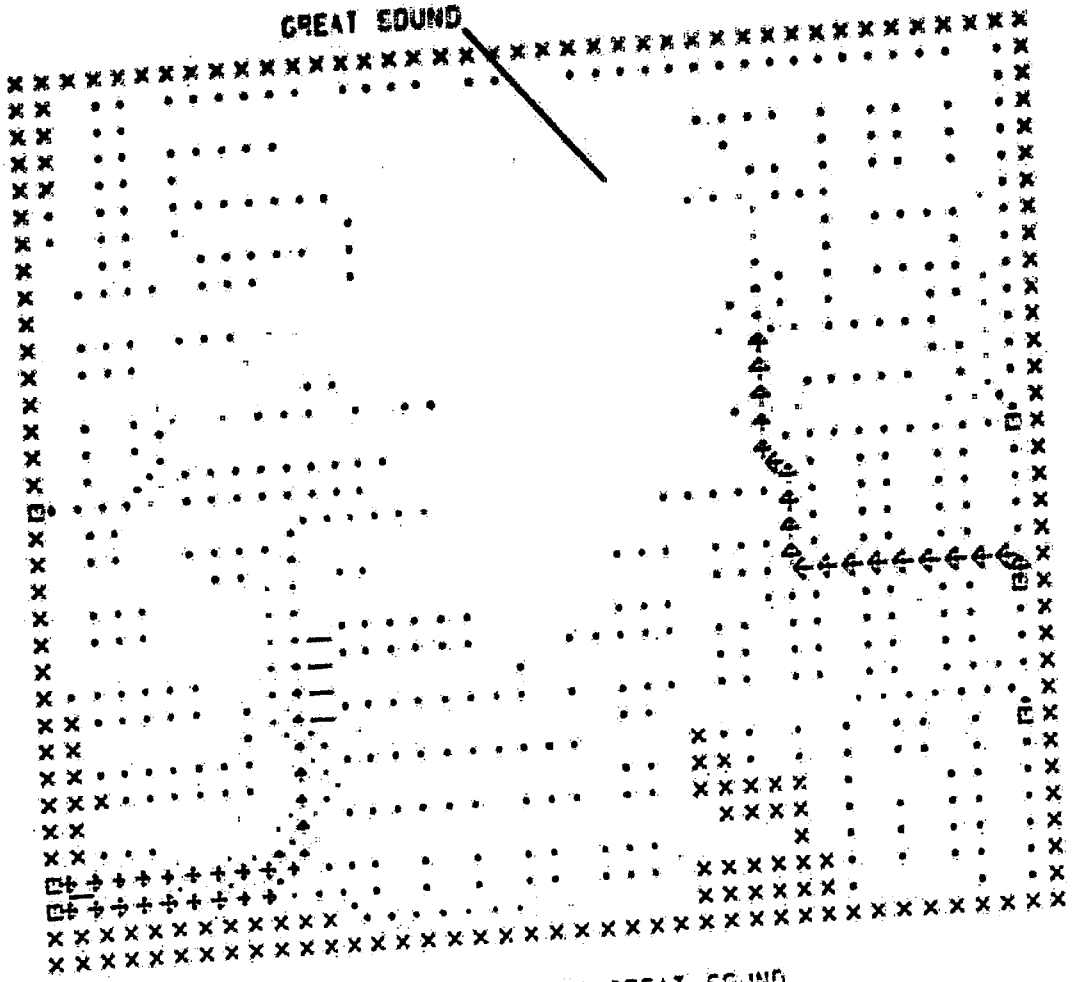

FLOW PATTERN FOR GREAT SOUND
1600 HRS 24 MAY 1981
X - LAND CELL
X - INUNDATION CELL
= - FORCING CELL
= - NO FLOW BOUNDARY
SCALE - 74000. CFS / INCH

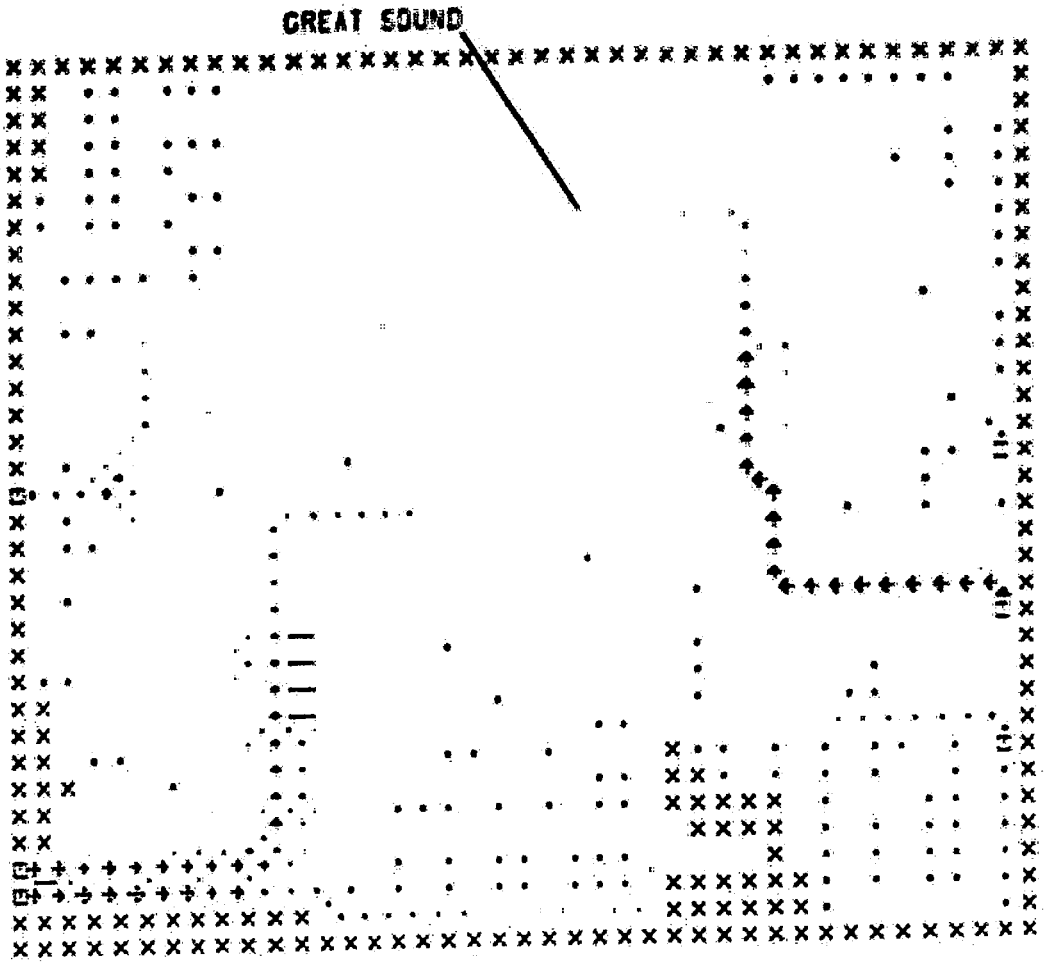

FLOW PATTERN FOR GREAT SOUND
1900 HRS 24 MAY 1983
X - LAND CELL
x - INUNDATION CELL
⊞ - FORCING CELL
— - NO FLOW BOUNDARY
SCALE - 74000. CFS / INCH

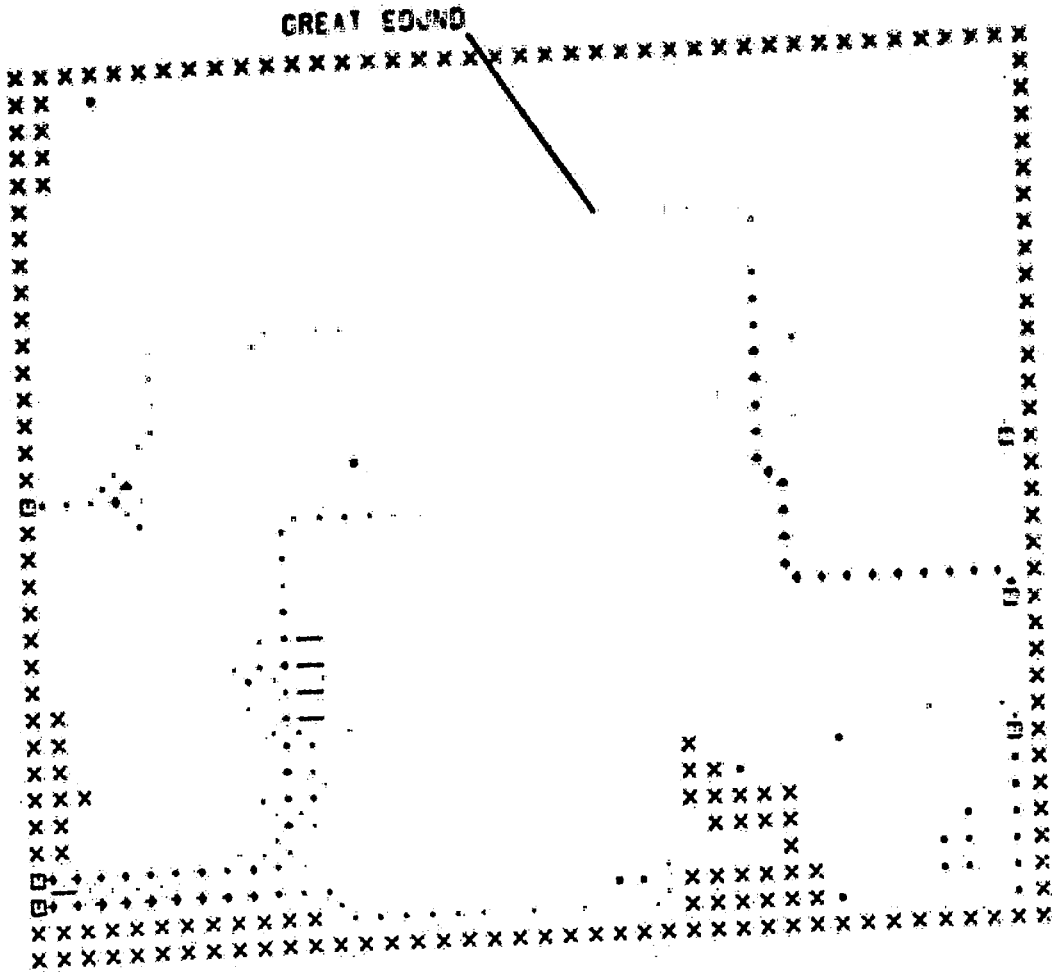

FLOW PATTERN FOR GREAT SOUND
2000 HRS 24 MAY 1983
X - LAND CELL
x - INUNDATION CELL
B - FORCING CELL
— - NO FLOW BOUNDARY
SCALE - 24000. CFS / INCH

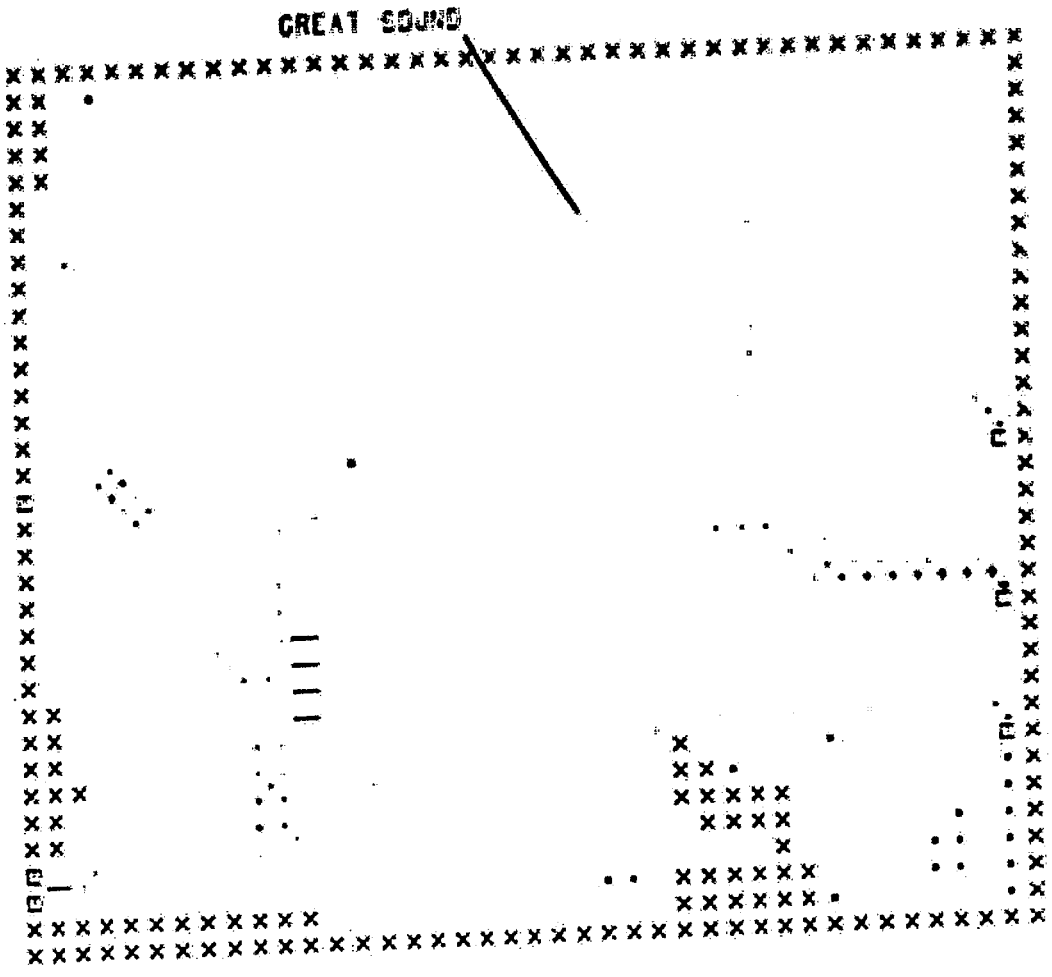

FLOW PATTERN FOR GREAT SOUND
2100 HRS 24 MAY 1983
X - LAND CELL
* - INUNDATION CELL
□ - FORCING CELL
— - NO FLOW BOUNDARY
SCALE - 74000. CFS / INCH

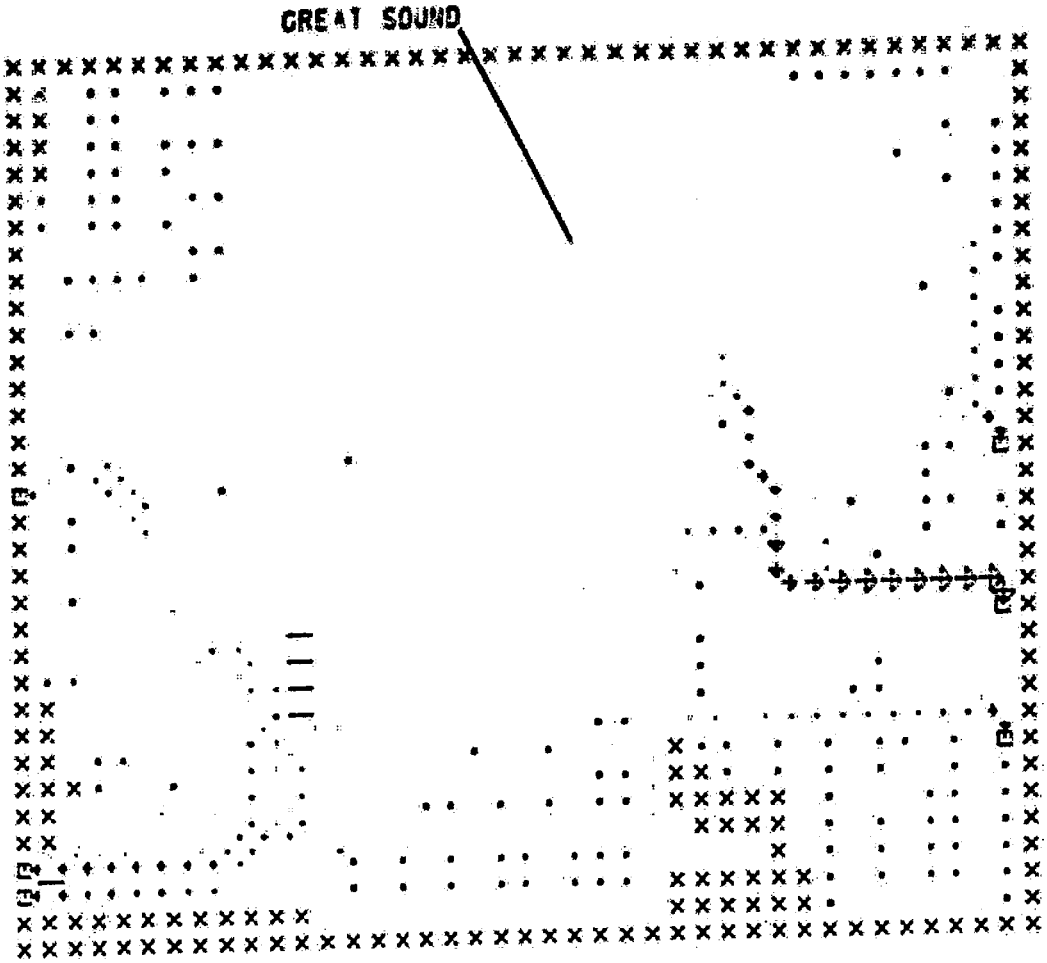

FLOW PATTERN FOR GREAT SOUND
2200 HRS 24 MAY 1983
X - LAND CELL
X - INUNDATION CELL
⊡ - FORCING CELL
— - NO FLOW BOUNDARY
SCALE - 74000. CFS / INCH

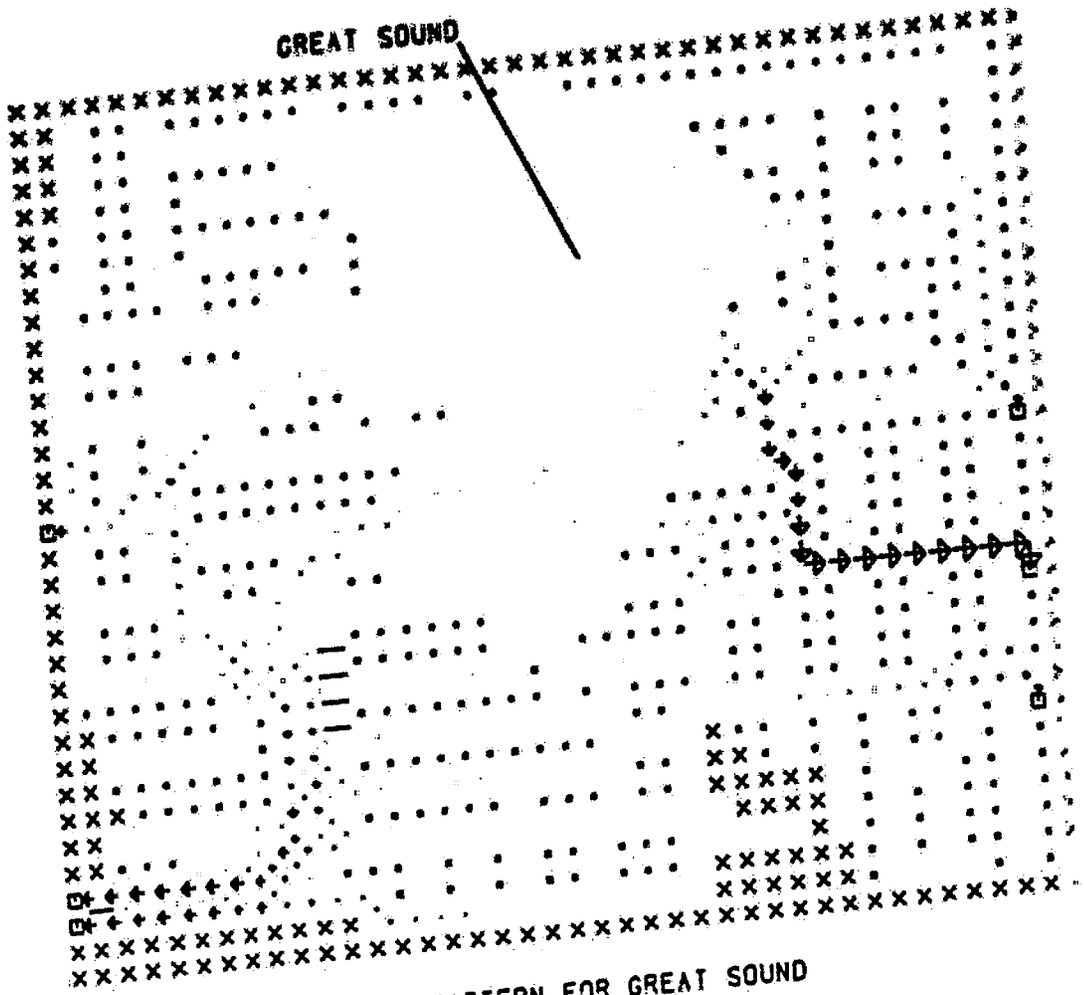

FLOW PATTERN FOR GREAT SOUND
2300 HRS 24 MAY 1983
X - LAND CELL
* - INUNDATION CELL
□ - FORCING CELL
— - NO FLOW BOUNDARY
SCALE - 74000. CFS / INCH

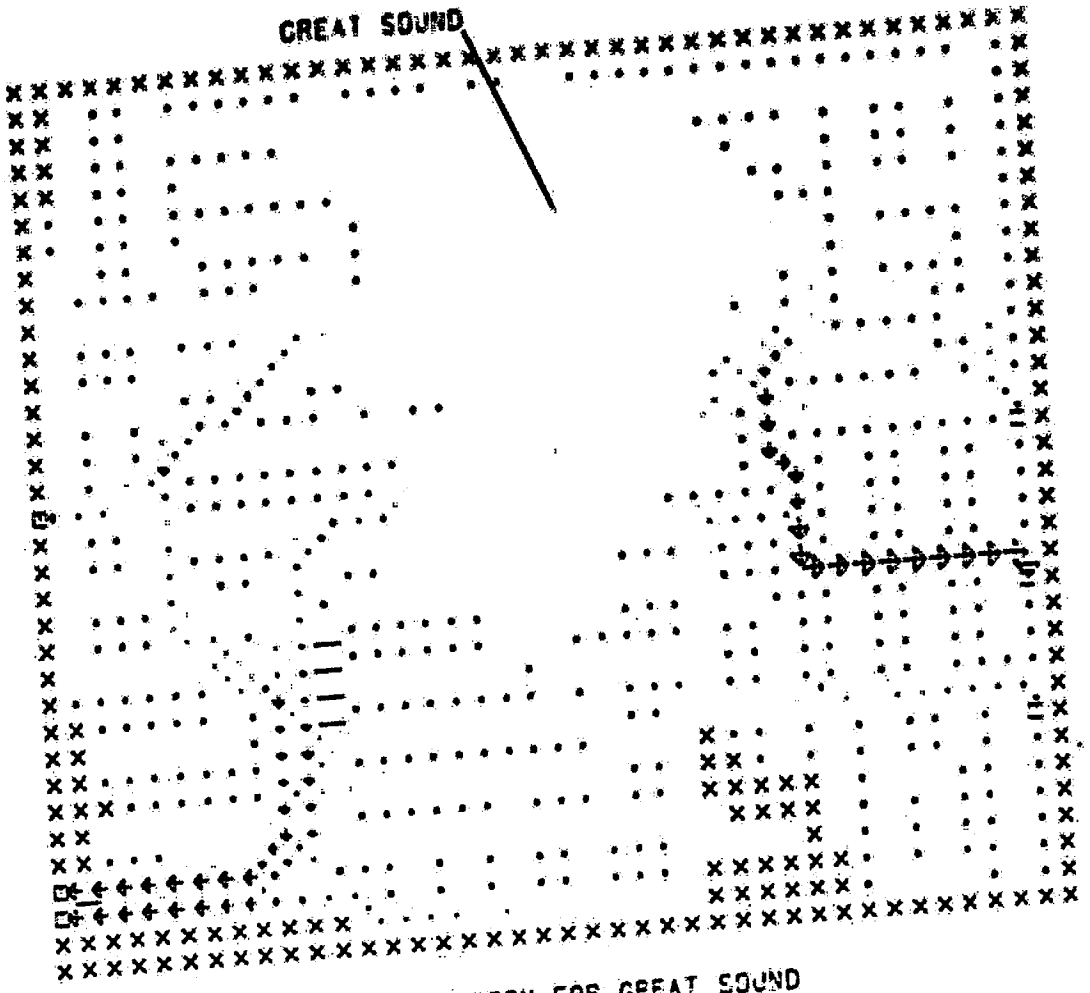

FLOW PATTERN FOR GREAT SOUND
2400 HRS 24 MAY 1963
X - LAND CELL
* - INUNDATION CELL
□ - FORCING CELL
— - NO FLOW BOUNDARY
SCALE - 74000. CFS / INCH

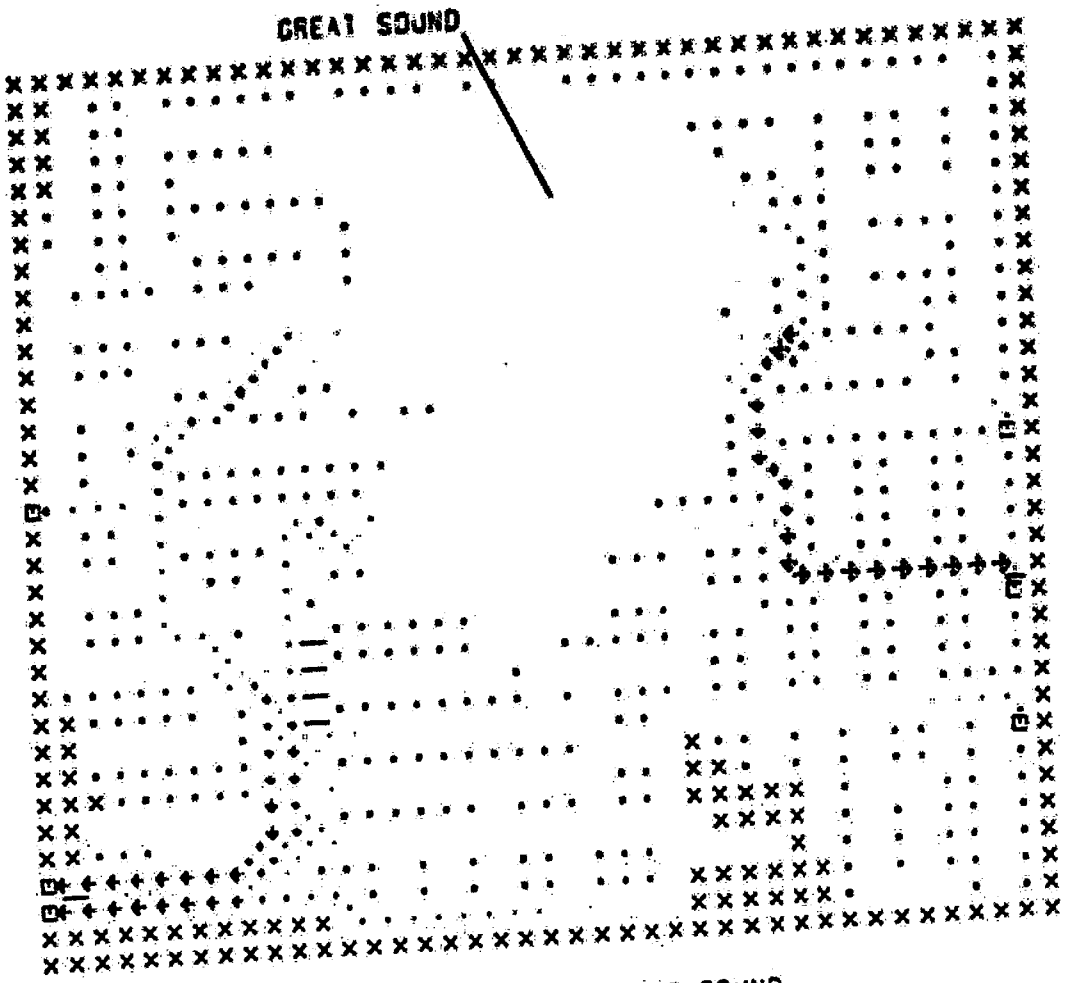

FLOW PATTERN FOR GREAT SOUND
0100 HRS 25 MAY 1983
X - LAND CELL
X - INUNDATION CELL
⊡ - FORCING CELL
— - NO FLOW BOUNDARY
SCALE - 74000. CFS / INCH

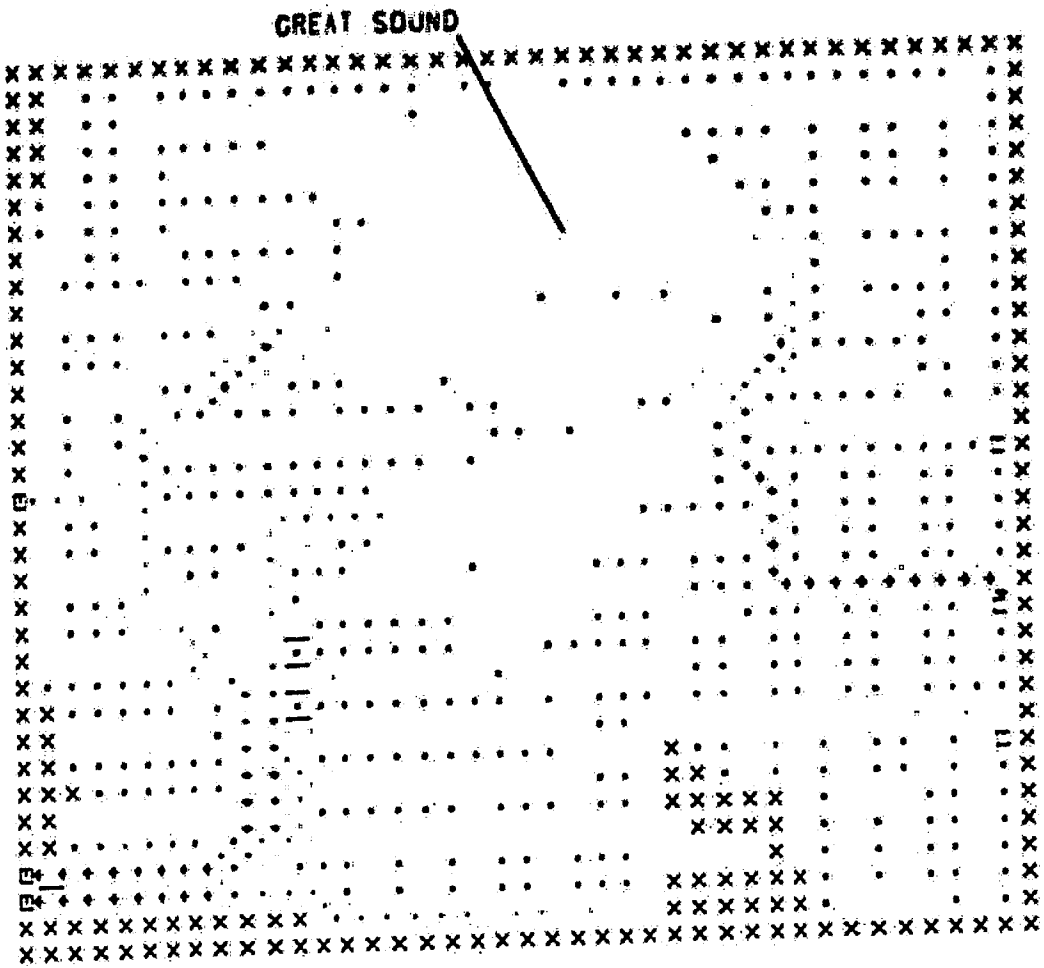

FLOW PATTERN FOR GREAT SOUND
0200 HRS 25 MAY 1983
X - LAND CELL
* - INUNDATION CELL
⊡ - FORCING CELL
— - NO FLOW BOUNDARY
SCALE - 74000. CFS / INCH

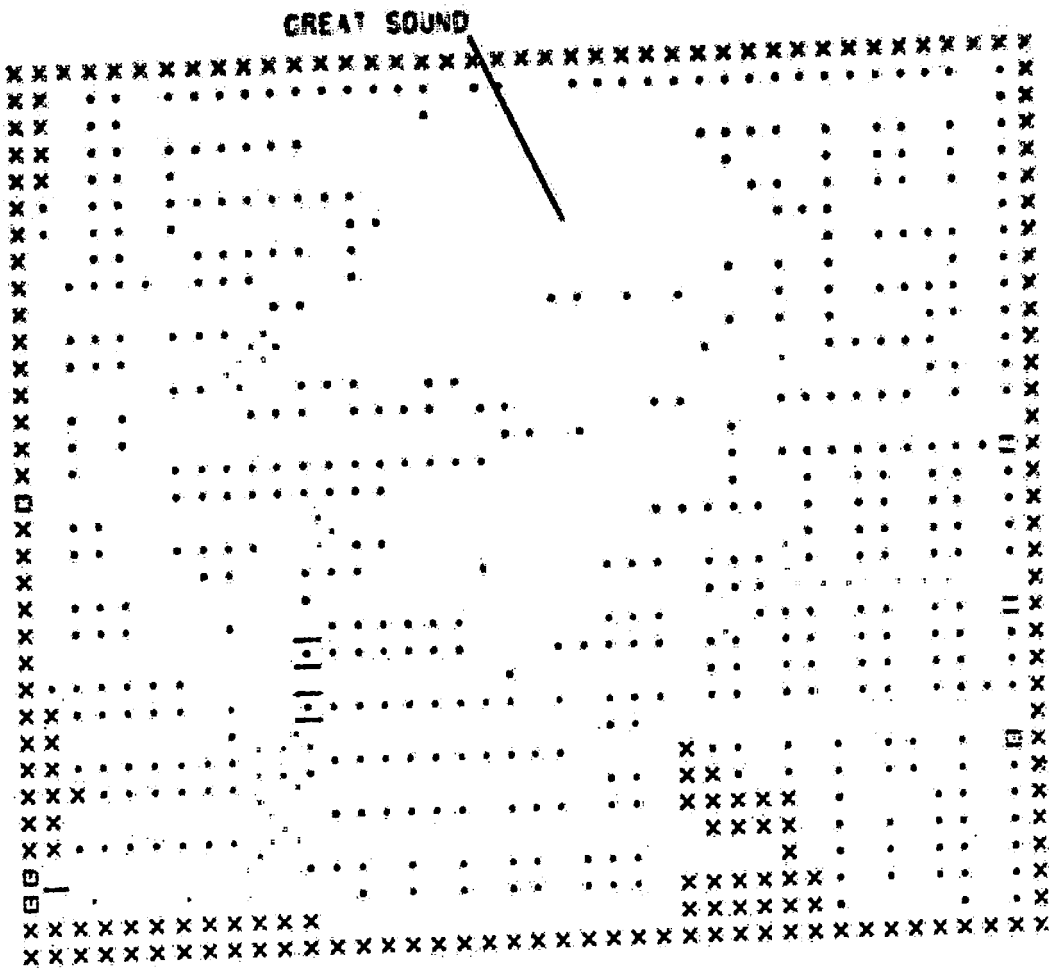

FLOW PATTERN FOR GREAT SOUND
0300 HRS 25 MAY 1963
X - LAND CELL
⊠ - INUNDATION CELL
⊡ - FORCING CELL
— - NO FLOW BOUNDARY
SCALE - 74000. CFS / INCH

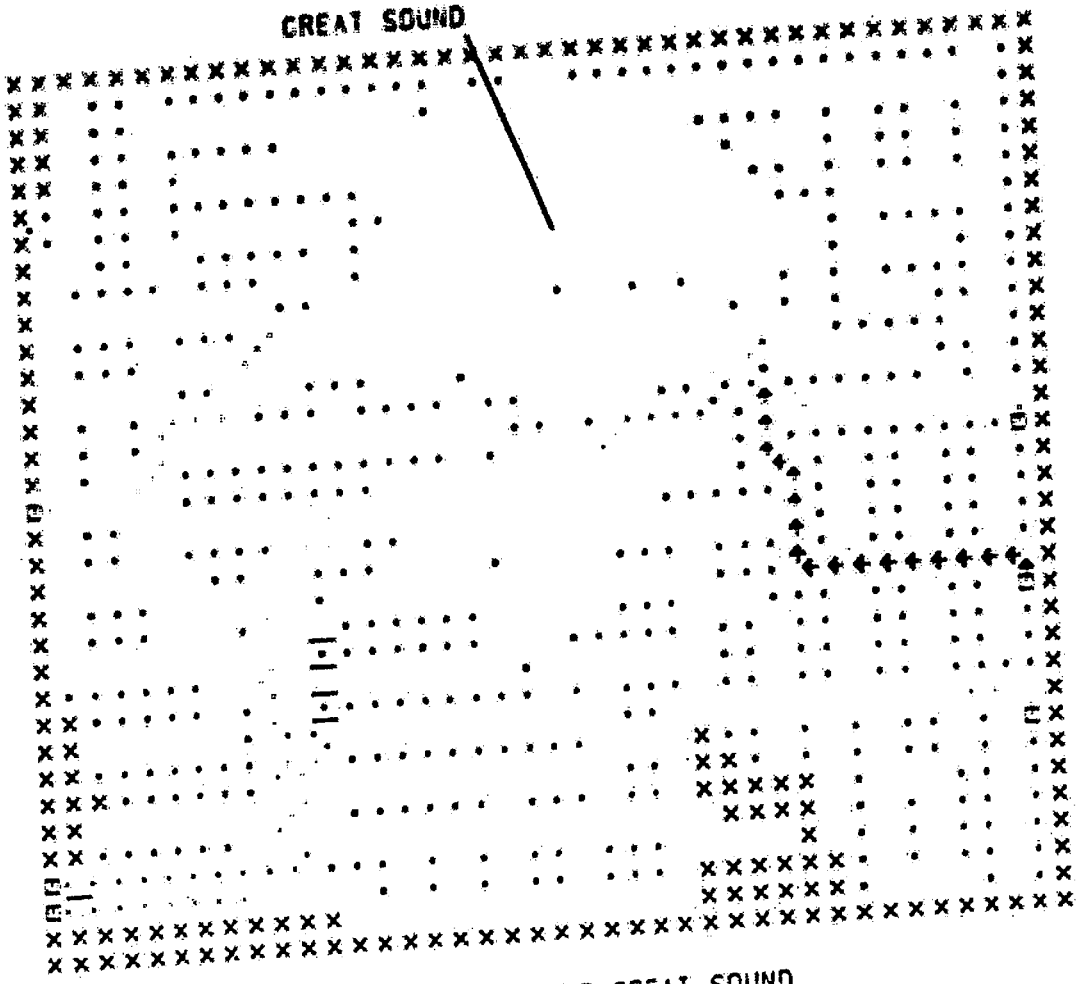

FLOW PATTERN FOR GREAT SOUND
0400 HRS 25 MAY 1983
X - LAND CELL
⊠ - INUNDATION CELL
⊡ - FORCING CELL
— - NO FLOW BOUNDARY
SCALE - 74000. CFS / INCH

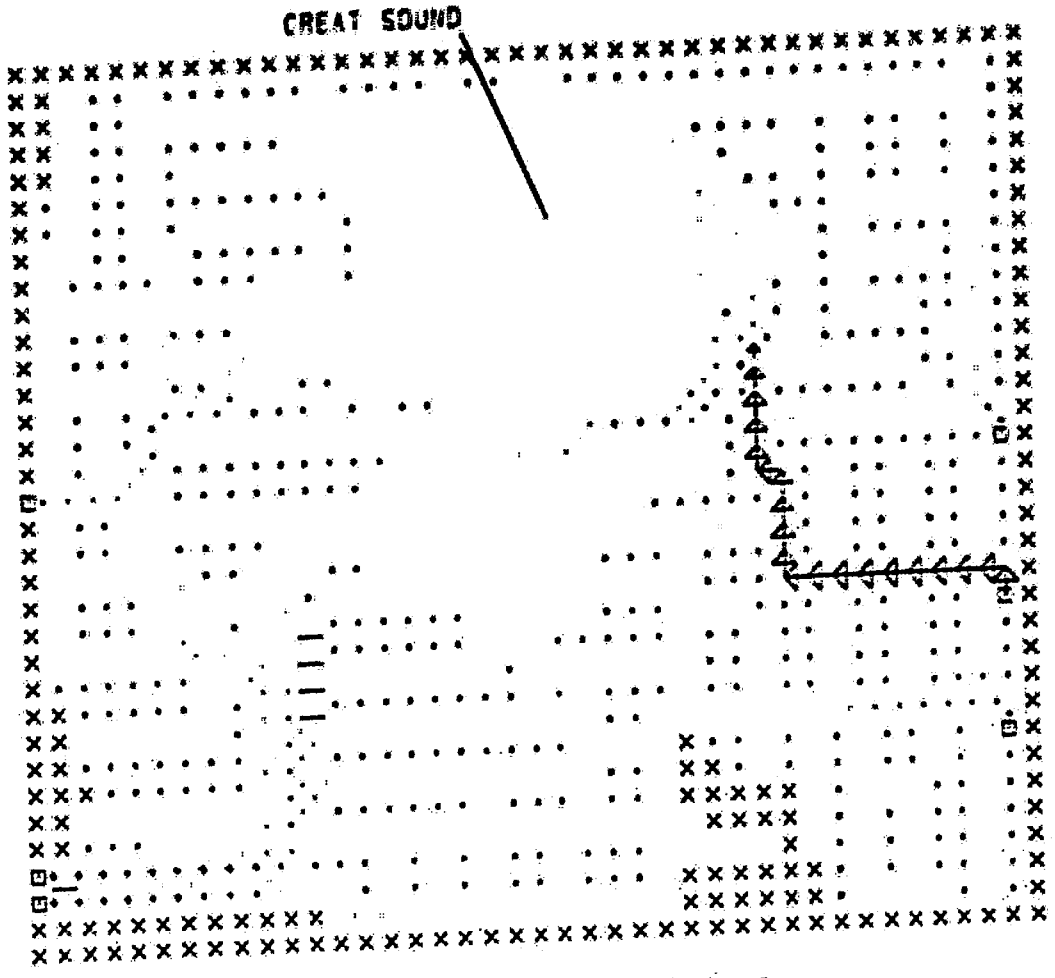

FLOW PATTERN FOR GREAT SOUND
0500 HRS 25 MAY 1983
X - LAND CELL
* - INUNDATION CELL
⊡ - FORCING CELL
— - NO FLOW BOUNDARY
SCALE - 74000. CFS / INCH

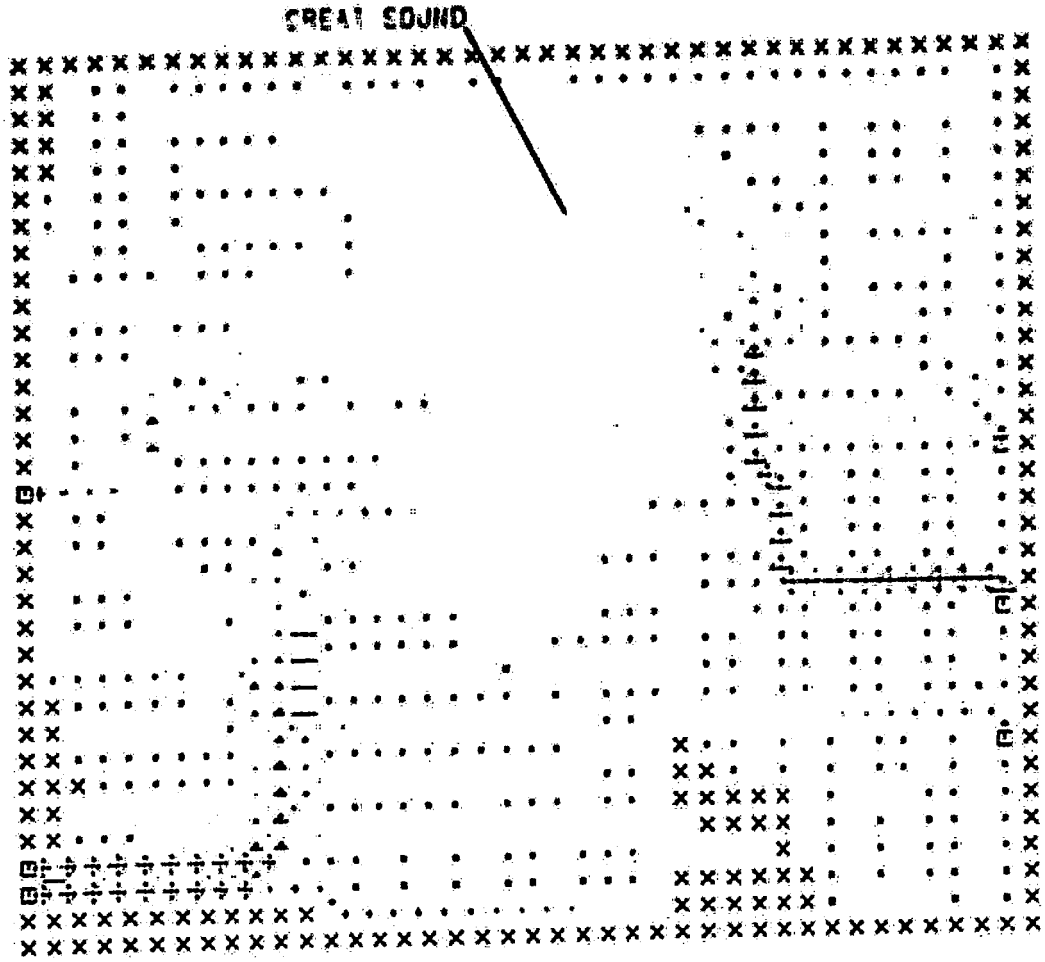

FLOW PATTERN FOR GREAT SOUND
CEGS HPS 25 MAY 1983
X - LAND CELL
⊠ - INUNDATION CELL
⊡ - FORCING CELL
— - NO FLOW BOUNDARY
SCALE - 74000 CFS / INCH

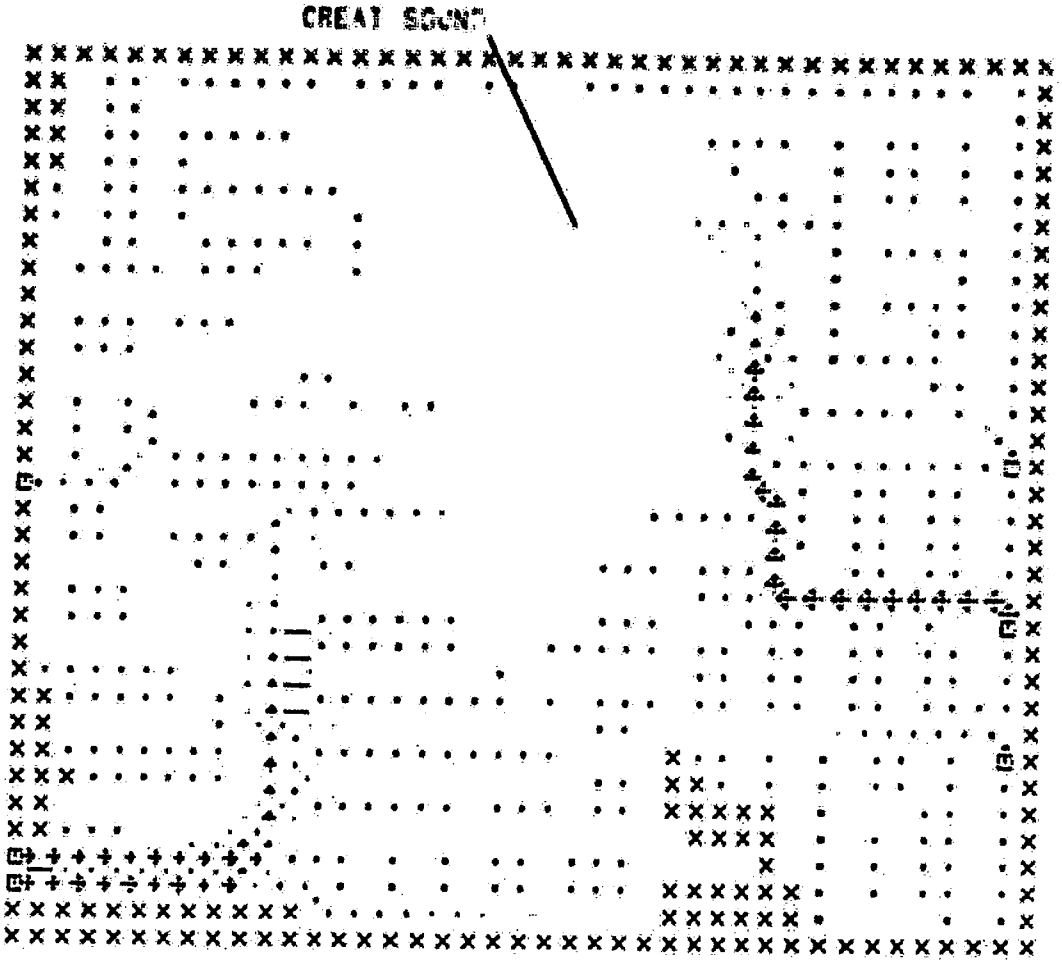

FLOW PATTERN FOR GREAT SOUND
0700 HRS 25 MAY 1982
X - LAND CELL
* - INUNDATION CELL
⊞ - FORCING CELL
— - A NO FLOW BOUNDARY
SCALE - 74000. CFS / INCH

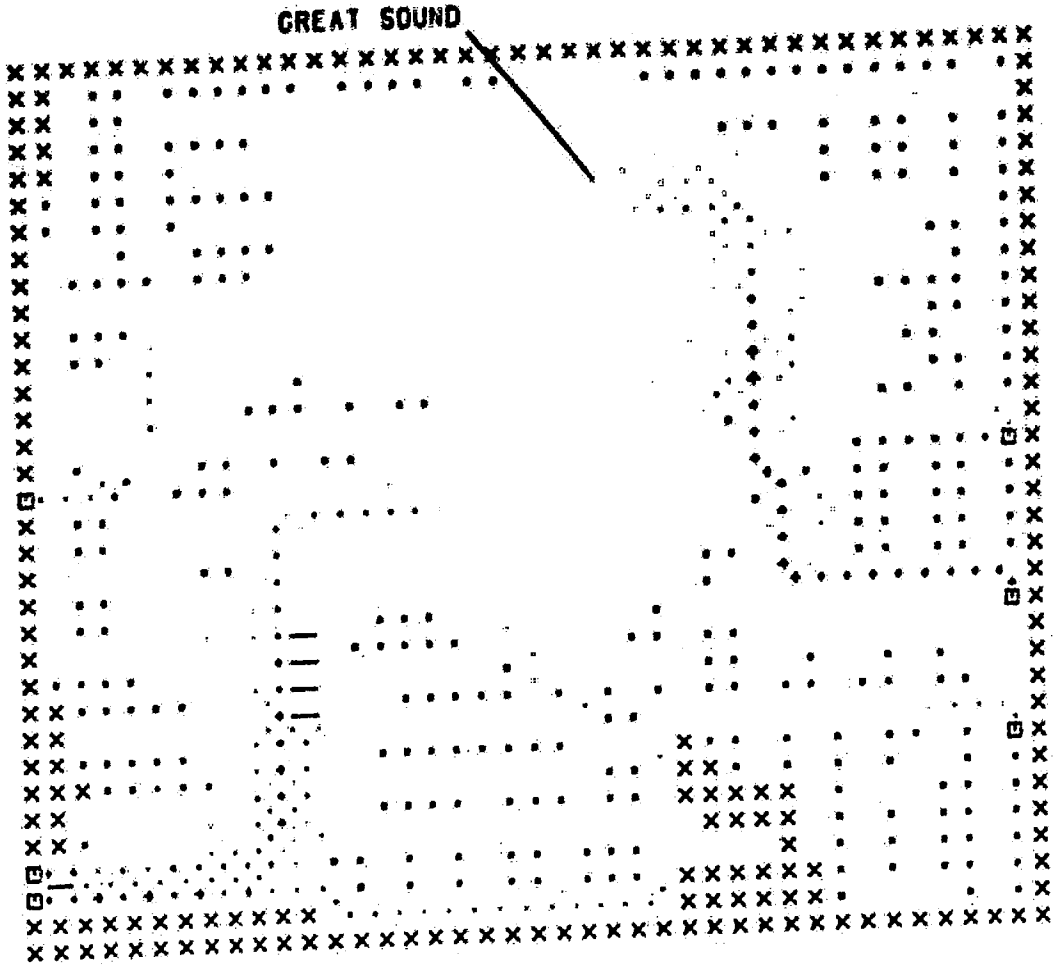

FLOW PATTERN FOR GREAT SOUND
0800 HRS 25 MAY 1963
X - LAND CELL
* - INUNDATION CELL
⊡ - FORCING CELL
— - NO FLOW BOUNDARY
SCALE - 74000. CFS / INCH

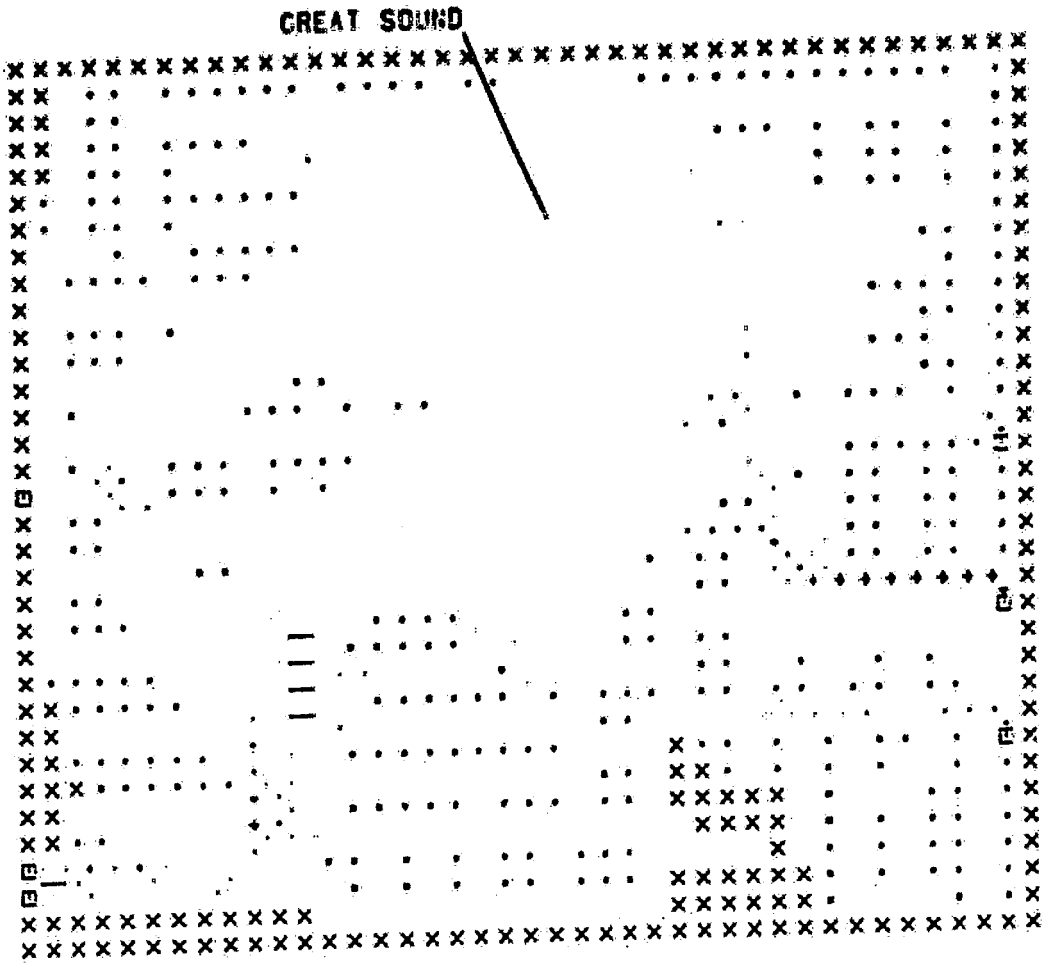

FLOW PATTERN FOR GREAT SOUND
0900 HRS 25 MAY 1983
X - LAND CELL
* - INUNDATION CELL
⊡ - FORCING CELL
— - NO FLOW BOUNDARY
SCALE - 74000 CFS / INCH

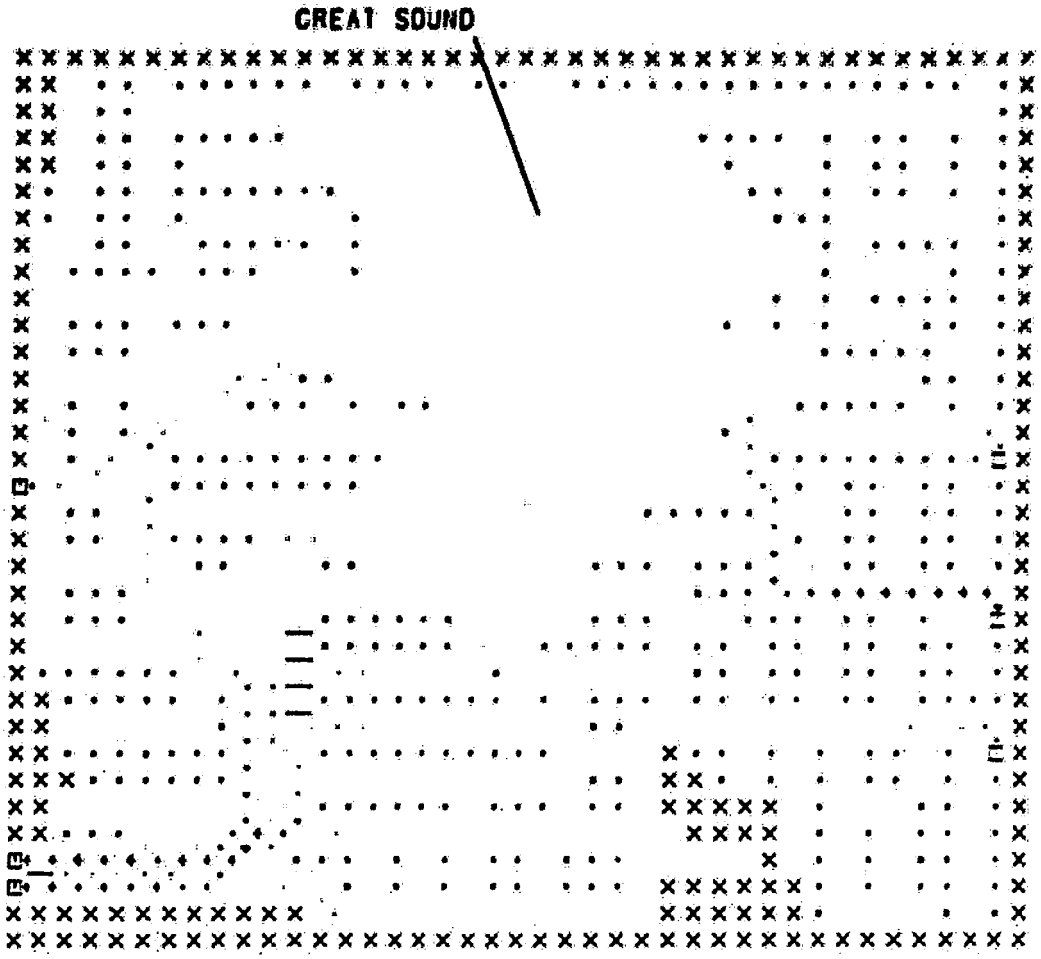

FLOW PATTERN FOR GREAT SOUND
1000 HRS 25 MAY 1983
X - LAND CELL
* - INUNDATION CELL
⊡ - FORCING CELL
— - NO FLOW BOUNDARY
SCALE - 74000. CFS / INCH

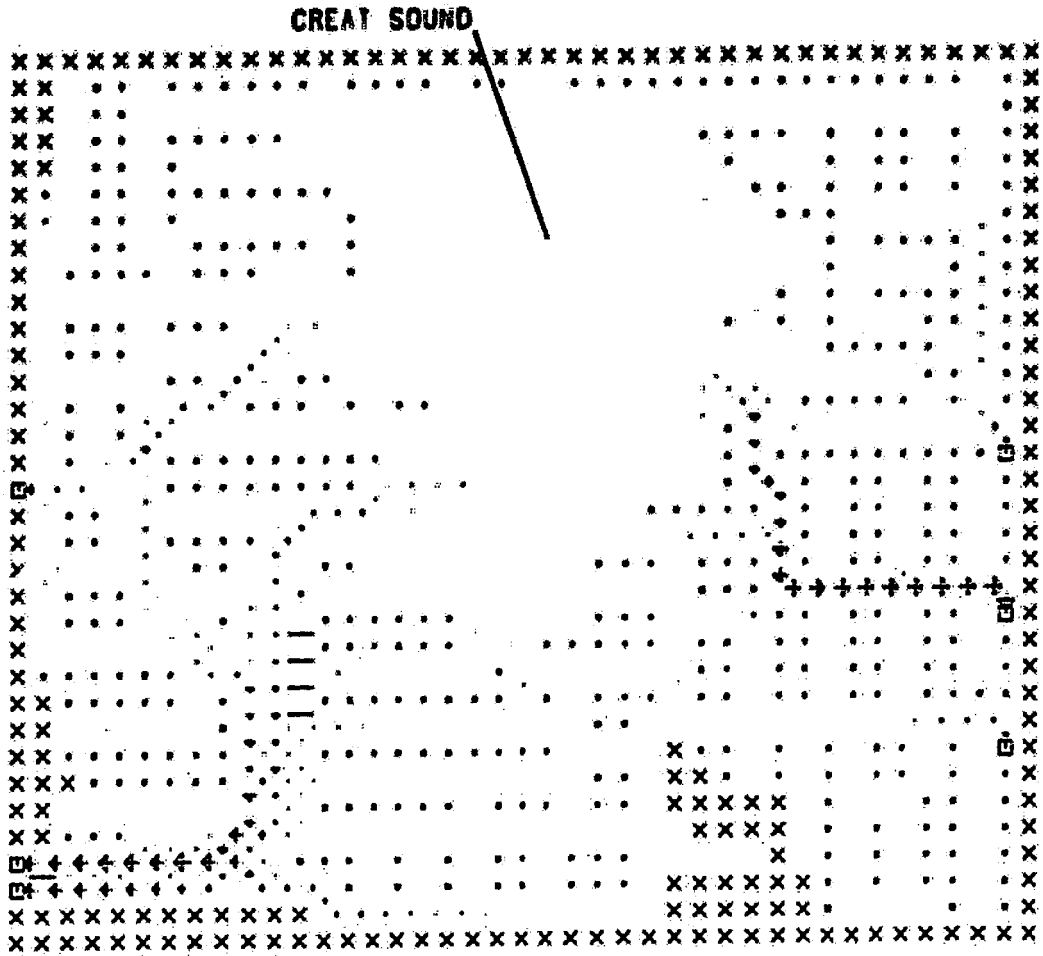

FLOW PATTERN FOR GREAT SOUND
1100 HRS 25 MAY 1983
X - LAND CELL
* - INUNDATION CELL
⊡ - FORCING CELL
— - NO FLOW BOUNDARY
SCALE - 74000 CFS / INCH

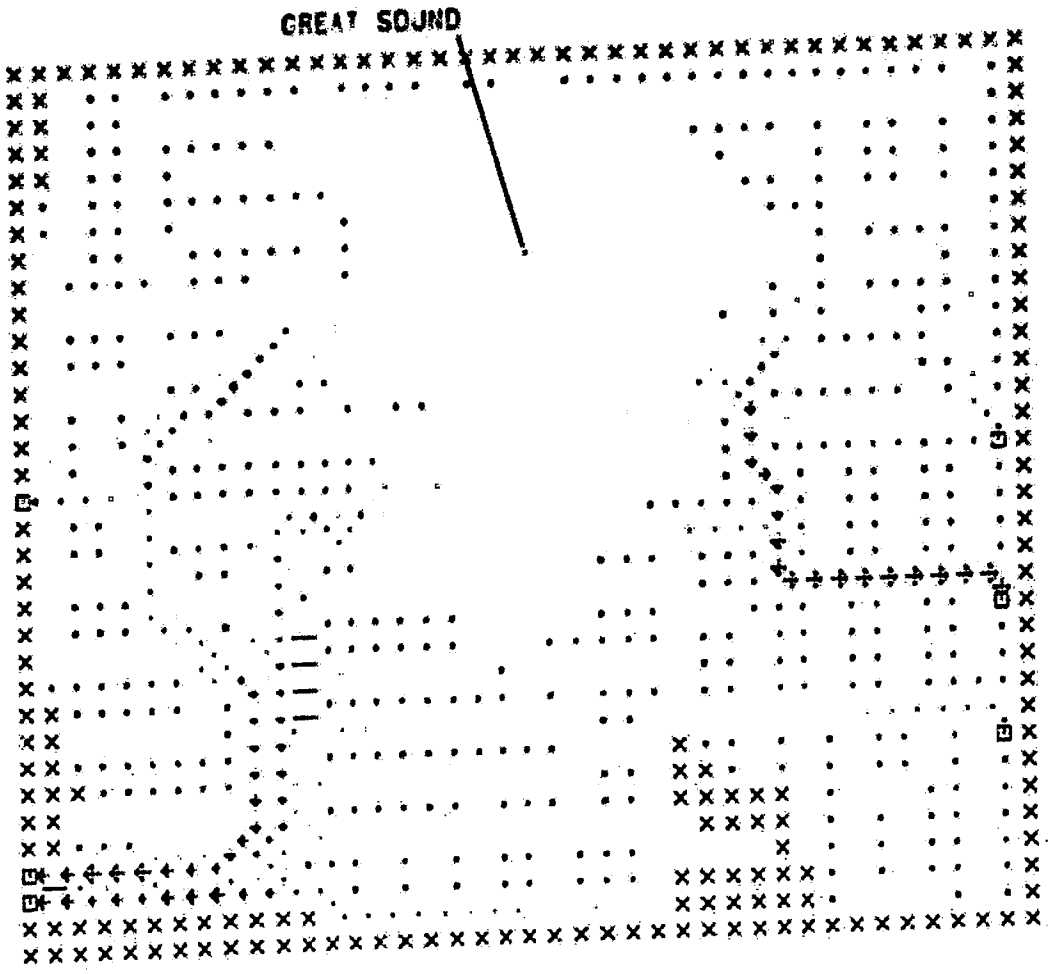

FLOW PATTERN FOR GREAT SOUND
1200 HRS 25 MAY 1983
X - LAND CELL
X - INUNDATION CELL
⊡ - FORCING CELL
— - NO FLOW BOUNDARY
SCALE - 74000. CFS / INCH

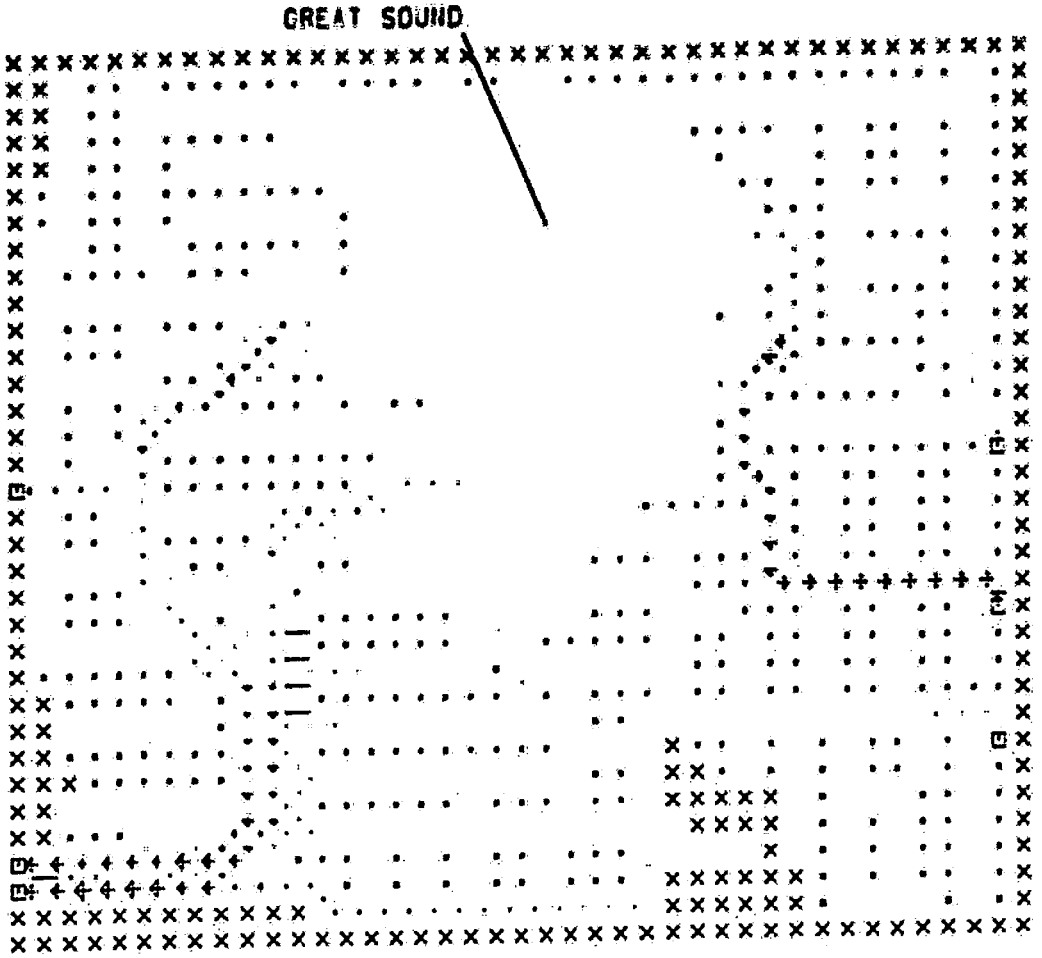

FLOW PATTERN FOR GREAT SOUND
1300 HRS 25 MAY 1963
X - LAND CELL
⋋ - INUNDATION CELL
⊡ - FORCING CELL
— - NO FLOW BOUNDARY
SCALE - 74000. CFS / INCH

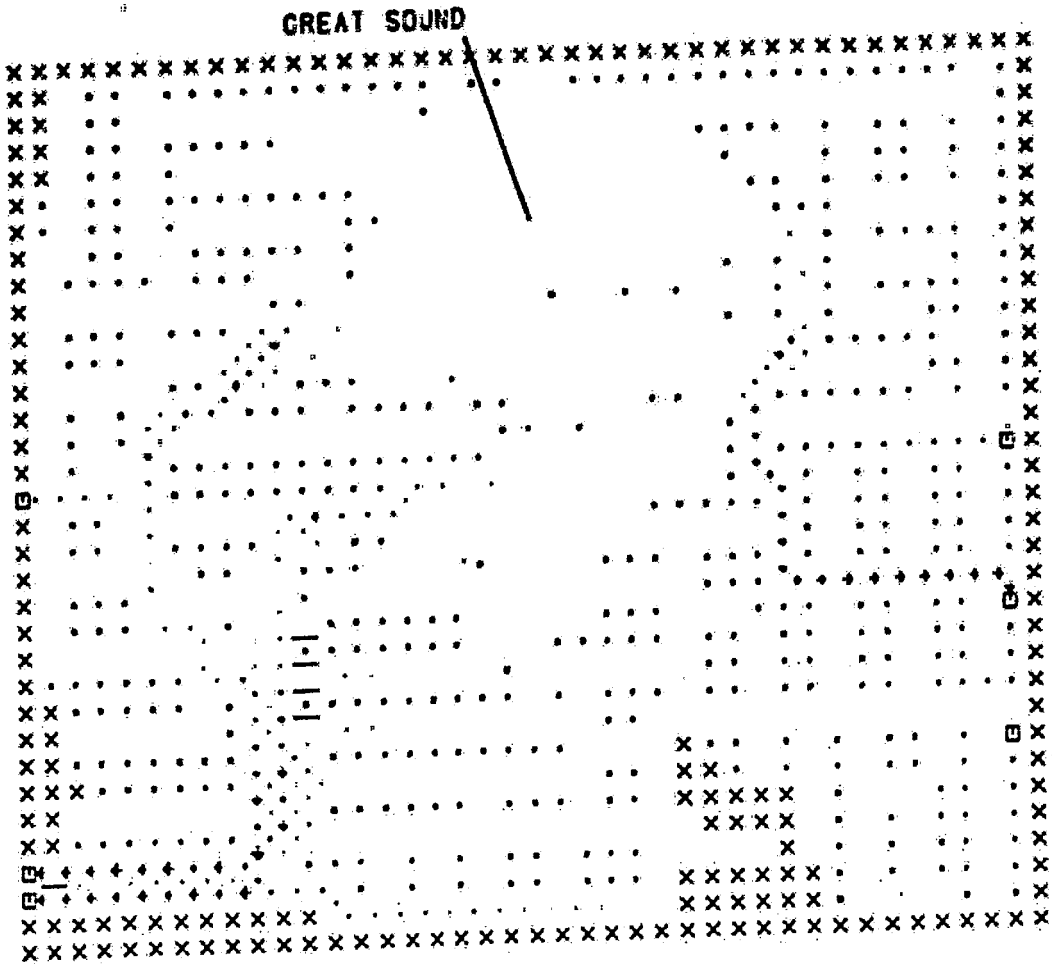

FLOW PATTERN FOR GREAT SOUND
1400 HRS 25 MAY 1983
X - LAND CELL
* - INUNDATION CELL
□ - FORCING CELL
— - NO FLOW BOUNDARY
SCALE - 74000. CFS / INCH

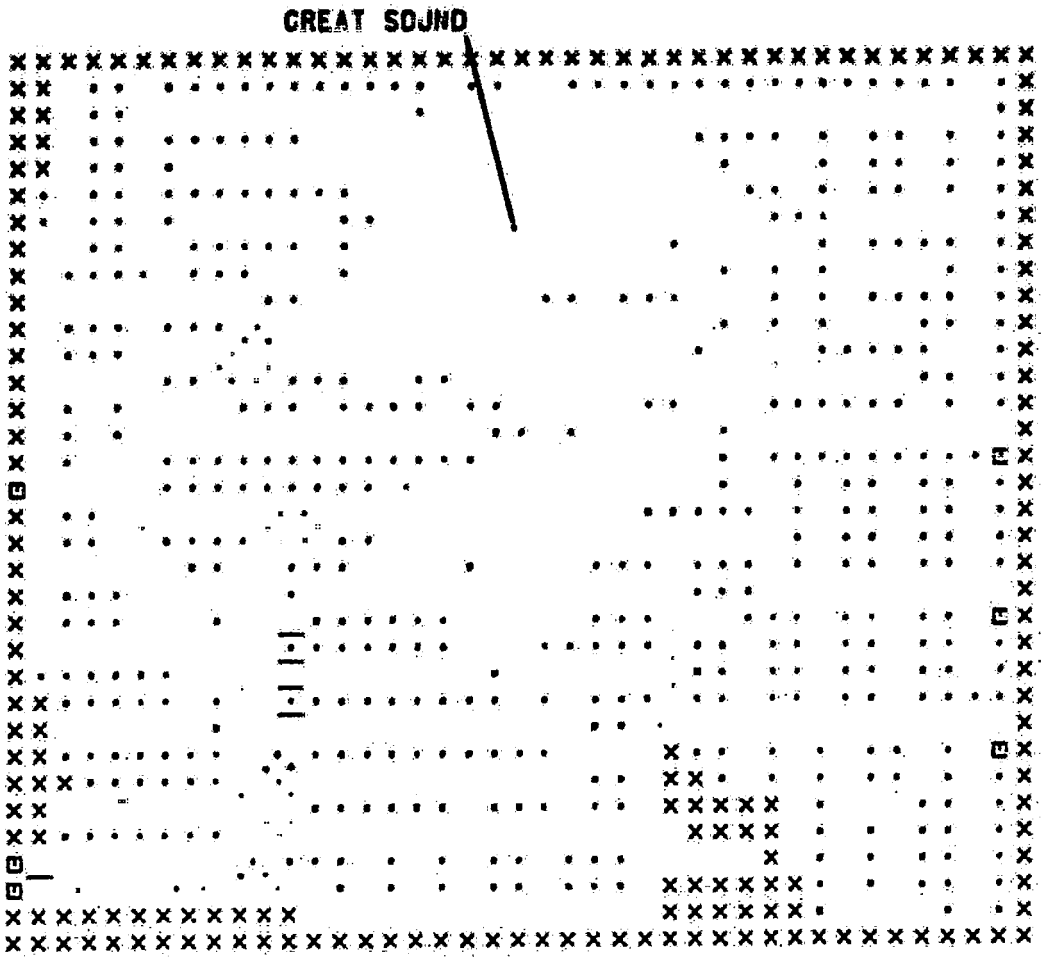

FLOW PATTERN FOR GREAT SOUND
1500 HRS 25 MAY 1983
X - LAND CELL
* - INUNDATION CELL
⊡ - FORCING CELL
– - NO FLOW BOUNDARY
SCALE - 74000. CFS / INCH

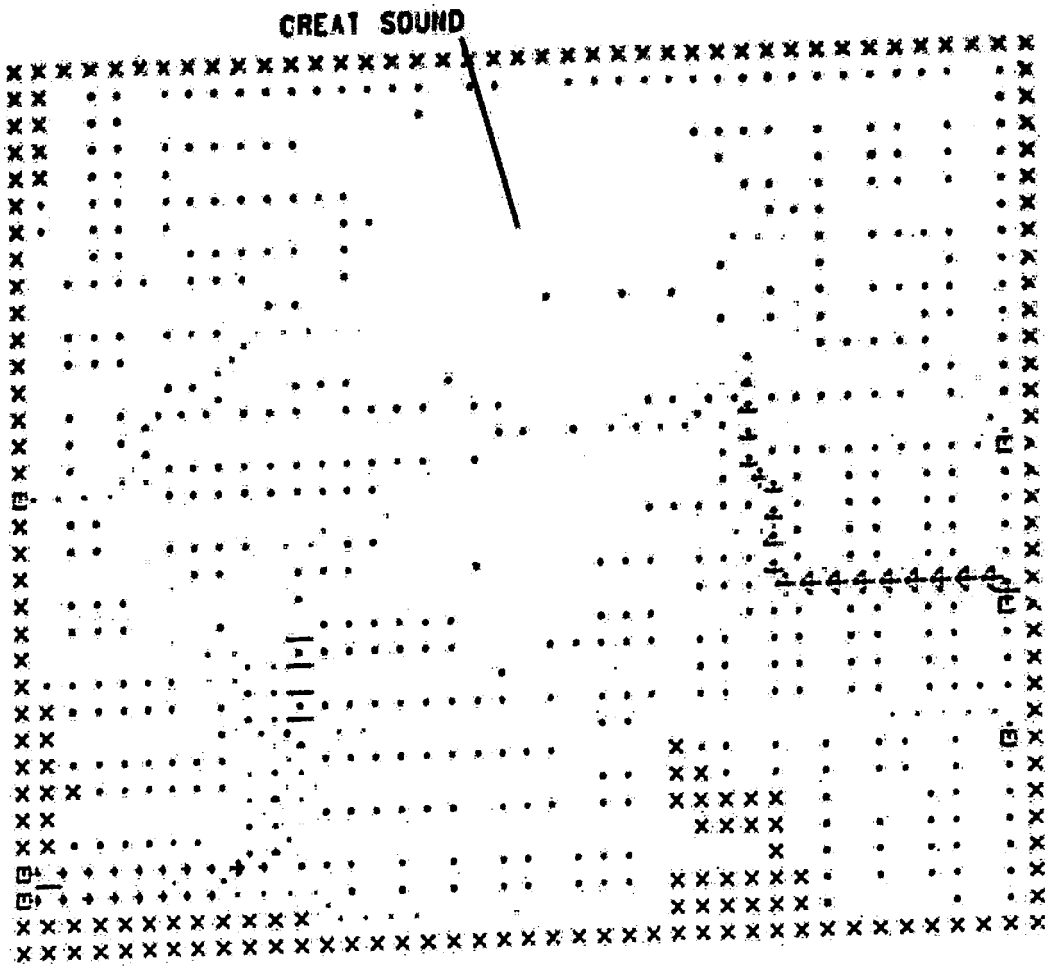

FLOW PATTERN FOR GREAT SOUND
1600 HRS 25 MAY 1983
X - LAND CELL
⊠ - INUNDATION CELL
⊡ - FORCING CELL
— - NO FLOW BOUNDARY
SCALE - 74000. CFS / INCH

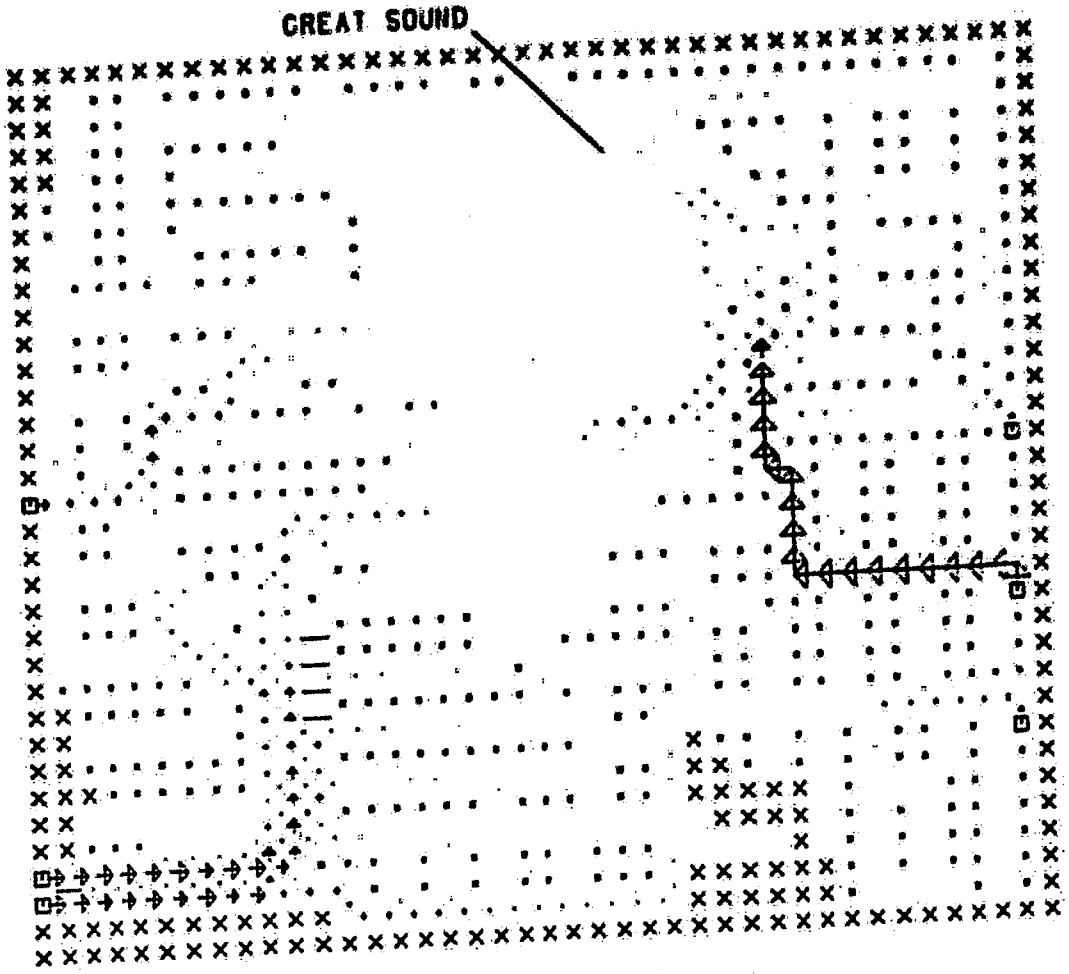

FLOW PATTERN FOR GREAT SOUND
1700 HRS 25 MAY 1983
X - LAND CELL
* - INUNDATION CELL
⊡ - FORCING CELL
— - NO FLOW BOUNDARY
SCALE - 74000. CFS / INCH

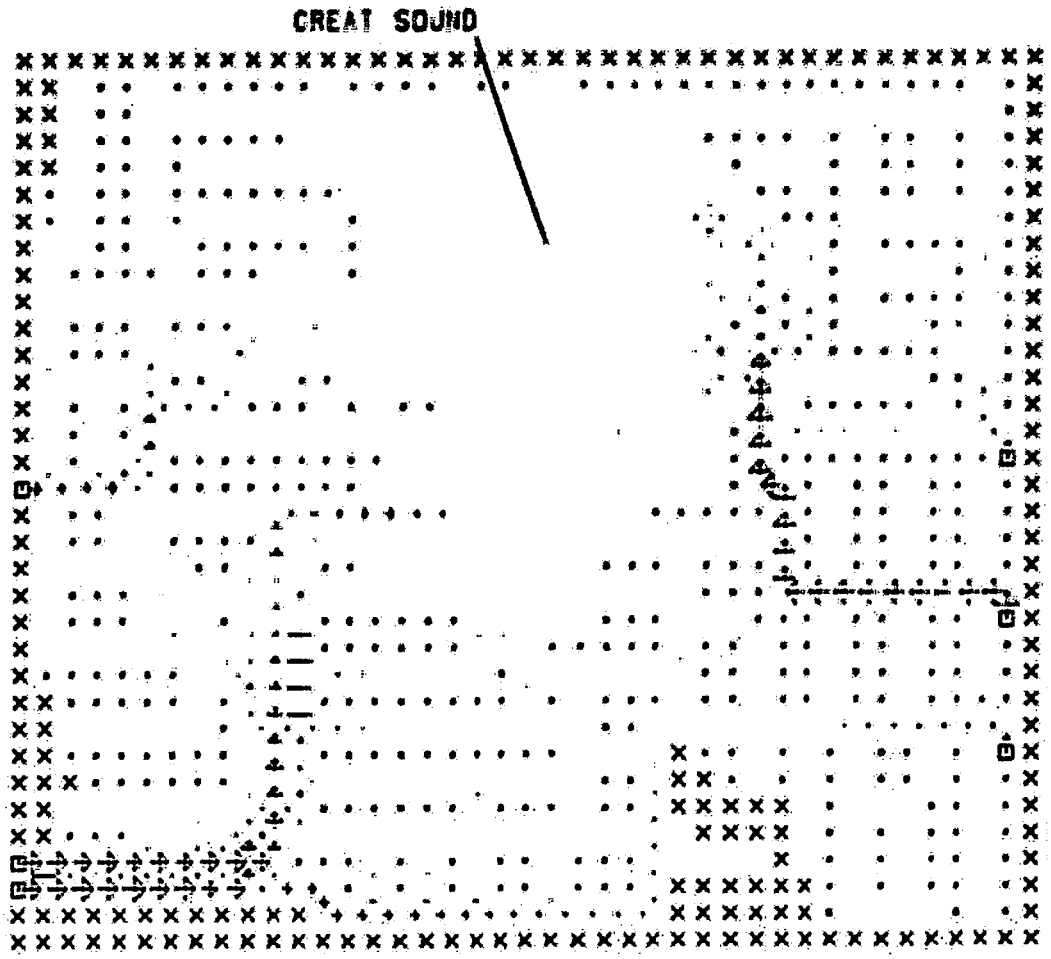

FLOW PATTERN FOR GREAT SOUND
:800 HRS 25 MAY :983
X - LAND CELL
* - INUNDATION CELL
□ - FORCING CELL
— - NO FLOW BOUNDARY
SCALE - 74000. CFS / INCH

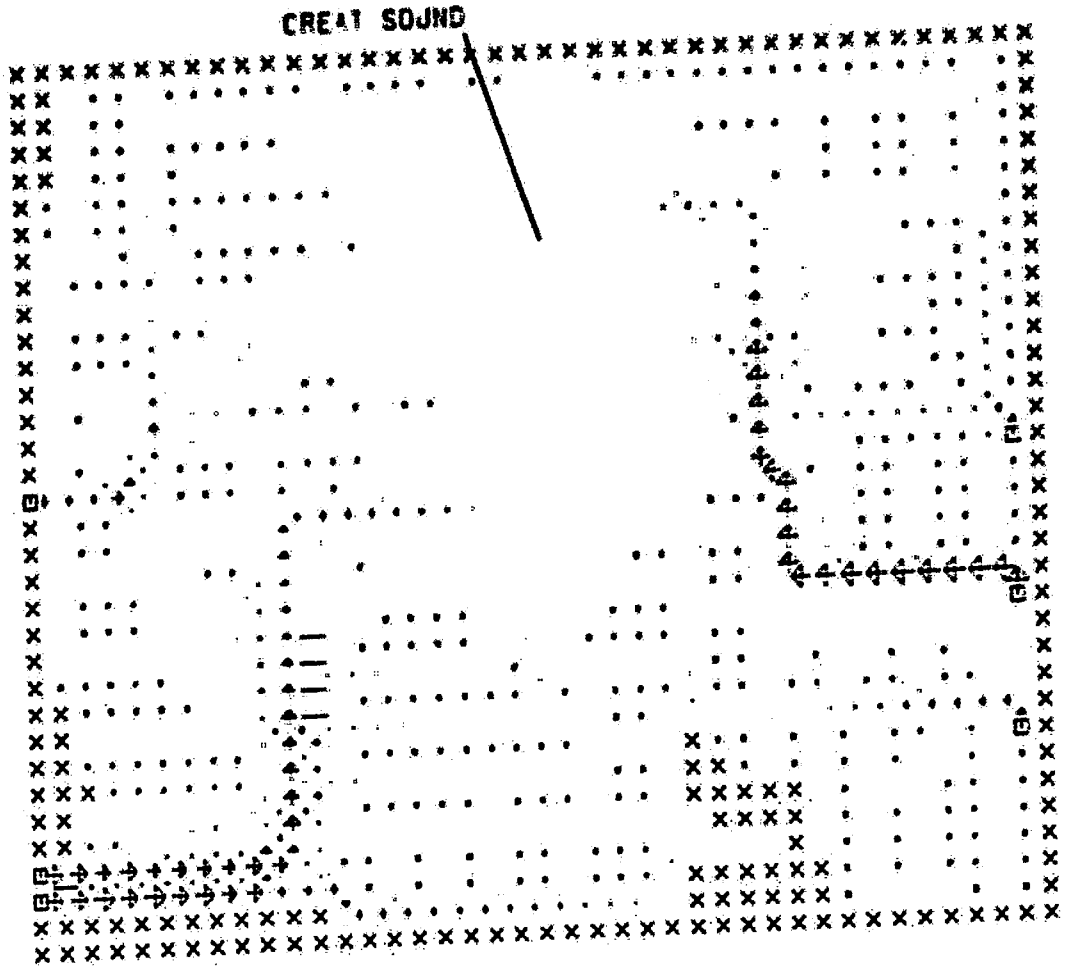

FLOW PATTERN FOR GREAT SOUND
1900 HRS 25 MAY 1983
X - LAND CELL
x - INUNDATION CELL
B - FORCING CELL
— - NO FLOW BOUNDARY
SCALE - 74000. CFS / INCH

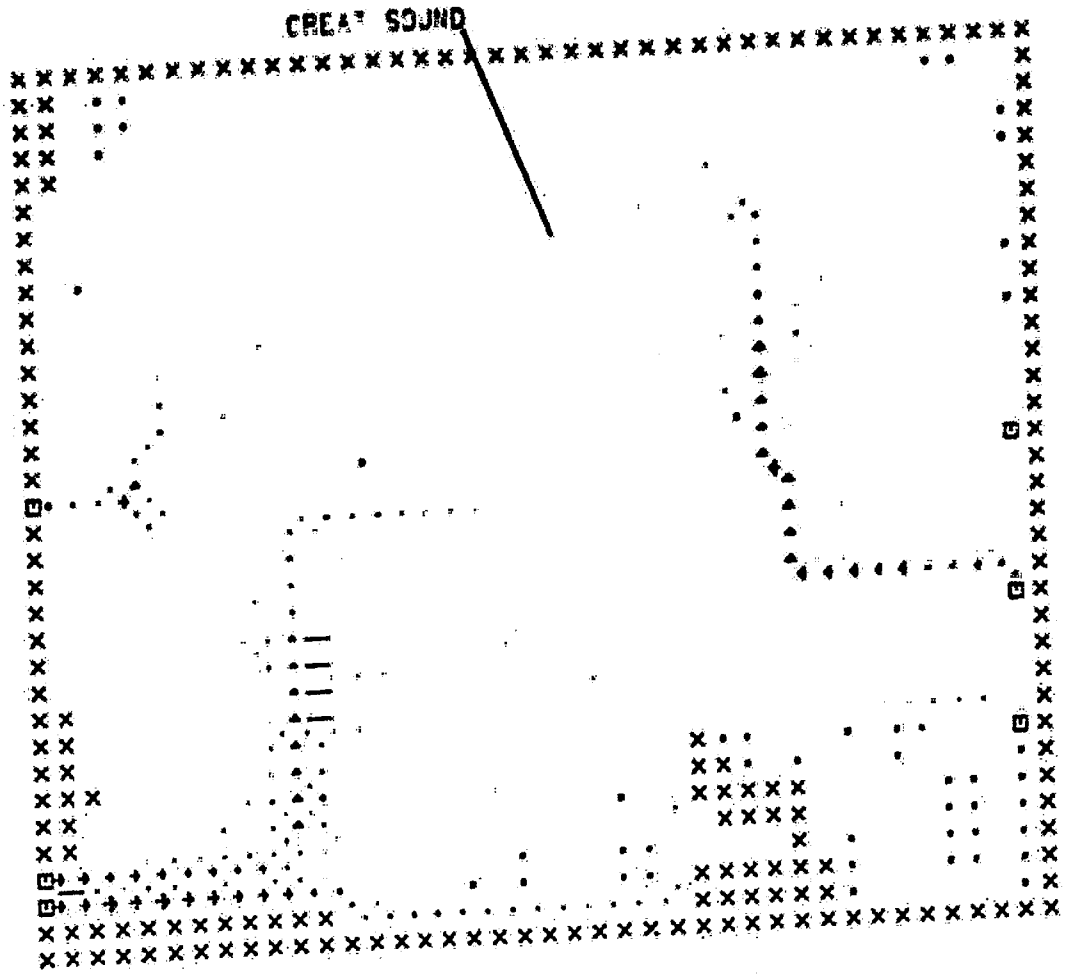

FLOW PATTERN FOR GREAT SOUND
2000 HRS 25 MAY 1983
X - LAND CELL
X - INUNDATION CELL
⊞ - FORCING CELL
— - NO FLOW BOUNDARY
SCALE - 24000. CFS / INCH

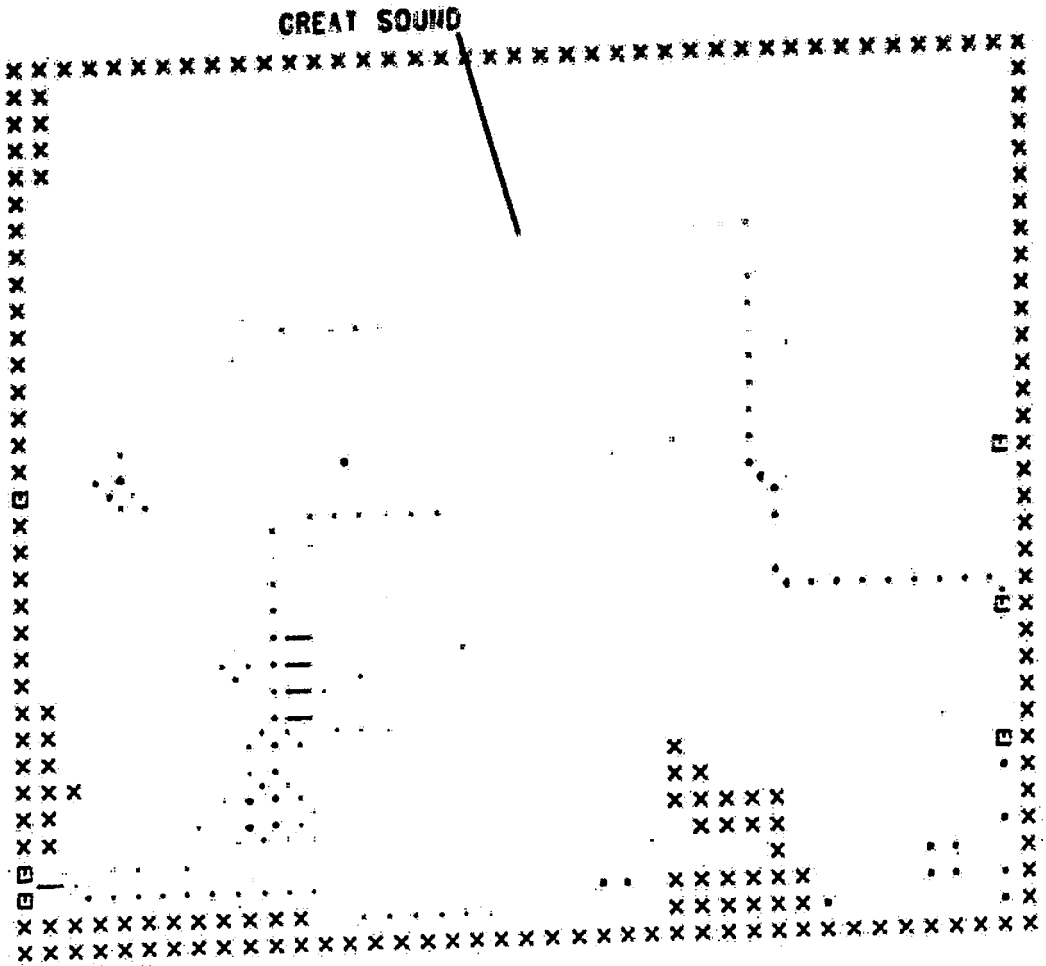

FLOW PATTERN FOR GREAT SOUND
2100 HRS 25 MAY 1983
X - LAND CELL
* - INUNDATION CELL
⊡ - FORCING CELL
— - NO FLOW BOUNDARY
SCALE - 74000. CFS / INCH

I.3 FLOW MAPS FOR NEAP TIDE CALIBRATION

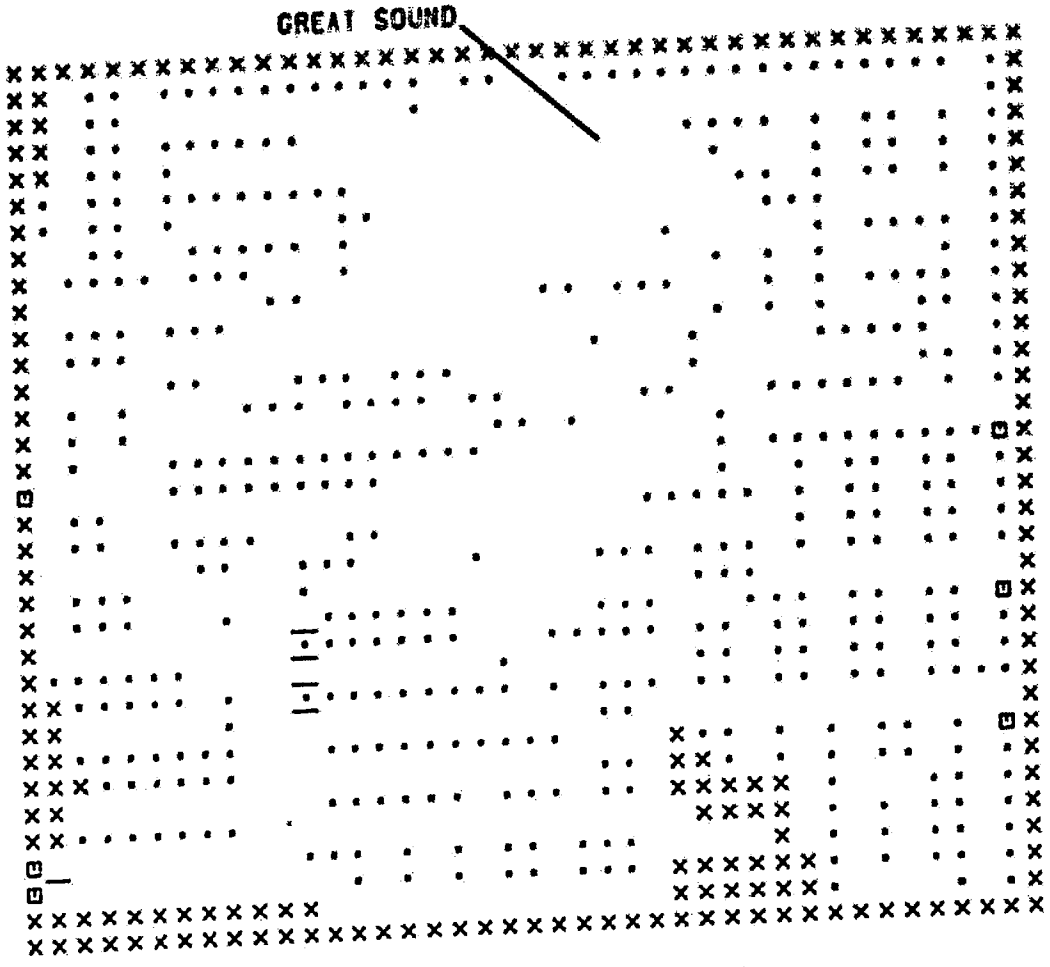

FLOW PATTERN FOR GREAT SOUND
0700 HRS 1 JUNE 1983
X - LAND CELL
* - INUNDATION CELL
⊡ - FORCING CELL
– - NO FLOW BOUNDARY
SCALE - 100000. CFS / INCH

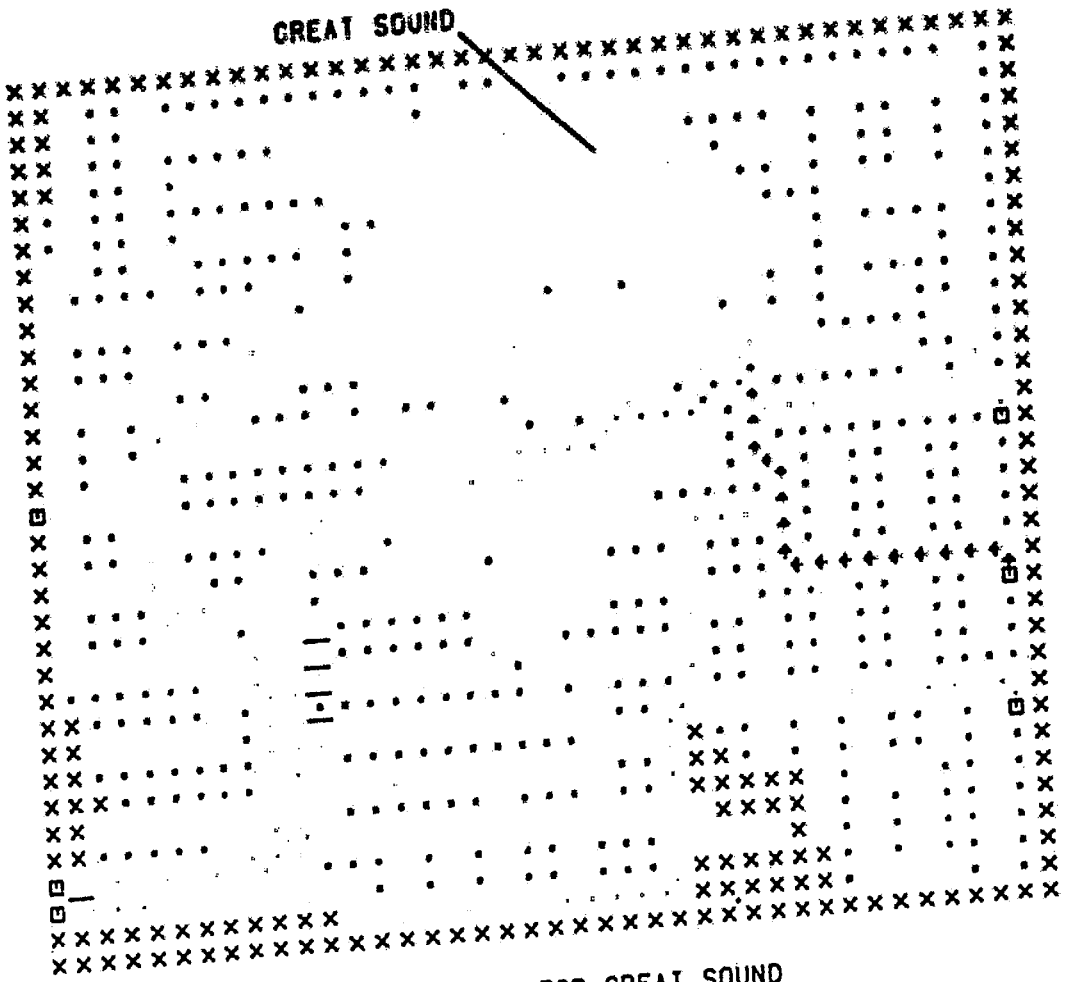

FLOW PATTERN FOR GREAT SOUND
0800 HRS 1 JUNE 1983
X - LAND CELL
* - INUNDATION CELL
⊡ - FORCING CELL
— - NO FLOW BOUNDARY
SCALE - 100000. CFS / INCH

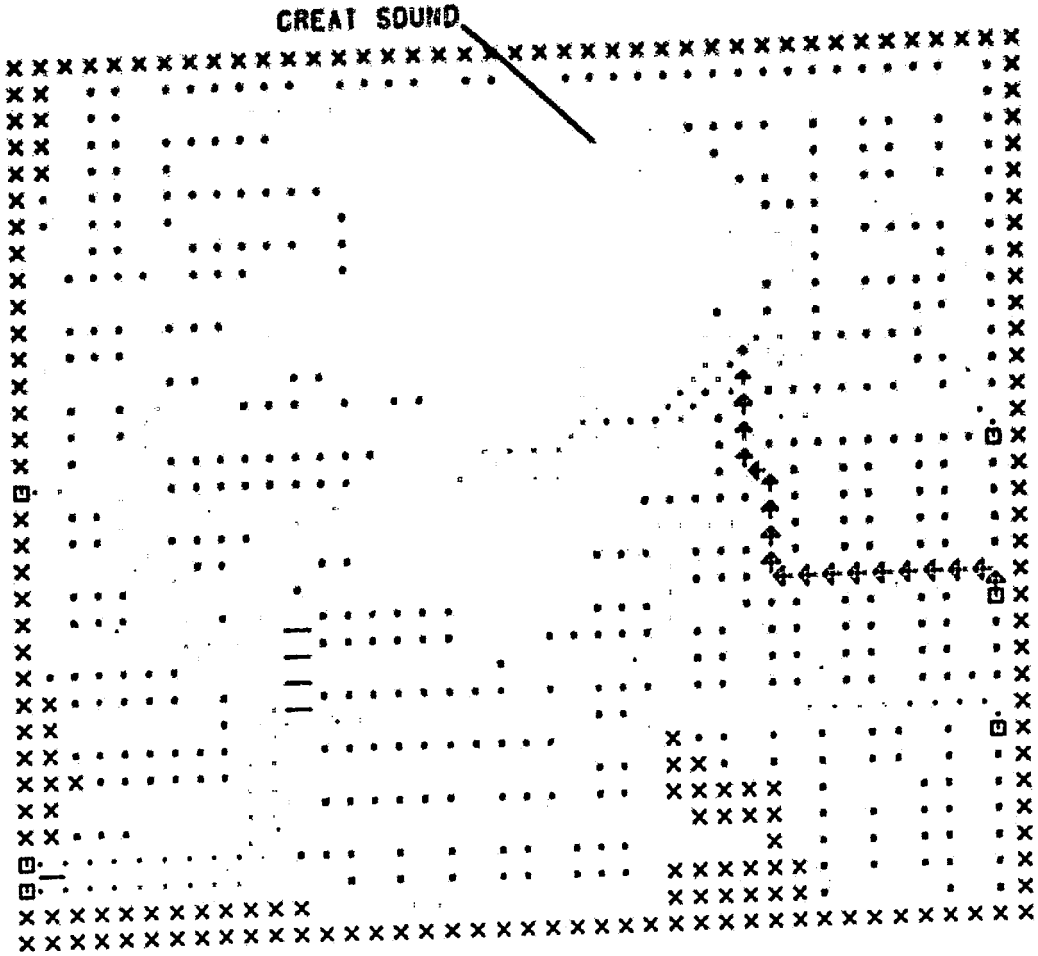

FLOW PATTERN FOR GREAT SOUND
0900 HRS 1 JUNE 1983
X - LAND CELL
* - INUNDATION CELL
⊡ - FORCING CELL
— - NO FLOW BOUNDARY
SCALE - 100000. CFS / INCH

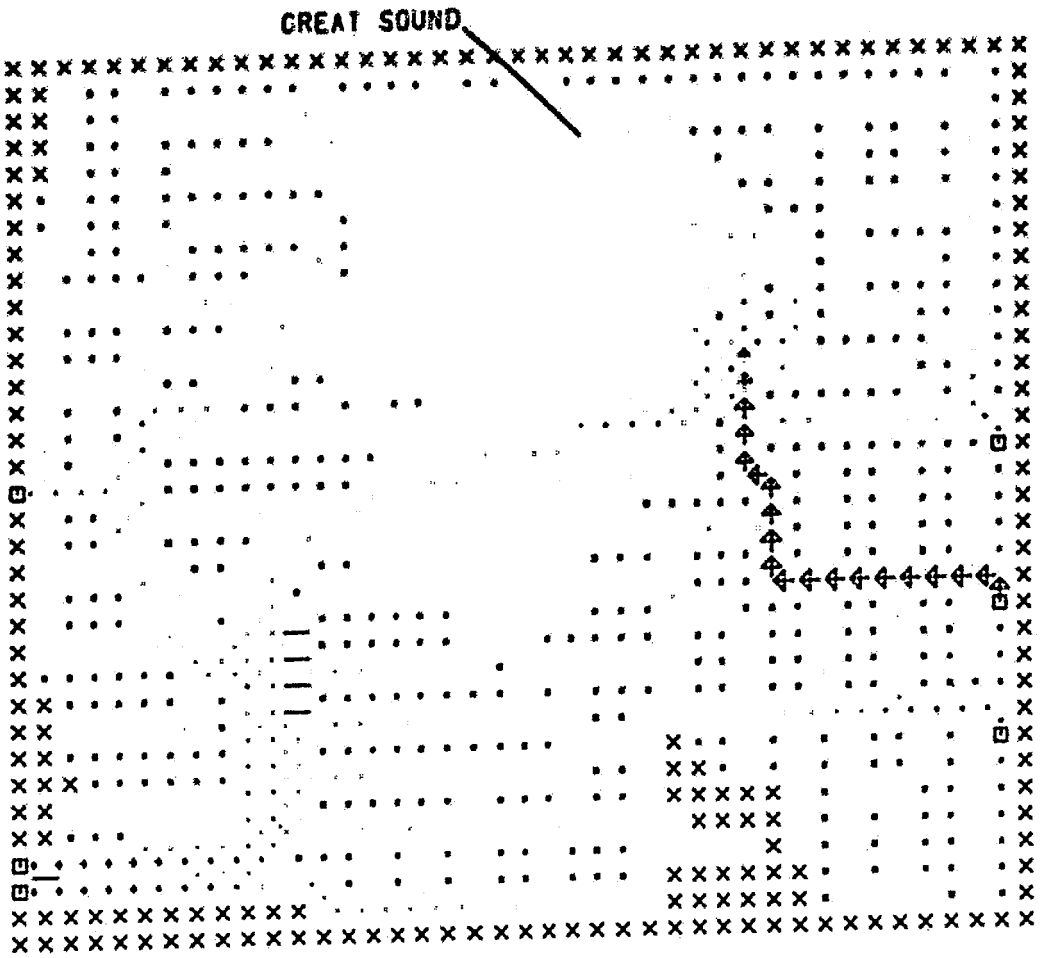

FLOW PATTERN FOR GREAT SOUND
1000 HRS 1 JUNE 1983
X - LAND CELL
* - INUNDATION CELL
⊡ - FORCING CELL
— - NO FLOW BOUNDARY
SCALE - 100000. CFS / INCH

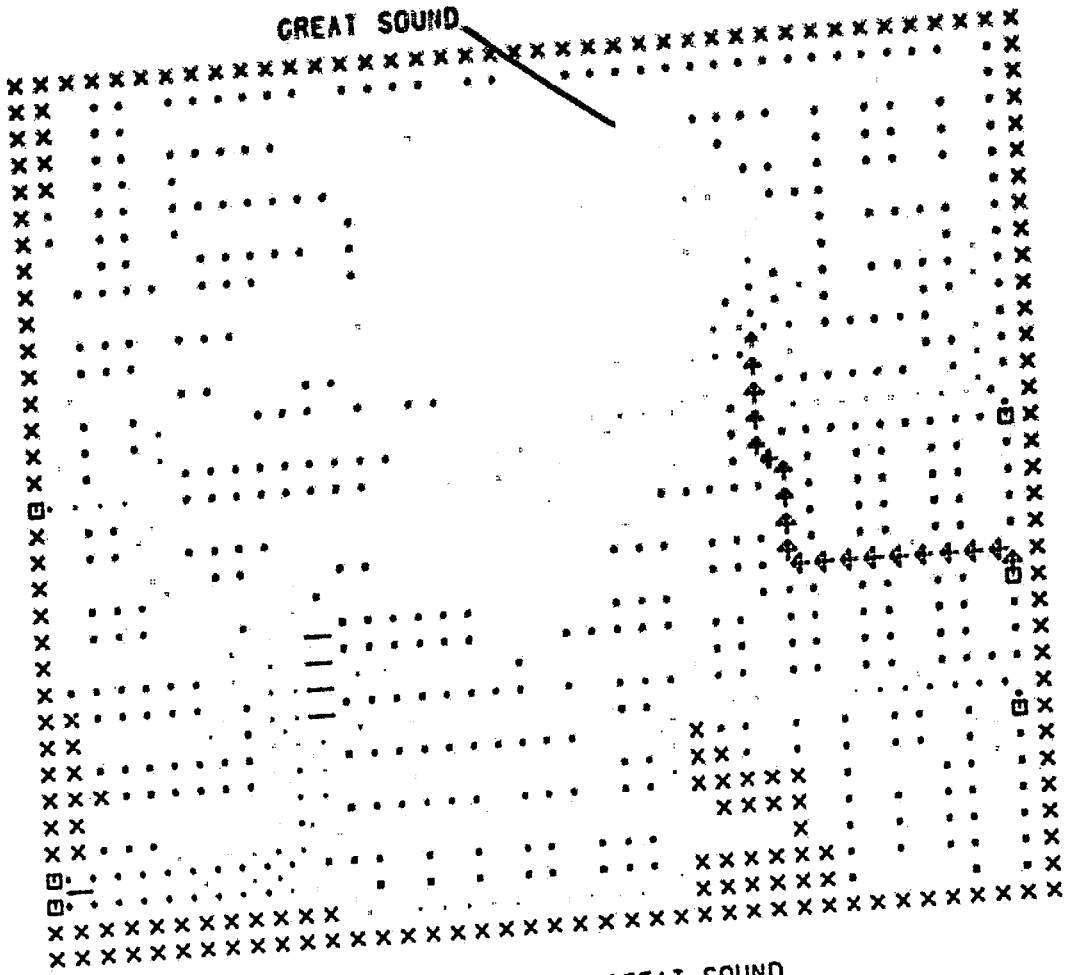

FLOW PATTERN FOR GREAT SOUND
1100 HRS 1 JUNE 1983
X - LAND CELL
* - INUNDATION CELL
⊡ - FORCING CELL
— - NO FLOW BOUNDARY
SCALE - 100000. CFS / INCH

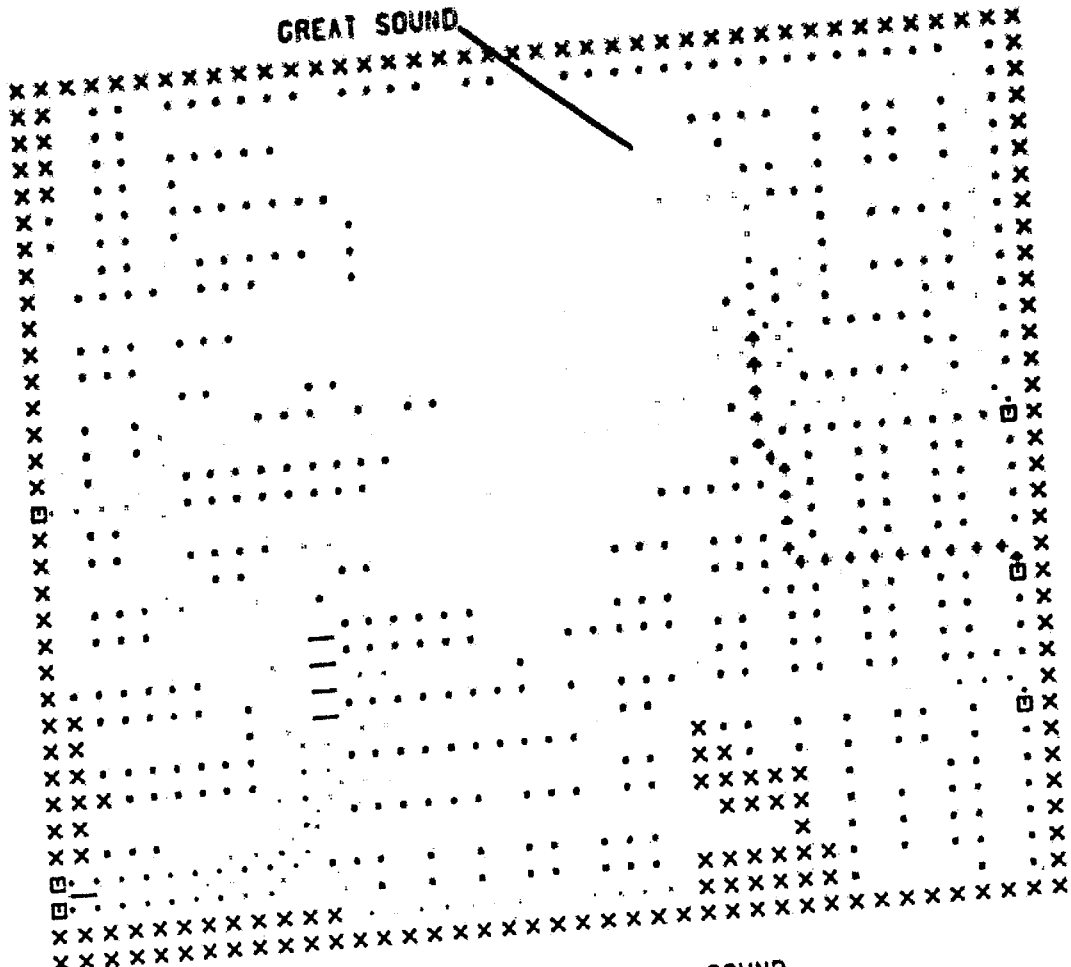

FLOW PATTERN FOR GREAT SOUND
1200 HRS 1 JUNE 1983
X - LAND CELL
* - INUNDATION CELL
⊡ - FORCING CELL
— - NO FLOW BOUNDARY
SCALE - 100000. CFS / INCH

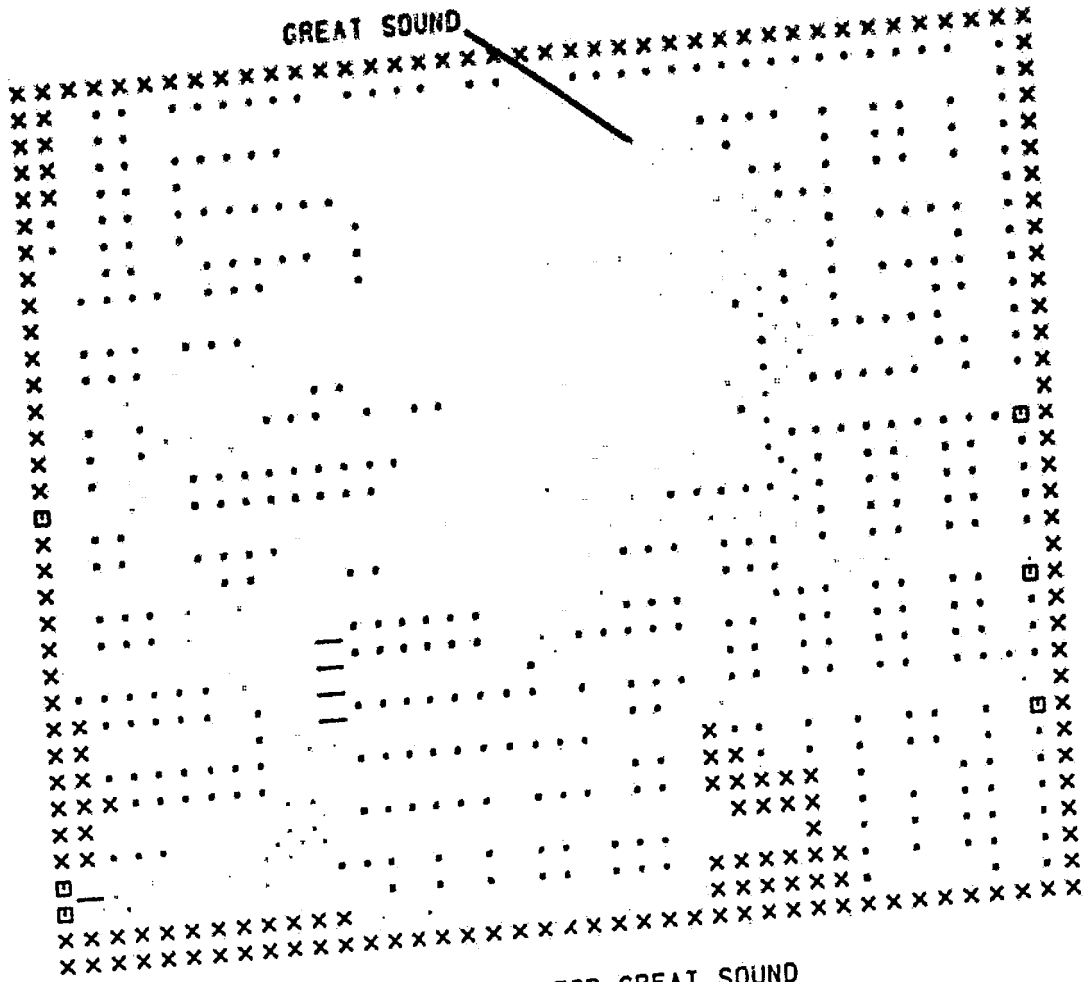

FLOW PATTERN FOR GREAT SOUND
1300 HRS 1 JUNE 1983
X - LAND CELL
* - INUNDATION CELL
⊡ - FORCING CELL
— - NO FLOW BOUNDARY
SCALE - 100000. CFS / INCH

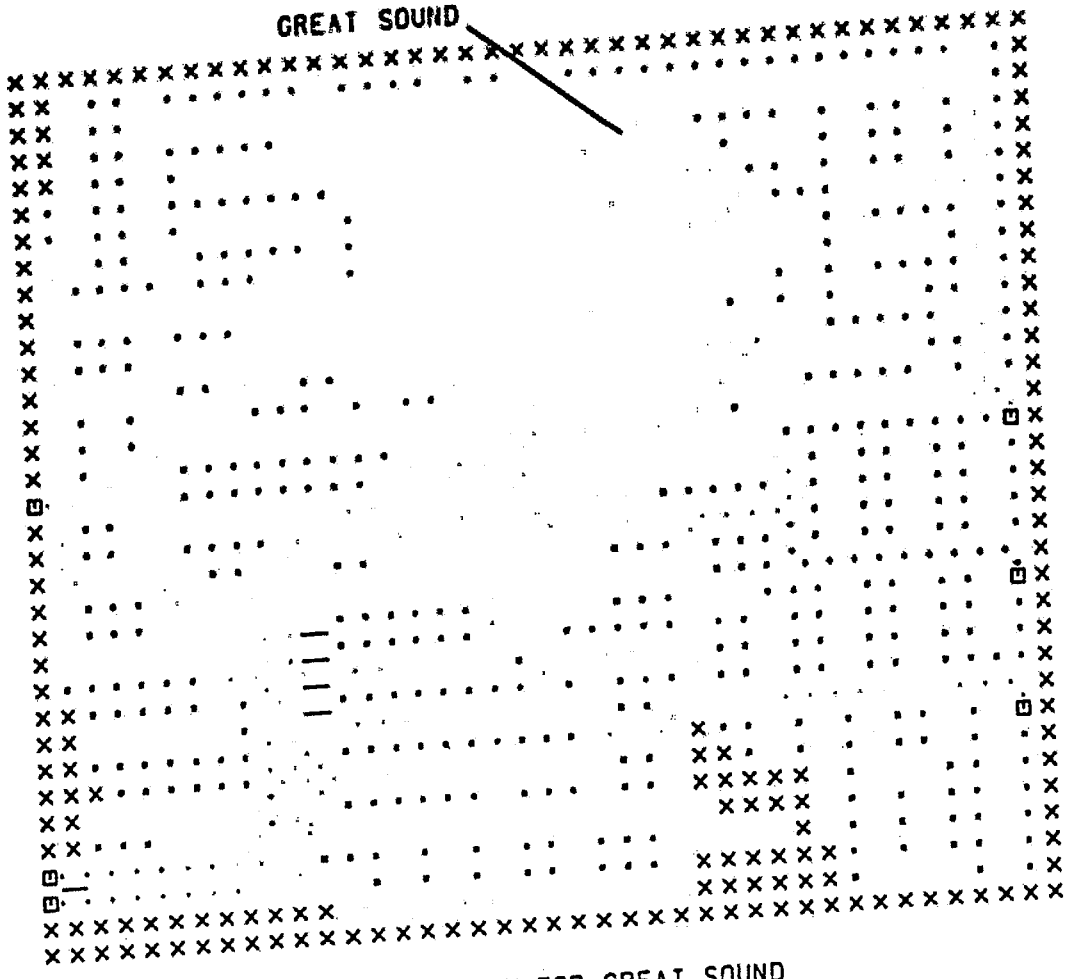

FLOW PATTERN FOR GREAT SOUND
1400 HRS 1 JUNE 1983
× - LAND CELL
* - INUNDATION CELL
⊡ - FORCING CELL
— - NO FLOW BOUNDARY
SCALE - 100000. CFS / INCH

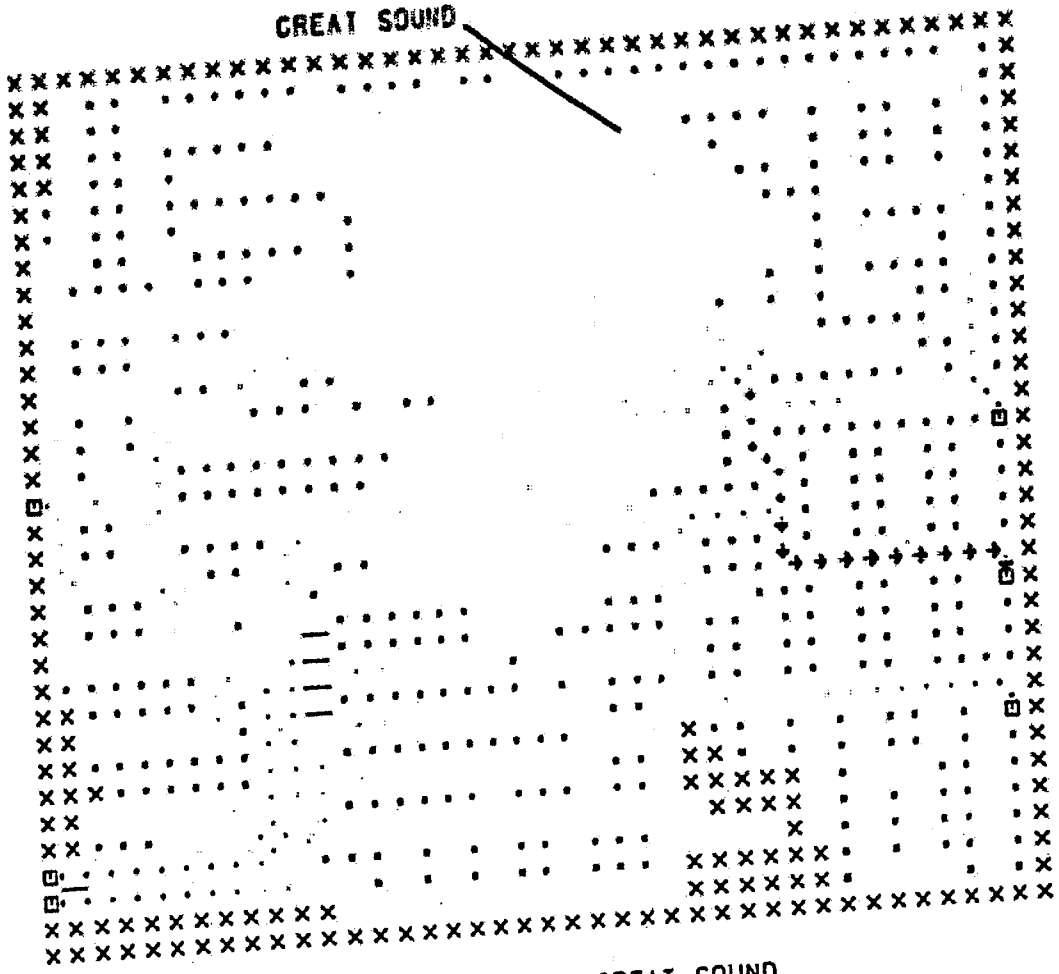

FLOW PATTERN FOR GREAT SOUND
1500 HRS 1 JUNE 1983
X - LAND CELL
* - INUNDATION CELL
⊡ - FORCING CELL
— - NO FLOW BOUNDARY
SCALE - 100000. CFS / INCH

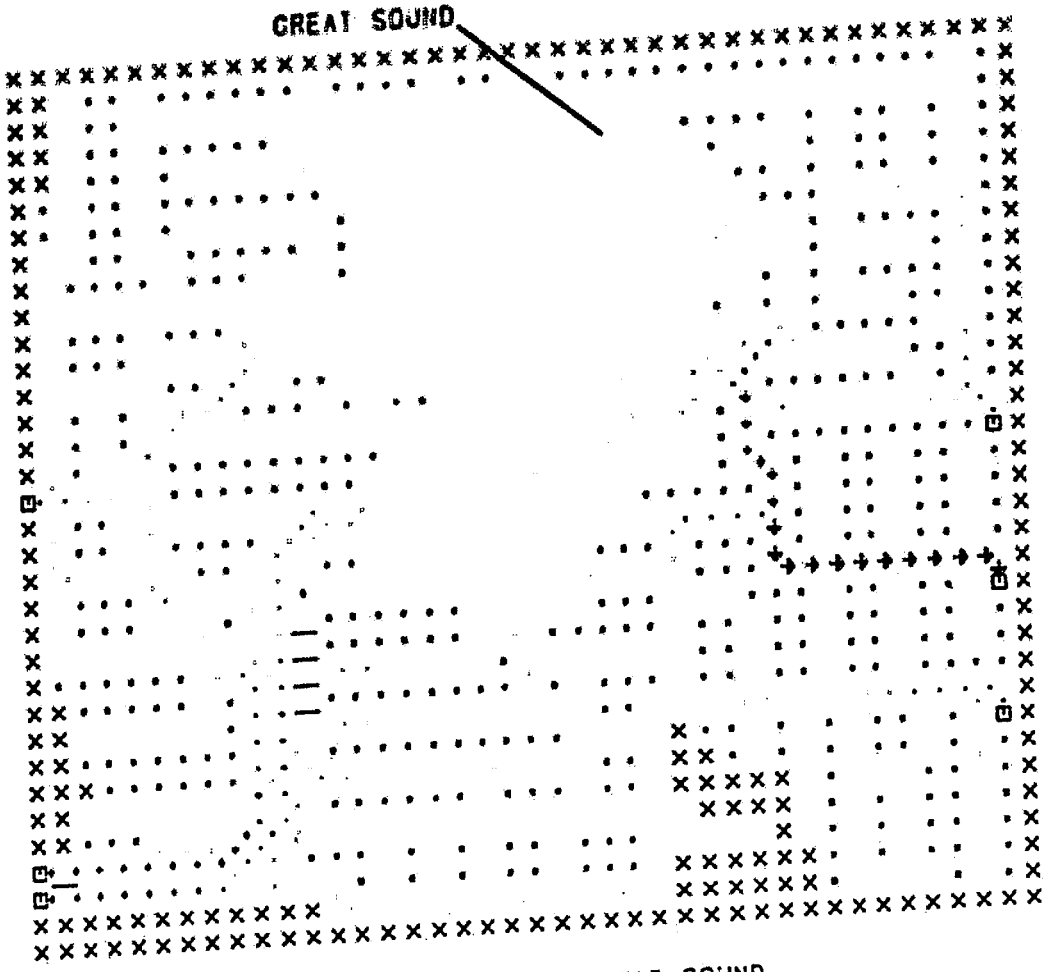

FLOW PATTERN FOR GREAT SOUND
1600 HRS 1 JUNE 1983
X - LAND CELL
* - INUNDATION CELL
⊡ - FORCING CELL
— - NO FLOW BOUNDARY
SCALE - 100000. CFS / INCH

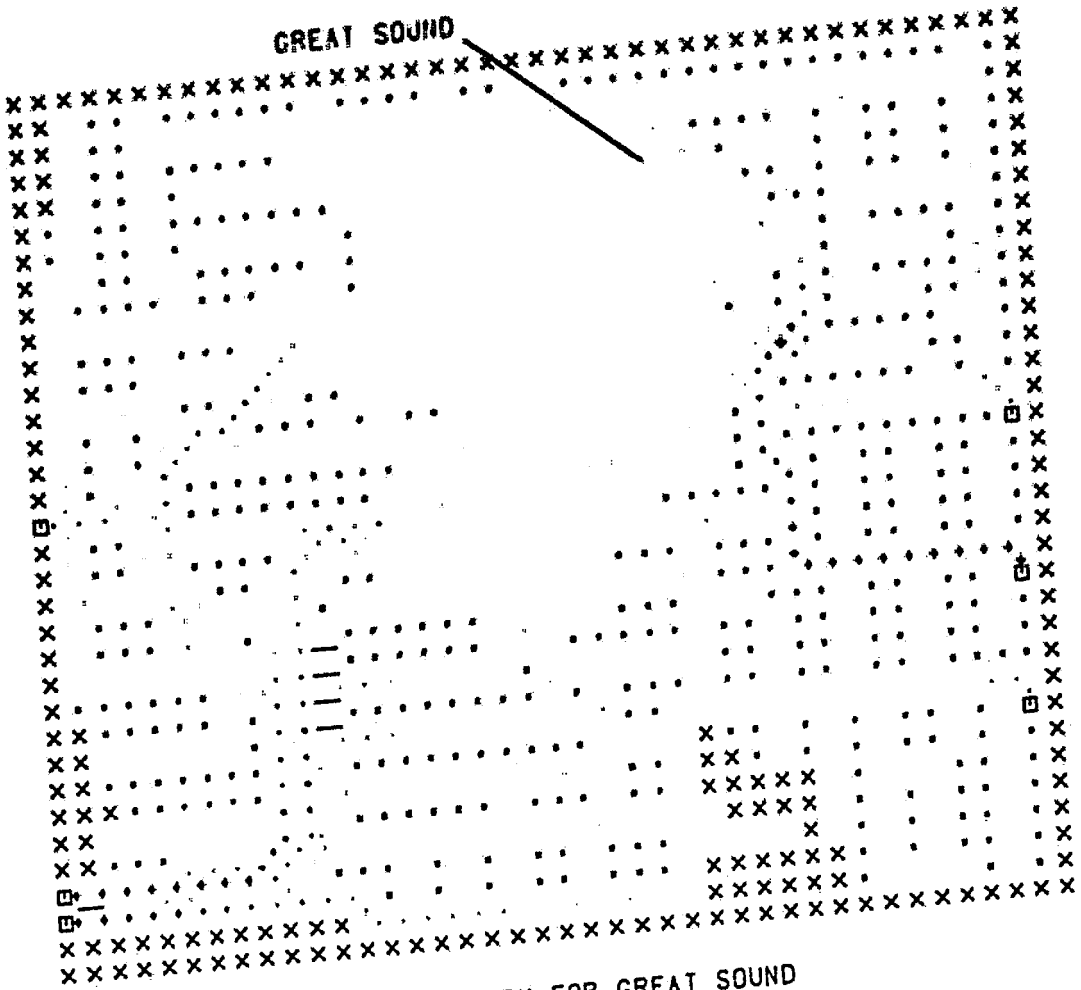

FLOW PATTERN FOR GREAT SOUND
1700 HRS 1 JUNE 1983
X - LAND CELL
* - INUNDATION CELL
⊡ - FORCING CELL
– - NO FLOW BOUNDARY
SCALE - 100000. CFS / INCH

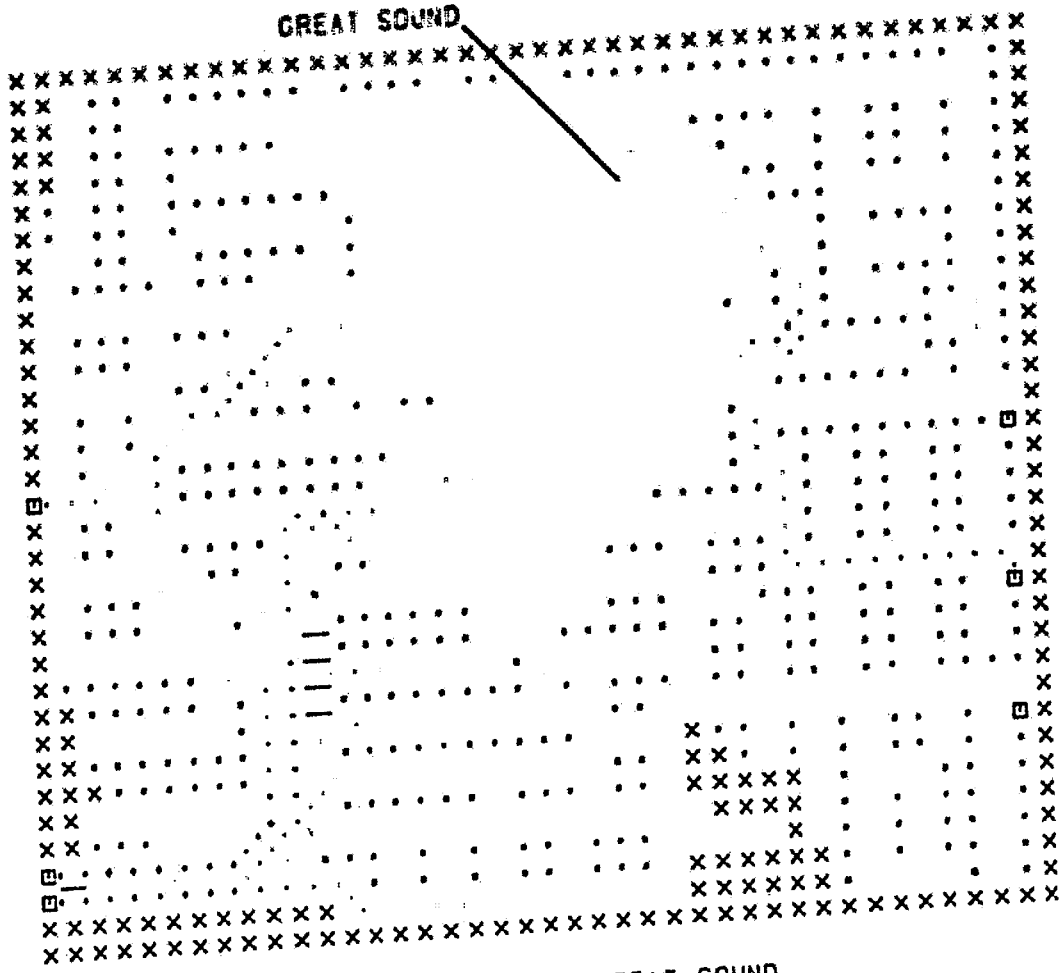

FLOW PATTERN FOR GREAT SOUND
1800 HRS 1 JUNE 1983
X - LAND CELL
* - INUNDATION CELL
⊡ - FORCING CELL
– - NO FLOW BOUNDARY
SCALE - 100000. CFS / INCH

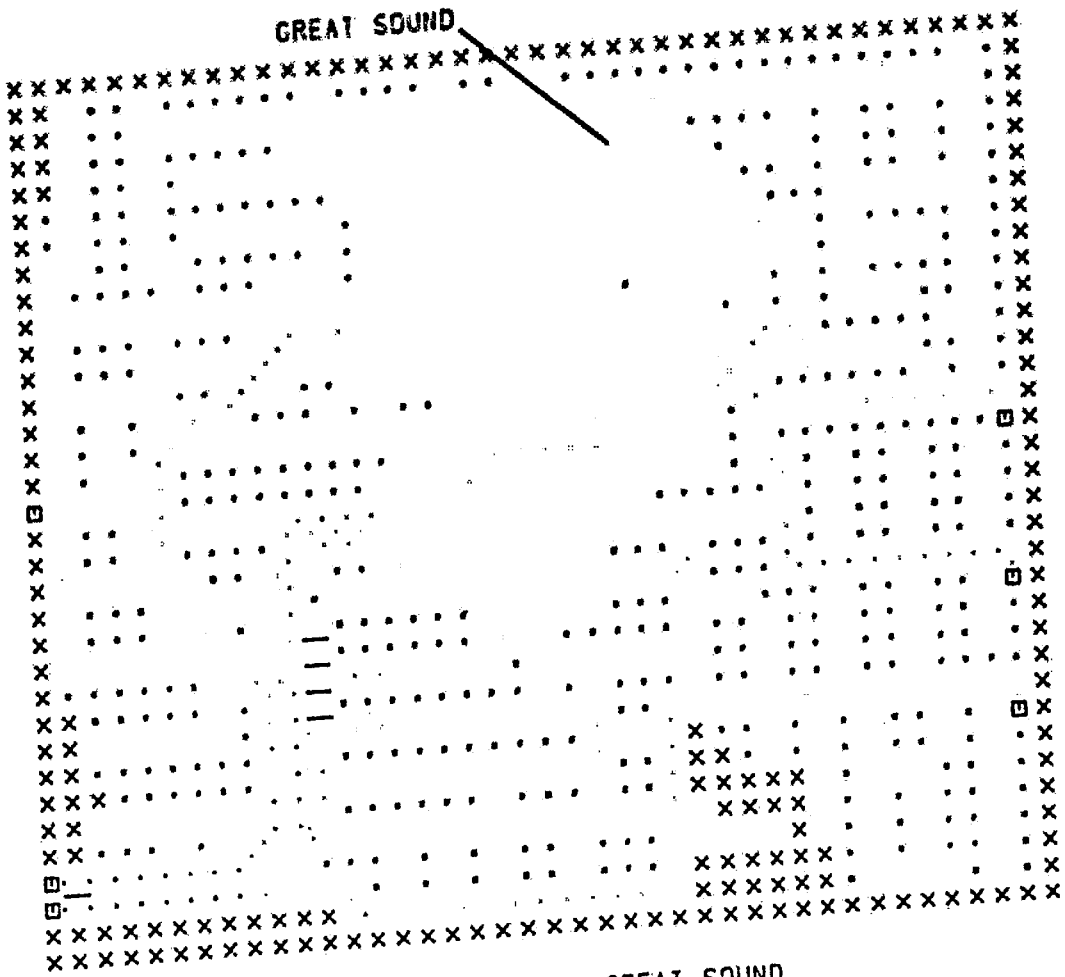

FLOW PATTERN FOR GREAT SOUND
1900 HRS 1 JUNE 1983
X - LAND CELL
* - INUNDATION CELL
⊡ - FORCING CELL
– – NO FLOW BOUNDARY
SCALE - 100000. CFS / INCH

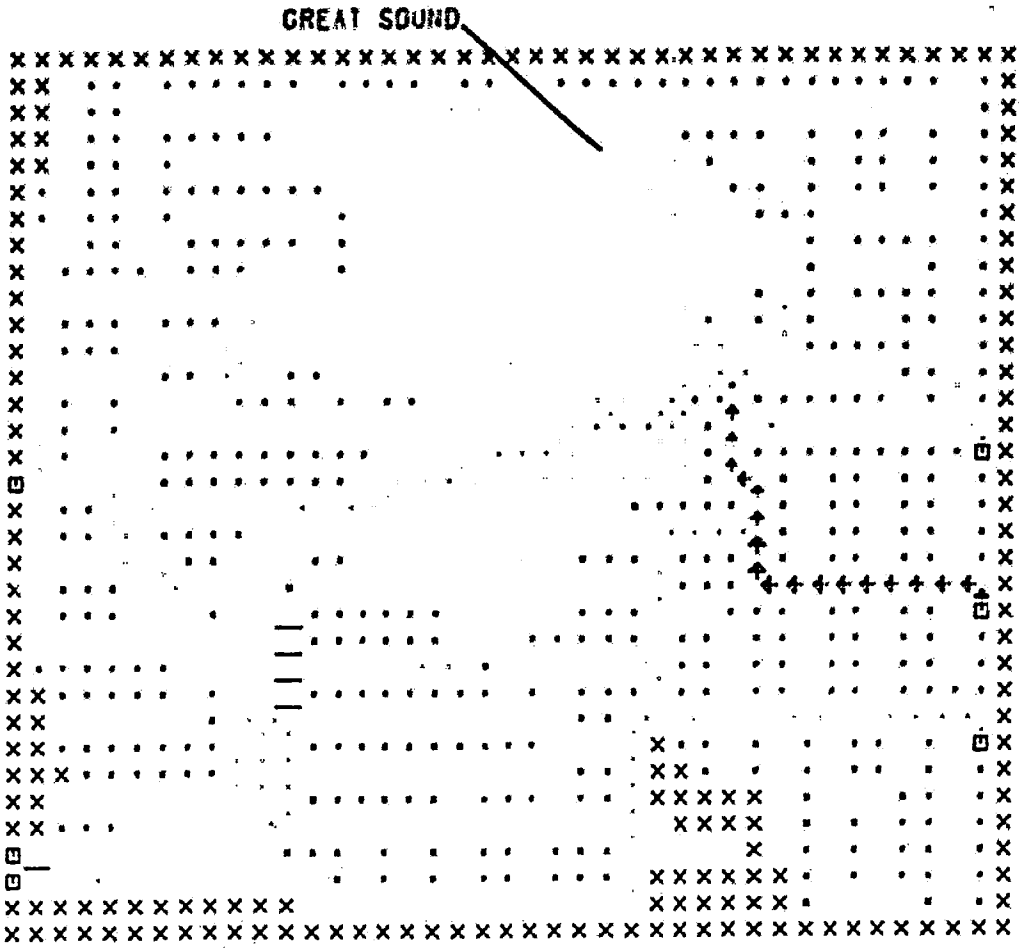

FLOW PATTERN FOR GREAT SOUND
2000 HRS 1 JUNE 1983
X - LAND CELL
⁂ - INUNDATION CELL
⊡ - FORCING CELL
— - NO FLOW BOUNDARY
SCALE - 100000. CFS / INCH

VITA

The author was born on October 24, 1960, to Fred C. and Theresa M. Schuepfer in Philadelphia, Pennsylvania. After completing high school, he attended Drexel University, studied towards a Bachelor of Science degree in Civil Engineering, and graduated with honors in 1983. While attending Drexel, he completed three cooperative education internships: one with the U. S. Geological Survey assisting in groundwater data base management and two with the U. S. Army Corps of Engineers performing spatial analysis work. In addition, he received a Bechtel Company Scholarship Award in his junior year at Drexel.

The author then continued his academic career at Lehigh University in September, 1983. For the next two years he worked as a research assistant in tidal and computational hydraulics. He expects to be granted a Master of Science degree in Civil Engineering in June, 1985, and then will begin work as a mathematical modeler with a private consulting firm.